AN INVESTIGATION OF THE TURBULENT MIXING OF PARALLEL TWO-DIMENSIONAL COMPRESSIBLE DISSIMILAR GAS STREAMS

By

SEYFEDDIN TANRIKUT

A DISSERTATION PRESENTED TO THE GRADUATE COUNCIL OF THE UNIVERSITY OF FLORIDA IN PARTIAL FULFILLMENT OF THE REQUIREMENTS FOR THE DEGREE OF DOCTOR OF PHILOSOPHY

UNIVERSITY OF FLORIDA
1973

ACKNOWLEDGEMENT

A research program, especially one involving an experimental investigation, is rarely completed with the sole efforts of one individual.

The author wishes to express his gratitude for the guidance and assistance of his major advisor, Dr. V. P. Roan. Special thanks are due to Dr. R. B. Gaither, Dr. R. A. Gater, Dr. C. K. Hsieh, Dr. U. H. Kurzweg and Dr. J. F. Kenkling for serving as members of the special supervisory committee. The financial support of the department of Mechanical Engineering throughout the doctoral program is gratefully acknowledged.

The construction and erection of the test apparatus was done by the personnel of the Mechanical Research Laboratories, headed by Professor E. P. Patterson and Mr. R. T. Tomlinson. Their suggestions and contributions to the effort are also gratefully acknowledged.

Finally, the author is indebted to his wife, Yasar, for her patience and confidence, in addition to her assistance in preparing this manuscript.

TABLE OF CONTENTS

TABLE OF CONTENTS (Continued)

TABLE OF CONTENTS (Continued)

LIST OF TABLES

LIST OF FIGURES

LIST OF FIGURES (Continued)

LIST OF FIGURES (Continued)

LIST OF FIGURES (Continued)

LIST OF FIGURES (Continued)

LIST OF SYMBOLS

a	slot height
b	mixing zone width
C_p	specific heat at constant pressure
C_r	Crocco number
H	total enthalpy
h	static enthalpy
J_i	mass diffusion
k	specific heat ratio
Le	Lewis number
M	Mach number
$\dot{m}$	mass flow rate
P	pressure
Pr	Prandtl number
R	gas constant
Sc	Schmidt number
T	temperature
u	velocity component in streamwise direction
v	velocity component in lateral direction
W	molecular weight
x,y	physical coordinate system

Greek Letters

α_j	mass fraction of specie i
β	mass flux ratio
γ	$\Delta x/(\Delta\psi)^2$
$\mathcal{E}$	error term in finite difference equation

ε_d eddy diffusivity

ε_h eddy conductivity

ε_m eddy viscosity

λ eigenvalue of difference equation velocity ratio

ξ $\rho u \varepsilon_m$

ρ density

ϕ excess velocity $(U - U_s)/(U_p - U_s)$

ψ stream function

μ dynamic viscosity

σ spread rate parameter

τ shearing stress

Subscripts

e nozzle exit plane

i specie (O_2, N_2, A, He)

m lateral grid increment in difference equation

n streamwise grid increment in difference equation

o stagnation conditions

p primary stream

s secondary stream

t turbulent quantities

Superscripts

' turbulent fluctuation

* incompressible initial condition

Abstract of Dissertation Presented to the
Graduate Council of the University of Florida in Partial
Fulfillment of the Requirements for the Degree of Doctor of Philosophy

AN INVESTIGATION OF THE TURBULENT MIXING OF PARALLEL TWO-DIMENSIONAL COMPRESSIBLE DISSIMILAR GAS STREAMS

By

Seyfeddin Tanrikut

December, 1973

Chairman: Dr. R. B. Gaither
Cochairman: Dr. V. P. Roan
Major Department: Mechanical Engineering

An investigation of the turbulent mixing in the initial region of a half-jet composed of dissimilar gas streams has been made. An iso-energetic, non-reacting and isobaric system with various velocity and mass flux ratios was studied both experimentally and theoretically.

The flow problem was formulated as an initial value problem using the turbulent boundary layer equations in conjunction with phenomenological models for the turbulent eddy viscosity. These models consisted of Prandtl's mixing length hypothesis, Ferri's differential mass flux formulation, Schetz's extension of the Clauser integral model and Alpinieri's momentum and mass flux model. The validity of the above models for the turbulent momentum transport mechanisms in the initial region of a half-jet was investigated on a consistent basis. The eddy diffusivity was obtained from the eddy viscosity model by considering the turbulent Schmidt number as a parameter. The analytical solution was obtained using an all-explicit forward marching finite difference scheme with the stability of this

scheme being ensured by satisfying the von Neumann stability criterion.

In the experimental phase of the study, a two-dimensional test section was designed and built to be used in conjunction with the existing blow-down wind tunnel facilities. Interchangeable nozzle blocks were designed with the two-dimensional method of characteristics to provide the supersonic flow. A primary stream of air at Mach numbers of 1.3 and 2.0 was allowed to mix with a secondary stream of either helium or argon at a Mach number of 1.3. Quantitative data in the form of total and static pressure measurements, total temperature and mass fraction measurements were collected. Qualitative data in the form of schlieren photographs were also obtained. These data were used to correlate and complement the analytical study.

Results of experimental static pressure measurements, both experimental and theoretical excess velocity and mass fraction profiles, are presented in graphical form for all configurations tested.

CHAPTER I

INTRODUCTION

The occurrence of free viscous layers and their consequent effect on the performance of many contemporary devices has stimulated considerable study of these flow processes. Some examples are slot cooling, supersonic diffusion flames, dumping of fuel at high velocities and thrust augmentation in jet and rocket engines. It is deemed worthwhile to briefly describe how the free viscous layers, resulting from the mixing of coflowing streams, are encountered in some of the physical applications cited above.

1) Slot (or film) cooling: The possible structural failure of modern aircraft due to excessive heating has been a major problem. This problem arises in rotating machinery components of aircraft engines as well as in all types of re-entry and high-speed vehicles. Some examples are turbine blades, rocket nozzles and leading edges of hypersonic aircraft. One method of solution to this problem lies in slot cooling. Slot cooling is a method whereby a coolant gas (or liquid) is injected into the boundary layer of the surface to be cooled. The purpose is to create a cold film layer of gas between the surface and the hot mainstream. If the film is maintained over a large portion of the surface to be cooled, it acts as a partial heat shield and therefore reduces the heating process sufficiently so as to ensure safe operation of the vehicle.

2) Diffusion flames: A mixing controlled combustion has several features. The heat release is distributed over a finite length in contrast to a premixed configuration wherein the heat may be released

abruptly through a detonation process. The inherent distribution of heat release in a mixing controlled system provides a mechanism for obtaining a controlled pressure variation enhancing the possible use of a fixed geometry system. Furthermore, the mixing controlled combustion process can take place in supersonic flow eliminating flow losses (i.e., total pressure loss due to shock waves) and critical design problems required for subsonic burning.

3) Dumping of fuel: Mixing of an injected gaseous fuel in combustible proportions, although desirable in combustion chambers, is usually undesirable when fuel is vented from a flight vehicle. In the case of the multistage chemical rocket using cryogenic propellant such as hydrogen, large quantities of waste gaseous fuel must be vented overboard. After the waste gas is dumped overboard, it may be exposed to regions of high temperature such as the surface boundary layer and the nozzle base area of the operating first-stage engine. A solution to this problem is the venting of the gas in such a manner that the mixture is diluted below the lower limit of flammability in a reasonably short distance from the point of injection.

4) Thrust augmentation: In addition to combustion and heat transfer problems, secondary injection is of importance in ejector systems for jet and rocket engines. High velocity secondary gases are ducted into the nozzles to increase the total exit momentum flux of the flow, thus obtaining higher thrust vectors.

For any kind of analytical study to be conducted on the above physical problems there is a need to know the rate of growth of the shear layer, subsequently referred to as the mixing region, the

variables affecting this growth and the velocity, concentration and temperature profiles inside the mixing region.

The mixing process may take place under a variety of conditions which determine the method of solution to the problem. Some of these conditions are summarized below:

i. The transport mechanism governing the mixing process may be laminar or turbulent.

ii. The mixing process may be steady or unsteady.

iii. Mixing may be isobaric or take place in the presence of pressure gradients.

iv. The compositions of the mixing streams may be similar or dissimilar.

v. The flow may be compressible or incompressible.

vi. The geometry of the system may be two-dimensional or axi-symmetric.

vii. Chemical reactions may take place in the mixing region or the flow could be frozen.

viii. The mixing may be isoenergetic or non-isoenergetic.

ix. The mixing streams could be contained by walls or the streams may be semi-infinite.

In most physical problems many of the complicating factors are present but some have to be neglected or simplified in order to obtain analytical solutions.

A brief investigation of the mixing problem first reveals that the mixing processes are almost unanimously turbulent. Second, one finds that at least one of the mixing streams will be compressible. Thus, the mixing process of interest must account for compressibility

of the streams. A third observation one might note is that the two streams are very likely to be at different thermal levels, requiring an assessment of these effects as well.

For all cases of mixing previous investigators [1][1] have concluded that for the purpose of analysis the mixing process may be divided into two regions. The first is the developing region where the velocity profiles are non-similar, and second the asymptotic (or fully developed) region where the velocity profiles are self-preserving. Figure 1 shows a schematic of the mixing region resulting from the "contact" of two uniform parallel semi-infinite streams which are initially separated by a thin splitter plate. The rate of growth of the mixing region is determined by the turbulent transport mechanisms of mass, momentum and energy.

Approach

There are essentially three methods in use today by which the mixing of parallel coflowing streams are studied. These consist of two methods that have been in use for some time, and a method that has become available within the last several years as a result of the rapid development and use of high-speed computers. The three methods are: 1) the simple momentum integral method, 2) solution of the equations of motion where certain assumptions are made which render these equations tractable to existing analytical techniques, and 3) step-by-step numerical solution of the equations on high-speed digital computers. All of these methods depend ultimately on experimental turbulent mixing

[1]Numbers in brackets designate references.

data since an essential part of all these techniques is the specification of the local turbulent transport coefficients (eddy viscosity, diffusivity, conductivity) of the particular turbulent flow in question at, at least, one general location in the mixing region.

In practical applications one is sometimes interested in the initial stage of mixing, where the upstream velocity has an important effect. The classical similarity solutions for the shear layer cannot account for the effect of the upstream boundary layer on the mixing process. The profile similarity assumption limits validity of the solution to the region past the developing region [2,3]. Solutions for the nonsimilar problems may be derived using the integral technique; however, this application is limited in practice to reasonably smooth profiles. Profiles that cannot be approximated by analytical expressions such as the step function, or profiles that exhibit large boundary layer deficits lie outside the scope of the integral method. In some of the analyses, transformations are made to obtain closed-form solutions that severly limit the variation in flow variables. In reference [4] a closed-form solution for this problem is obtained, but the linearization of transformed equations that is employed again limits the variation in flow variables.

Therefore, the analytical approach taken in this investigation was to develop a solution that would be numerical in nature and permit initial variations of density, velocity and temperature profiles, and would be valid close to the flow inlet as well as far downstream. The flow field was treated by employing the von Mises transformation to the boundary layer equations and utilizing several different hypothesized models for the eddy viscosity. The resulting conservation equations were solved numerically with an explicit type "marching" technique.

As stated earlier, experimental data are essential to evaluate the validity of any formulated turbulent transport coefficient. Such data on the mixing of compressible streams of different compositions are available in literature only in scarce quantity. The main body of available material deals with the fully developed flow region of axi-symmetric jets. Data on the two-dimensional mixing in the initial region are practically nonexistent.

Thus, an experimental investigation was done to provide data for the two-dimensional mixing of dissimilar streams. The data were used to complement and verify the analytical approach taken in this study.

The gas dynamics facilities in the mechanical engineering department were adapted to utilize different species of gas for the mixing analysis. The high pressure air supply system was utilized in the primary stream and a bank of commercial bottled gases, i.e., argon and helium, was used to supply the secondary stream. A test section was designed which permitted the use of interchangeable nozzle blocks. The isoenergetic mixing took place in this two-dimensional test section where both the primary and secondary streams were supersonic. Static and total pressure measurements were made in the test section. Gas samples were withdrawn from the mixing region and collected in a series of vacuum bottles. These samples were subsequently analyzed with a gas chromatograph. A schlieren system was also employed to obtain qualitative results.

CHAPTER II

LITERATURE REVIEW

The analyses of the mixing of turbulent flow fields have been performed by employing the laminar flow boundary layer equations modified by replacing the laminar viscosity with the eddy viscosity and by replacing the laminar Prandtl, Lewis and Schmidt numbers by their turbulent counterparts. The use of the boundary layer equations is justified by the fact that the region of space in which a solution is being sought does not extend far in the transverse direction, as compared with the main direction of flow, and that the transverse gradients are large. The assumptions and details involved in the reduction of the general Navier-Stokes equations to the boundary layer form are well documented in references [1], [2] and [3], and will not be reviewed here. The two-dimensional continuity and momentum equations for steady flow are presented below to aid in understanding some of the assumptions and techniques used by various investigators in obtaining solutions. These equations are discussed in detail in Chapter III.

Continuity:
$$\frac{\partial \rho u}{\partial x} + \frac{\partial \rho v}{\partial y} = 0 \tag{2.1}$$

X-Momentum:
$$\rho u \frac{\partial u}{\partial x} + \rho v \frac{\partial u}{\partial y} = \frac{\partial \tau}{\partial y} - \frac{\partial P}{\partial x} \tag{2.2}$$

Y-Momentum:
$$0 = \frac{\partial P}{\partial y} \tag{2.3}$$

(Here τ denotes the turbulent shearing stress or the Reynolds stress and is usually expressed in terms of the time mean average of the velocity perturbations, i.e., $\tau = - \overline{(\rho v)' u'}$.)

The works of previous investigators will be reviewed in three sections; 1) mixing of semi-infinite streams, 2) mixing of contained (ducted) streams, and 3) some experimental investigations on the mixing of dissimilar gases. The first two sections will primarily be involved in the analytical approaches. The last section is included because it has a definite bearing on the experimental aspect of the present investigation.

Mixing of Semi-Infinite Streams

An excellent bibliography of both experimental and theoretical work on turbulent mixing prior to 1950 is given in a paper by Forstall and Shapiro [5]. Two of the works in this paper should be mentioned here since they formed the starting point and basis for some of the more recent investigations.

The mixing of semi-infinite incompressible streams was considered analytically as early as 1926 by Tollmien [6]. Using a similarity transformation of the type $\eta = y/x$ and Prandtl's [7] mixing length hypothesis[1] for the turbulent transport mechanism, he obtained a numerical solution for the fully developed region of a two-dimensional turbulent jet exhausting into a quiescent atmosphere. This solution was later extended by Kuethe [8] for various boundary conditions.

Görtler [9] utilized Prandtl's [10] second hypothesis for the eddy viscosity to obtain a new analytical solution for the incompressible mixing of two parallel streams. The result was a series solution in contrast to Tollmien's numerical solution and offered the further

---

[1] A detailed discussion on the turbulent transport mechanisms is presented in Chapter IV.

advantage that for sufficiently large secondary velocities, the velocity profile could be approximated by the error function.

Both Tollmien's and Görtler's solutions involved the utilization of a stream function which was proportional to a function, F, of the similarity variable $\eta = \sigma y/x$. Thus, the partial differential equations of motion were reduced to a single ordinary differential equation:

Tollmien's problem: $F''' + F = 0$

Görtler's problem: $F''' + 2\sigma FF'' = 0$

Tollmien experimentally determined a value of 12 for σ from low subsonic turbulent mixing experiments.

It was desired to extend this type of solution to compressible flows. Thus, mixing analyses have primarily been concerned with the development of the theoretical expressions for the mixing similarity parameters; specifically, the evaluation of the "spread rate parameter", σ. One widely used method is to apply a coordinate transformation to the compressible flow equations such that the transformed equations are in the form of the incompressible ones. Then, data from both the compressible and incompressible domain may be used to predict σ. One such method is the extension of Howarth's [11] transformation which was developed for the analysis of compressible laminar boundary layers. The transformation is essentially stretching of the y-coordinate and may be defined in one form by

$$\frac{\partial}{\partial x} = \frac{\partial}{\partial x^*} + \frac{\partial y^*}{\partial x}\frac{\partial}{\partial y} \tag{2.4}$$

$$\frac{\partial}{\partial y} = \left(\frac{\rho}{\rho_r}\right)\frac{\partial}{\partial y^*} \tag{2.5}$$

These relations will reduce the compressible flow equations to the incompressible flow equations in the absence of external pressure gradients. Mager [12] removed the restriction on the pressure gradient by postulating that the shear stress was invariant under the transformation.

There are a number of theoretical estimates of the effects of compressibility on the spread rate parameter. These estimates relate the ratio σ/σ^* to the free stream Mach or Crocco[1] numbers; σ^* is the similarity parameter for incompressible, isoenergetic flow. Abramovich [1] estimated lateral turbulent transport using the classical Prandtl hypothesis for eddy viscosity in conjunction with a hypothetical characteristic longitudinal velocity in the shear layer in order to predict the growth rate of the mixing region. Bauer [13] based his model on a compressible analog of the mixing length concept; together with the error function approximation of the velocity profile, he was able to estimate the spread rate.

Channapragada and Woolley[14], using the Howarth transformation in conjunction with Mager's postulate, reduced the governing equations to the form of Tollmien's or Görtler's problem depending on the model for the eddy viscosity. From the transformation they concluded that the parameter σ varied across the mixing region for compressible flow fields. For the two stream mixing problem, they related σ to the total temperature and velocity ratios of the two streams in addition to the primary stream Crocco number. This model for σ agreed well with the

---

[1] The Mach and Crocco numbers are related through the equation

$$M = C_r^2 / \sqrt{\frac{K-1}{2}(1 - C_r^2)} \ .$$

empirical relation of Korst and Tripp [15] for total temperature ratios of unity, and exhibited similar trends to the predictions of Channapragada [16]. This work was later extended by Woolley [17] to the case of two dissimilar streams (with same specific heat ratios) in the presence of small pressure gradients.

Laufer [18] applied a Howarth type of transformation to the time-dependent rather than the mean equations of motion, as had been done in the past. When the transformed equations were averaged and the correlation between the fluctuations of the temperature and velocity gradients neglected, the incompressible turbulent equations for the mean flow were obtained; and these could be solved with conventional methods.

Utilizing Prandtl's second hypothesis and an extension of Warren's [19] momentum integral method, Donaldson and Gray [20] analyzed the turbulent mixing and decay of axially symmetric, compressible free jets of dissimilar gases. They concluded from a comparison of data with theoretical results that a general relationship existed, at each axial position in the jet, between a local mixing rate parameter and the local Mach number. Furthermore, this relationship was independent of the physical properties or the thermodynamic state of the mixing gases (i.e., independent of molecular weight and enthalpy). This method of analysis was later extended to the case of coflowing streams by Smoot and Purcell [21].

Peters [22] presented a detailed discussion on various eddy viscosity theories and compressibility transformations during the development of a transport model incorporating a dual scale of eddy sizes which was used to predict σ in the compressible regime. Lamb [23]

developed a theory which permitted the estimation of the effect of compressibility and heat transfer on the spread rate parameter for fully developed mixing zones. Integral forms of the conservation equations were used to specify the flow characteristics along the "dividing streamline" between the two streams. By the application of the Navier-Stokes equations to this streamline he was able to calculate a position parameter which in turn yielded an expression for σ.

In a later work by Lamb and Bass [24] an analysis of the methods involved in the correlation of the parameter σ was made. It was observed that differences in the various predictions at high Mach numbers (on the order to 6-8) were as much as 50 percent. It was also seen that the trends of the Channapragada and Woolley theory appeared to be opposite to those of the other analyses, showing a large effect of compressibility at low Mach numbers and very little influence at higher values of M_∞.

In an effort to compare and consolidate different theoretical velocity profiles and expressions for σ, Korst and Chow [25] pointed out that the spread rate parameter depended on 1) the selected eddy viscosity model, 2) the methods of theoretical analysis and 3) the definition of profile matching. On this basis they established theoretical relations which attempted to reconcile discrepancies between different analytical solutions so that all available information on σ could be utilized.

It can be concluded that many of the compressible mixing investigations have placed an emphasis on obtaining similarity solutions which are valid for regions far removed from the initial point of

contact of the two streams. Major effort has gone into methods which attempted to predict the behavior of the spread rate parameter in the compressible domain. Unfortunately there is no widely accepted relation for σ. This may be coupled to the fact that there is no universal model for the turbulent transport mechanism due to the lack of understanding of the physics of the phenomena. Another drawback is that no information can be extracted about the initial and transitional regions of mixing from the spread rate parameter or similarity solutions.

Little work has been done on the effect of nonuniform initial velocity profiles on the mixing process. Wygnanski and Hawaleshka [26] attempted a series solution to the case of the incompressible asymmetric jet (i.e., created by the mixing of a wall jet with quiescent surrounding fluid downstream of the trailing edge). However, the region of validity of this method as well as its accuracy depended critically on an accurate knowledge of the initial velocity profile and its derivatives with respect to y and the number of terms retained in the series expansion. Korst and Chow [27] used integral methods to account for the effects of initially disturbed profiles on the mixing region. Lamb's [23,28] "dividing streamline" solution using the momentum integral method yielded some information on the transition region.

Most of the investigators have assumed a value of unity for the turbulent Prandtl and Lewis numbers. This assumption enabled them to obtain a solution to the momentum equation and use this solution in conjunction with the Crocco integral relation to automatically satisfy the species and energy equations. Although a value of unity for the turbulent Prandtl number may be justified in most cases, the turbulent Schmidt number (Pr/Le) has been shown experimentally to vary between 0.5 and 2.0 [29,30,31].

Another widely used method in obtaining solutions to the mixing problem is one which is based on the linearization of the conservation equations in the plane of the von Mises variables while retaining the essential non-linear nature of the equations in the physical plane. This results in a linear partial differential equation in the form of the unsteady heat equation which can be treated with conventional methods [32] subject to initial and boundary conditions. However, relating the intrinsic coordinate system to the physical plane by means of integral forms of the conservation equations is rather involved and requires the specification of a compressible eddy viscosity model. The works of Libby [33], Ferri et al. [34], Alpinieri [35], Kleinstein [4], and Schetz [36] were all based on this type of a solution with each solution deviating from the other in the formulation of the turbulent transport mechanisms. These formulations will be analyzed in Chapter IV.

Numerical solutions have been utilized recently to obtain mixing characteristics throughout the flow field [37,38,39]. These, however, required appropriate models for the Reynolds transport terms for each region of mixing; that is, the initial, transition and fully developed regions.

Mixing of Confined (Ducted) Streams

Integral techniques have been used in general to obtain solutions to confined turbulent jet mixing problems. In most of the analyses the axial velocity and the shear stress were assumed to obey similarity laws, so that expressions for the turbulent transport coefficients were not needed. In 1955, Craya and Curtet [40]

established an approximate theory for confined jet mixing of streams of identical composition. This theory was further developed by Curtet [41,42] and was followed by additional theoretical and experimental studies by Curtet and Ricou [43] and Curtet and Barchilon [44]. The theoretical analysis was based on assumptions of zero radial pressure gradient, uniform and non-turbulent axial velocity outside the mixing region, and similarity of the axial velocity profiles inside the mixing region. Experimental observations led to the assumption of similar Gaussian velocity profiles in the developing region.

In 1965, Hill [45,46] carried out analytical studies of an isothermal homogeneous confined jet mixing in order to predict the mean velocity field in the flow. In this analysis, an integral technique was also used and the shear integrals were evaluated using free jet data. However, the assumptions made were such that the effects of a confining wall were not significantly taken into consideration.

Dealy [47] studied the effects of conditions at the inlet on the flow phenomena in a confined jet mixing system. Dealy concluded that, for systems with low jet-to-confining tube radius ratio, the flow in the near regime was indeed independent of the nature of the jet source; had similar velocity profiles and was amenable to analysis by the common momentum integral technique. But for large jet-to-confining tube radius ratios, the mixing mechanism was found to be dependent strongly on the flow conditions in the jet exit. Further experiments by Dealy also showed that, for fully developed turbulent flow at the jet source, mixing took place more rapidly (because of

larger turbulent stresses) than for the case corresponding to a uniform flow at the jet source.

Trapani [48] carried out an experimental study of turbulent jets with solid boundaries in the transverse direction in order to investigate their application in certain fluidic devices. Comparison with the flow characteristics of a two-dimensional turbulent free jet showed that the presence of solid transverse boundaries definitely alters the behavior of the flow. The bounded jet (i.e., the jet bounded by plates above and below) was seen to spread less rapidly than the free jet. On the other hand, the confined jet (i.e., the jet enclosed on all sides) was observed to spread more rapidly than the free jet; this effect was attributed to the development of an adverse axial pressure gradient in the confined flow.

An extensive study of the ducted turbulent mixing process for supersonic flows was carried out by Peters et al. [39,49,50] experimentally as well as analytically. An integral theory for the ducted flow was presented for arbitrary axi-symmetric duct geometry. Cases of both frozen and equilibrium chemistry were considered as the mode of chemical reaction in the mixing zone. At initiation of mixing, the boundary layer was considered negligible as were the viscous effects at the duct wall. The velocity profiles in the turbulent mixing zone were assumed to be similar and were represented by a cosine function. The turbulent shear stress in this variable density mixing layer was treated by the use of a modified Prandtl eddy viscosity model. The free mixing concept of shear and velocity profile similarity were assumed to be applicable in the main region. The turbulent Prandtl

and Lewis numbers of unity were used in the analysis. From the results of analysis and experiment, it was concluded that the integral method developed permitted reasonably accurate computations of the flow in complex mixing systems such as air-air ejectors and air-augmented rockets.

Emmons [51] also developed an analysis for predicting the flow characteristics in the mixing region of a particle-laden turbulent rocket exhaust and the surrounding air stream. Neglecting the boundary layer at the confining wall, the turbulent boundary layer equations were used to describe the flow in the mixing zone. The eddy viscosity model was assumed to vary with the streamwise coordinate. The system of partial differential equations governing the flow was transformed using the von Mises transformation and then solved by finite difference methods. Similar approaches were taken by Cohen [52], Edelman and Fortune [38] and Chia et al. [53].

Mixing of Dissimilar Gases

Major Experimental Investigations

Perhaps the earliest experimental study on the relative rates of diffusion of momentum and energy in turbulent jets was done by Ruden [54], who found that energy diffused more rapidly than momentum in isobaric incompressible jets. Forstall and Shapiro [5] studied the diffusion of mass and momentum between coaxial jets of air where the central jet was composed of approximately 10 percent of helium for use as a tracer gas. The velocities considered in their experiments were in the low subsonic range. They concluded that mass diffusion was more rapid than momentum diffusion. Furthermore, the Schmidt number, which measures the relative rates of transfer of mass and momentum,

was found to be independent of the velocity ratio. A similar result was obtained by Keagy and Weller [55] from their experiments on helium and carbon dioxide jets exhausting into quiescent air.

Corrsin and Uberoi [56], using a heated jet exhausting into a quiescent region of different density, investigated the effect of large density differences in the mixing zone. They found that a decrease of jet density with respect to that of the receiving medium caused an increase in the rate of spread of the jet.

Isoenergetic mixing between carbon dioxide and hydrogen central jets exhausting into a moving concentric stream of air was investigated by Alpinieri [35]. Using velocities in the low to high subsonic range, he concluded that the Schmidt number was essentially constant and, in agreement with previous results, that mass appeared to diffuse more readily than momentum. It was also observed that no tendency toward segregation of the two jets was evident when either the velocity ratio, mass flow ratio or momentum flux ratio was made equal to unity. Yates [57] studied the supersonic slot injection of hydrogen into a supersonic air stream. He found that the concentration profiles exhibited similarity before the velocity profiles did. The rate of growth of the energy and concentration layers was observed to be about the same and exceeded the growth of the momentum layer.

Zakkay et al. [58] undertook an extensive experimental investigation of the turbulent mixing of two dissimilar gases. The axisymmetric mixing analysis was carried out to determine the turbulent transport coefficients for hydrogen-, helium-, and argon-air mixtures. The external stream of air was maintained at a constant Mach number of

1.6 and the inner jet was either subsonic or supersonic. Their conclusions may be summarized as, 1) the centerline decay was not influenced by the molecular weight or the initial boundary layer of the jet; 2) the radial velocity profiles exhibited similarity past the potential core and could be correlated by the mass flux ratio; 3) no dependence of Schmidt number on molecular weight could be observed; 4) the deviation of the turbulent Schmidt number from unity was considerable in several cases.

However, from their experimental investigation of the axisymmetric turbulent jets of air, helium and Freon 12, Abramovich et al. [59] concluded that it was ineffective to attempt to describe the characteristics of the jet by any cojoint complex of the variables (ρ,u) such as the mass flux ratio or the momentum flux ratio.

CHAPTER III

ANALYSIS FOR THE MIXING OF DISSIMILAR STREAMS

Introduction

The literature survey presented shows that several simplifying assumptions were made to render the analytical model tractable from the mathematical point of view. The "boundary layer" forms of the conservation equations have been shown to be applicable to the cases of both confined and unconfined mixing problems. In a great majority of the investigations, the correlation of the analysis with data was restricted to the main region of mixing, where similarity of the velocity profiles was assumed.

In the present study, the mixing problem is formulated as an initial value problem in the von Mises plane using the turbulent boundary layer equations. Unlike the laminar problem, the transport mechanisms in turbulent mixing do not depend on the fluid properties alone, but also on geometric and dynamic factors of the flow system. Determination of the necessary transfer coefficients by an exact theoretical analysis is presently not possible due to the lack of understanding of the turbulence phenomena; therefore, a semi-empirical approach is employed in order to correlate the data obtained in the experimental phase of the investigation. The governing conservation equations of the flow are approximated by their finite difference forms and the solution is obtained by an explicit numerical scheme. Numerical stability is ensured by satisfying the von Neumann stability criterion. A typical geometry of the problem is shown in Figure 2.

Boundary Layer Equations

The Prandtl boundary layer equations used in the analysis of two-dimensional mixing problems are:

Global Continuity

$$\frac{\partial \rho}{\partial t} + \frac{\partial (\rho u)}{\partial x} + \frac{\partial (\rho v)}{\partial y} = 0 \tag{3.1}$$

X-Momentum

$$\frac{\partial (\rho u)}{\partial t} + \frac{\partial (\rho u) u}{\partial x} + \frac{\partial (\rho v) u}{\partial y} = - \frac{\partial P}{\partial x} + \frac{\partial \tau}{\partial y} \tag{3.2}$$

Y-Momentum

$$0 = \frac{\partial P}{\partial y} \tag{3.3}$$

Specie Continuity

$$\frac{\partial \rho \alpha_i}{\partial t} + \frac{\partial (\rho u) \alpha_i}{\partial x} + \frac{\partial (\rho v) \alpha_i}{\partial y} = \frac{\partial J_i}{\partial y} \tag{3.4}$$

Total Energy

$$\frac{\partial \rho H}{\partial t} + \frac{\partial (\rho u) H}{\partial x} + \frac{\partial (\rho v) H}{\partial y} = - \frac{\partial q}{\partial y} + \frac{\partial u \tau}{\partial y} + \frac{\partial P}{\partial t} \tag{3.5}$$

where

$$\tau = \mu \frac{\partial u}{\partial y} \qquad \text{(molecular shear)} \tag{3.6a}$$

$$J_i = - D_i \frac{\partial \alpha_i}{\partial y} \qquad \text{(molecular diffusion)} \tag{3.6b}$$

$$q = q_c + q_d = - k \frac{\partial T}{\partial y} + \sum_i h_i J_i$$

$$= \frac{k}{C_p} \sum_i \alpha_i \frac{\partial h_i}{\partial y} + \sum_i h_i J_i \quad \text{(molecular heat flux)} \tag{3.6c}$$

If the differentiations in Equations (3.2), (3.4) and (3.5) are carried out, the global continuity equation can be extracted and the equations

reduce to their more conventional form. The equations are written in the above forms for the sake of mathematical expediency in the time-averaging technique necessary to obtain the turbulent forms.

Inherent in the above equations are the assumptions that the body force terms in the x- and y-momentum equations are small, the species are inert chemically (i.e., non-reacting flow) and thermal diffusion is negligible. From the first of these assumptions, the only information available from the y-momentum equation is the result that pressure is invariant in the lateral direction. Pressure gradients (if any) are restricted to the axial direction and no further use of the y-momentum equation can be made.

Further assumptions necessary for the present analysis are summarized below:

i. Flow outside the mixing zone is inviscid, non-conducting and uniform.

ii. Boundary layers on the confining walls will be neglected. No correlation will be attempted for regions downstream of the point of interaction of the wall with the mixing zone.

iii. The mixing region of interest is under isobaric conditions; that is, in addition to $\partial P/\partial y = 0$, it is assumed that $\partial P/\partial x = 0$. Although some streamwise pressure changes are expected since the experimental configuration under consideration is one of confined supersonic flow, these pressure changes are expected to be small (i.e., 5-8 percent of the exit plane value) since the region of interest is the

initial mixing region (i.e., 5-10 inches downstream of the nozzle exit) where there is no interaction of the confining walls with the mixing zone. Data from the experimental investigation justify this assumption as does other literature [1].

Turbulent Equations

In the analysis of turbulent flows, it is customary to assume that the instantaneous value of each property is the sum of the mean value which varies with a time-mean average value and a fluctuating component which is a function of time [3]. In addition to fluctuations of velocity, density, temperature and mass fractions, Van Driest [60] hypothesized that there are fluctuations of mass flow (ρu), (ρv) regarded as a single property. Hence, the following relation is defined for any property ϕ:

$$\phi = \bar{\phi} + \phi' \tag{3.7}$$

where "bar" quantities are time-mean-averages defined by

$$\bar{\phi} = \frac{1}{t^*} \int_{t_o}^{t_o+t^*} \phi dt \tag{3.8}$$

and the "prime" quantities are fluctuating components. It is readily seen from Equation (3.8) that the time-mean value of any linear fluctuating quantity and its derivatives vanisles;i.e., $\overline{u'}$, $\overline{v'}$, $\overline{\partial u'/\partial y}$, etc. are all zero.

Since turbulent flow is unsteady in nature, it is somewhat of a contradiction in terms to speak of a "steady turbulent flow", but

the term has usually been used to denote a turbulent flow which is steady in the mean, i.e., quasi-steady. Moreover, at each point the fluid properties and velocity may be observed to fluctuate wildly, but, when averaged over time periods comprising many cyclic fluctuations, the time-mean properties are constant with respect to time.

Thus, a state of quasi-steady turbulent flow is assumed; the instantaneous values of the quantities are replaced by the relation in Equation (3.7) and the flow is considered in the mean by time averaging as defined in Equation (3.8).

Global Continuity

$$\frac{\partial \overline{\rho u}}{\partial x} + \frac{\partial \overline{\rho v}}{\partial y} = 0 \tag{3.9}$$

X-Momentum

$$\overline{\rho u}\,\frac{\partial \bar{u}}{\partial x} + \overline{\rho v}\,\frac{\partial \bar{u}}{\partial y} = \frac{\partial \bar{\tau}}{\partial y} - \frac{\partial}{\partial y}\,\overline{(\rho v)'u'} - \frac{\partial}{\partial x}\,\overline{(\rho u)'u'}$$

This equation differs from the laminar counterpart by the last two terms. The last term is the derivative of the turbulent normal stress and is usually neglected by assuming that boundary layer approximations are valid for cojoint complex perturbation quantities, i.e.,

$$\frac{\partial}{\partial x}\,\overline{\tau_1' \tau_2'} << \frac{\partial}{\partial y}\,\overline{\tau_1' \tau_2'} \tag{3.10}$$

The second term on the right-hand side is the Reynolds (or apparent) stress which cannot be neglected. Thus, a turbulent stress is defined as

$$\bar{\tau}_t = -\,\overline{(\rho v)'u'}$$

and the momentum equation takes the form:

$$\overline{\rho u}\,\frac{\partial \bar{u}}{\partial x} + \overline{\rho v}\,\frac{\partial \bar{u}}{\partial y} = \frac{\partial}{\partial y}\left[\bar{\tau} + \tau_t\right] \tag{3.11}$$

Species

$$\overline{\rho u}\,\frac{\partial \bar{\alpha}_i}{\partial x} + \overline{\rho v}\,\frac{\partial \bar{\alpha}_i}{\partial y} = \frac{\partial \bar{J}_i}{\partial y} - \frac{\partial}{\partial y}\,\overline{(\rho v)'\alpha_i'} - \frac{\partial}{\partial x}\,\overline{(\rho u)'\alpha_i'}$$

With the approximation of Equation (3.10) and defining turbulent mass diffusion as

$$\bar{J}_{it} = -\,\overline{(\rho v)'\alpha_i'}$$

the species equation takes the same form as the momentum equation:

$$\overline{\rho u}\,\frac{\partial \bar{\alpha}_i}{\partial x} + \overline{\rho v}\,\frac{\partial \bar{\alpha}_i}{\partial y} = \frac{\partial}{\partial y}\left[\bar{J}_i + \bar{J}_{it}\right] \tag{3.12}$$

Total Energy

$$\overline{\rho u}\,\frac{\partial H}{\partial x} + \overline{\rho v}\,\frac{\partial H}{\partial y} = -\frac{\partial \bar{q}_c}{\partial y} - \frac{\partial \bar{q}_d}{\partial y} + \frac{\partial}{\partial y}\left[\bar{u}\bar{\tau} + \overline{u'\tau'}\right] - \frac{\partial}{\partial y}\,\overline{(\rho v)'H'} - \frac{\partial}{\partial x}\,\overline{(\rho v)'H'}$$

Although the last term can be neglected with the aid of Equation (3.10), the present form of the equation does not permit a comparison between the molecular and turbulent transport properties. To overcome this difficulty, some assumptions have to be made. From Equation (3.6a), the third term on the right may be written as

$$\frac{1}{2}\,\frac{\partial}{\partial y}\,\bar{\mu}\,\frac{\partial}{\partial y}\left[\bar{u}^2 + \overline{u'^2}\right]$$

Along the lines of Van Driest's [60] work, it is expected that $\overline{u'^2}$ is small compared to $\bar{u}^2$; since $\bar{u}^2$ is assumed to be of the same order as h, $\overline{u'^2}$ can be dropped from the equation.

Now an equivalent expression for the perturbation term, H',

will be formulated. From the definition of total enthalpy and assuming $v^2 << u^2$, which is a valid boundary layer assumption:

$$H \doteq h + \frac{u^2}{2} = \sum_i \alpha_i h_i + \frac{u^2}{2}$$

$$\bar{H} + H' = \sum_i \{\bar{\alpha}_i\bar{h}_i + \bar{\alpha}_i h_i' + \alpha_i'\bar{h}_i + \alpha_i' h_i'\} + \frac{\bar{u}^2}{2} + \bar{u}u' + \frac{u'^2}{2}$$

Noting that $\sum_i \bar{\alpha}_i\bar{h}_i = \bar{h} - \sum_i \overline{\alpha_i' h_i'}$ and $\frac{\bar{u}^2}{2} = \frac{\overline{u^2}}{2} - \overline{\frac{u'^2}{2}}$

$$\bar{H} + H' = (\bar{h} + \frac{\bar{u}^2}{2}) + \sum_i \{\bar{\alpha}_i h_i' + \alpha_i'\bar{h}_i + \alpha_i' h_i' - \overline{\alpha_i' h_i'}\} + \bar{u}u' + \frac{u'^2}{2} - \overline{\frac{u'^2}{2}}$$

Thus,

$$H' = -\sum_i \overline{\alpha_i' h_i'} - \overline{\frac{u'^2}{2}} + \sum_i \bar{h}_i\alpha_i' + \sum_i h_i'\bar{\alpha}_i + \sum_i \alpha_i' h_i' + \bar{u}u' + \frac{u'^2}{2} \quad (3.13)$$

It is also noted that Equation (3.13) satisfies the condition $\overline{H'} \equiv 0$. When Equation (3.13) is multiplied by $(\rho v)'$, time averaged and the third order correlations neglected, the result is

$$-\overline{(\rho u)'H'} = -\sum_i \bar{h}_i\overline{(\rho v)'\alpha_i'} - \bar{u}\,\overline{(\rho v)'u'} - \sum_i \bar{\alpha}_i\,\overline{(\rho v)'h_i'} \quad (3.14)$$

The first and second terms on the right may be recognized as containing the turbulent diffusion and shear terms, respectively. The third term is similar to q_c in Equation (3.6c) and is defined as the turbulent "conduction" term:

$$\bar{q}_{ct} = -\sum_i \bar{\alpha}_i\,\overline{(\rho v)'h_i'}$$

Equation (3.14) now has terms analogous to the molecular terms and the total energy equation is written as

$$\overline{\rho u}\,\frac{\partial \bar{H}}{\partial x} + \overline{\rho v}\,\frac{\partial \bar{H}}{\partial y} = \frac{\partial}{\partial y}\,(\bar{q}_{ct} - \bar{q}) + \frac{\partial}{\partial y}\,(\bar{q}_{dt} - \bar{q}_{d}) + \frac{\partial}{\partial y}\,\bar{u}(\bar{\tau}_{t} + \bar{\tau}) \tag{3.15}$$

It is now assumed that the boundary layer is fully turbulent and, thus, molecular transports are negligible, i.e.,

$$\bar{q}_{ct} >> \bar{q}_{c}$$

$$\bar{q}_{dt} >> \bar{q}_{d}$$

$$\bar{\tau}_{t} >> \bar{\tau}$$

$$\bar{J}_{it} >> \bar{J}_{i}$$

The turbulent shear is related to the mean flow variables following Boussinesq [61]

$$\bar{\tau}_{t} = -\,\overline{(\rho v)'u'} = \varepsilon_{m}\,\frac{\partial \bar{u}}{\partial y} \tag{3.16}$$

where ε_{m} is the turbulent momentum transfer coefficient and has the same units as the molecular dynamic viscosity. Similarly, the turbulent diffusion and conduction terms are related to the mean flow variables:

$$\bar{J}_{it} = -\,\overline{(\rho v)'\alpha_{i}'} = \varepsilon_{d}\,\frac{\partial \bar{\alpha}_{i}}{\partial y} \tag{3.17}$$

$$\bar{q}_{ct} = -\sum_{i} \bar{\alpha}_{i}\,\overline{(\rho v)'h_{i}'} = \sum_{i} \bar{\alpha}_{i}\varepsilon_{h}\,\frac{\partial \bar{h}_{i}}{\partial y} \tag{3.18}$$

The relation indicated by Equation (3.17) implies that all mass transfer coefficients, ε_{di}, of the various species are equal. Woolley [17] argued that if two streams, each composed of multiple chemical species in homogeneous mixtures were considered, then, upon exposing

the two streams to each other, all gradients of concentration differences for species between the streams would be identical. If their mass transport coefficients were also equal, they would diffuse through the mixing zone at the same rate. The relative concentrations of the species from a given stream would, then, remain unchanged at any position in the mixing zone. However, this was equivalent to each stream behaving as a single species. Thus, under the present assumption, each homogeneous stream, no matter what its detailed composition, may be treated as a single species in the mixing study. Therefore, it is only necessary to treat the mixing of two dissimilar gases, each having the average chemical and thermodynamic properties of their respective mixtures. This is particularly true for the primary stream of air which is usually considered as a single species [62].

Also of interest are some dimensionless turbulent quantities which measure the relative rates of different transport mechanisms. The turbulent Prandtl number is a measure of the relative rates of transport of momentum and energy; the turbulent Lewis number is a measure of the relative rates of transport of mass and energy.

These quantities together with the turbulent Schmidt number are defined as

$$Pr_t = \frac{\varepsilon_m}{\varepsilon_h}$$

$$Le_t = \frac{\varepsilon_d}{\varepsilon_h} \qquad (3.19)$$

$$Sc_t = \frac{Pr_t}{Le_t} = \frac{\varepsilon_m}{\varepsilon_d}$$

Since all equations are time averaged and all transports are turbulent, the bar notation and the subscript "t" will be dropped from here on. With the definitions in Equations (3.16) through (3.19) and after some rearrangement, the governing equations take the final form:

Global Continuity

$$\frac{\partial \rho u}{\partial x} + \frac{\partial \rho v}{\partial y} = 0 \tag{3.20}$$

Momentum

$$\rho u \frac{\partial u}{\partial x} + \rho v \frac{\partial u}{\partial y} = \frac{\partial}{\partial y}\left(\varepsilon_m \frac{\partial u}{\partial y}\right) \tag{3.21}$$

Species

$$\rho u \frac{\partial \alpha_i}{\partial x} + \rho v \frac{\partial \alpha_i}{\partial y} = \frac{\partial}{\partial y}\left(\frac{\varepsilon_m}{Sc} \frac{\partial \alpha_i}{\partial y}\right) \tag{3.22}$$

Total Energy

$$\rho u \frac{\partial H}{\partial x} + \rho v \frac{\partial H}{\partial y} = \frac{\partial}{\partial y}\left[\varepsilon_m \left\{ \frac{1}{Pr} \frac{\partial H}{\partial y} + \left(1 - \frac{1}{Pr}\right) \frac{\partial u^2/2}{\partial y} + \sum_i \left(\frac{Le - 1}{Pr} \right) h_i \frac{\partial \alpha_i}{\partial y} \right\}\right] \tag{3.23}$$

The von Mises Transformation

The solution of Equations (3.20) through (3.23) provides the details of the flow field including the velocity, species and enthalpy (thus temperature) fields. The global continuity equation, Equation (3.20), can be eliminated from the system of differential equations by introducing the von Mises coordinates as the independent variables. The transformation $(x,y) \rightarrow (x,\psi(x,y))$ is defined according to the relations:

$$\frac{\partial \psi}{\partial x} = - \rho v \quad ; \quad \frac{\partial \psi}{\partial y} = \rho u$$

The derivatives in the physical coordinates are mapped onto the von Mises plane via

$$\left(\frac{d}{dy} \right)_x = \left(\frac{d\psi}{dy} \right)_x \left(\frac{\partial}{\partial \psi} \right)_x + \left(\frac{dx}{dy} \right)_x \left(\frac{\partial}{\partial x} \right)_\psi = \rho u \left(\frac{\partial}{\partial \psi} \right)_x \tag{3.24}$$

$$\left(\frac{d}{dx} \right)_y = \left(\frac{d\psi}{dx} \right)_y \left(\frac{\partial}{\partial \psi} \right)_x + \left(\frac{dx}{dx} \right)_y \left(\frac{\partial}{\partial x} \right)_\psi = - \rho v \left(\frac{\partial}{\partial \psi} \right)_x + \left(\frac{\partial}{\partial x} \right)_\psi \tag{3.25}$$

Substitution of the above relations into the system of equations completes the formulation of the problem in the von Mises plane.

Momentum

$$\frac{\partial u}{\partial x} = \frac{\partial}{\partial \psi} \left[\rho u \varepsilon_m \frac{\partial u}{\partial \psi} \right] \tag{3.26}$$

Specie

$$\frac{\partial \alpha_i}{\partial x} = \frac{\partial}{\partial \psi} \left[\frac{1}{Sc} \rho u \varepsilon_m \frac{\partial \alpha_i}{\partial \psi} \right] \tag{3.27}$$

Total Energy

$$\frac{\partial H}{\partial x} = \frac{\partial}{\partial \psi} \left[\rho u \varepsilon_m \left[\frac{1}{Pr} \frac{\partial H}{\partial \psi} + \frac{Pr - 1}{Pr} \frac{\partial u^2/2}{\partial \psi} + \frac{Le - 1}{Pr} \sum_i h_i \frac{\partial \alpha_i}{\partial \psi} \right] \right] \tag{3.28}$$

The physical y-coordinate is obtained by the inverse transformation:

$$y = \int_0^\psi \frac{d\psi}{\rho u} \tag{3.29}$$

and the transverse component of velocity, v, is given by:

$$v = - \frac{1}{\rho} \frac{\partial \psi}{\partial x} \tag{3.30}$$

Boundary Conditions

The governing equations exhibit parabolic characteristics and thus require initial conditions at some $x = x^*$ and boundary conditions at $\psi = 0$ and $\psi = \infty$.

In any real experimental situation, there is an inevitable accumulation of boundary layer on the jet dividing boundary. In order to avoid making an error in initial conditions by assuming either a step profile or a computed boundary layer, the calculation of the mixing region is started at a position downstream of the mixing interface where measured data are available. Hence, the initial conditions may be expressed as:

$$
\begin{aligned}
&@\ x = x^* \quad ; \quad 0 \leq \psi \leq \infty \\
&u(x^*,\psi) = u^*(\psi) \\
&H(x^*,\psi) = H^*(\psi) \\
&\alpha_i(x^*,\psi) = \alpha_i^*(\psi)
\end{aligned}
\tag{3.31}
$$

Since the wall boundary layer is assumed to be negligible, constant flow conditions equal to the secondary stream conditions are assumed at the wall, i.e., slip condition. It is observed that zero axial velocities are not permissible at any location in the flow field due to the inverse transformation of Equation (3.29). Then, the boundary conditions become:

$$
\begin{aligned}
&@\ y = 0 \rightarrow \psi = 0 \quad ; \quad x^* \leq x \leq x_{max} \\
&\qquad u(x,0) = u_s = \text{constant} \\
&\qquad H(x,0) = H_s = \text{constant} \\
&\alpha_{O_2}(x,0) = 0 \ ; \ \alpha_{N_2}(x,0) = 0 \ ; \ \alpha_{A,He}(x,0) = 1
\end{aligned}
\tag{3.32}
$$

$$@\ Y = \infty \rightarrow y = \infty\ ;\ x^* < x < x_{max}$$

$$\begin{aligned} u(x,\infty) &= u_p = \text{constant} \\ H(x,\infty) &= H_p = \text{constant} \end{aligned} \tag{3.33}$$

$$\alpha_{O_2}(x,\infty) = 0.23\ ;\ \alpha_{N_2}(x,\infty) = 0.77\ ;\ \alpha_{A,He}(x,\infty) = 0$$

The condition of $y = \infty$ ($\psi = \infty$) are all regions beyond the upper boundary of the mixing zone.

Finite Difference Equations

A forward marching all-explicit numerical method was used in this analysis. Accordingly, for the transverse derivatives, central differences are used in the interior grid points. Forward differences are used for the longitudinal derivatives everywhere. Figure 3 shows a generic point (n+1,m) in the (x,ψ) grid network, for which the solution is obtained by using the following explicit difference relations [63] where F is any one of the three pertinent variables u, α_i, or H:

$$\frac{\partial F}{\partial x} = \frac{F_{n+1,m} - F_{n,m}}{\Delta x} \tag{3.34}$$

$$\frac{\partial F}{\partial y} = \frac{F_{n,m+1} - F_{n,m-1}}{2\Delta\psi} \tag{3.35}$$

$$\frac{\partial}{\partial\psi}\left[\xi \frac{\partial F}{\partial\psi}\right] = \frac{\xi_{n,m+1/2}(F_{n,m+1} - F_{n,m}) - \xi_{n,m-1/2}(F_{n,m} - F_{n,m-1})}{(\Delta\psi)^2} \tag{3.36}$$

where

$$\xi = \rho u \varepsilon_m \tag{3.37}$$

$$\xi_{n,m\pm1/2} = \frac{1}{2}(\xi_{n,m} + \xi_{n,m\pm1}) \tag{3.38}$$

Then, the non-linear parabolic equation may be approximated by the finite difference equation

$$F_{n+1,m} = F_{n,m} + \gamma[\xi_{n,m+1/2}F_{n,m+1} - (\xi_{n,m+1/2} + \xi_{n,m-1/2})F_{n,m}$$

$$+ \xi_{n,m-1/2}F_{n,m-1}] + \mathcal{E} \tag{3.39}$$

where $\gamma = \Delta x/(\Delta\psi)^2$ and $\mathcal{E}$ is the error introduced by the finite difference approximation of the differential equation and may be defined as [63]:

$$\mathcal{E} = k_1[\theta(\Delta x)] + k_2[\theta(\Delta\psi)^2] \tag{3.40}$$

Equation (3.40) implies that Δx and $\Delta\psi$ have to be sufficiently small for the difference scheme to be accurate. This point will be discussed further with respect to consistency and stability of the scheme.

It should be recognized that, although the partial differential equations are non-linear, the present explicit difference formulation results in a locally linear system. Inherent in this result is the assumption that the solution is "fairly smooth" and the quantity, ξ, is a "slowly varying" function. These two assumptions imply that discontinuities such as shock waves cannot be present in the flow field, and thus pose no major restriction on the solution since no such phenomena are considered.

The conservation equations for the interior grid points (i.e., $m \neq 0$) in difference form are:

Momentum

$$u_{n+1,m} = u_{n,m} + \gamma[\xi_{n,m+1/2}u_{n,m+1} - (\xi_{n,m+1/2} + \xi_{n,m-1/2})u_{n,m}$$

$$+ \xi_{n,m-1/2}u_{n,m-1}] \tag{3.41}$$

Species

$$(\alpha_i)_{n+1,m} = (\alpha_i)_{n,m} + \frac{\gamma}{Sc}\left[\xi_{n,m+1/2}(\alpha_i)_{n,m+1} - (\xi_{n,m+1/2} + \xi_{n,m-1/2})(\alpha_i)_{n,m} + \xi_{n,m-1/2}(\alpha_i)_{n,m-1}\right] \tag{3.42}$$

Energy

$$\begin{aligned} H_{n+1,m} = H_{n,m} &+ \frac{\gamma}{Pr}\left[\xi_{n,m+1/2}H_{n,m+1} - (\xi_{n,m+1/2} + \xi_{n,m-1/2})H_{n,m}\right. \\ &\left. + \xi_{n,m-1/2}H_{n,m-1}\right] + \frac{\gamma(Pr-1)}{2Pr}\left[\xi_{n,m+1/2}u^2_{n,m+1}\right. \\ &\left. - (\xi_{n,m+1/2} + \xi_{n,m-1/2})u^2_{n,m} + \xi_{n,m-1/2}u^2_{n,m-1}\right] \\ &+ \sum_i \frac{\gamma(Le-1)}{Pr}\left[(\xi h_i)_{n,m+1/2}(\alpha_i)_{n,m+1} - [(\xi h_i)_{n,m+1/2}\right. \\ &\left. + (\xi h_i)_{n,m-1/2}](\alpha_i)_{n,m} + (\xi h_i)_{n,m-1/2}(\alpha_i)_{n,m-1}\right] \end{aligned} \tag{3.43}$$

Boundary Conditions for the Difference Equation

The initial and boundary conditions for the difference equations are similar to their counterparts for the differential equation and are input in equal intervals of $\Delta\psi$.

$$\begin{aligned} &@\ x = x^* \ ;\ 0 \le \psi \le N\Delta\psi \\ &u_{o,m} = u_m(\Delta\psi) \\ &H_{o,m} = H_m(\Delta\psi) \\ &(\alpha_i)_{o,m} = [\alpha_i(\Delta\psi)]_m \end{aligned} \tag{3.44}$$

An interesting characteristic of the general difference equation, Equation (3.39), is observed when the boundary condition at $\psi = 0$, i.e.,

$m = 0$, is applied; that is, the terms $F_{n,-1}$ and $\xi_{n,-1/2}$ are undefined. The conventional method employed to circumvent this difficulty is to define an "artificial" boundary condition such that the value of $F_{n,-1}$ is equal to $F_{n,1}$. This implies that the gradient of the quantity F is zero at the boundary and, in the physical sense, is equivalent to a condition of symmetry at the axis of a jet. Since an assumption of constant velocity at the wall has already been made for the physical boundary condition, the application of the above principle will not introduce any new assumptions into the analysis. With the application of the condition of symmetry, the difference equations at the wall become:

Momentum:

$$u_{n+1,o} = u_{n,o} + 2\gamma\xi_{n,o}(u_{n,1} - u_{n,o}) \tag{3.45}$$

Species

$$(\alpha_i)_{n+1,o} = (\alpha_i)_{n,o} + \frac{2\gamma}{Sc}\,\xi_{n,o}[(\alpha_i)_{n,1} - (\alpha_i)_{n,o}] \tag{3.46}$$

Energy

$$H_{n+1,o} = H_{n,o} + \frac{2\gamma}{Pr}\,\xi_{n,o}(H_{n,1} - H_{n,o}) + \frac{\gamma(Pr - 1)}{Pr}\,\xi_{n,o}(u^2_{n,1} - u^2_{n,o}) + \frac{2\gamma(Le - 1)}{Pr}\,\xi_{n,o}\sum_i (h_i)_{n,o}[(\alpha_i)_{n,1} - (\alpha_i)_{n,o}] \tag{3.47}$$

Together with the boundary condition:

$$\begin{aligned} u_{n,o} &= u_s = \text{constant} \\ H_{n,o} &= H_s = \text{constant} \\ (\alpha_{O_2})_{n,o} &= 0 \;;\; (\alpha_{N_2})_{n,o} = 0 \;;\; (\alpha_{A,He})_{n,o} = 1 \end{aligned} \tag{3.48}$$

The boundary condition at $\psi = \infty$ is one of "floating" type; that is, calculations proceed until the condition $F_{n,m+1} = F_{n,m}$ is satisfied.

Analysis of the Difference Scheme

Once a finite difference scheme is set up, it must satisfy three conditions [64]:

i. The difference equation must be "consistent" with the differential equation. That is, the error involved in approximating a differential equation by a difference equation must vanish in the limit $\Delta x, \Delta\psi \to 0$.

ii. The difference scheme must be "convergent". That is, the solution to the difference equation must approach the solution of the differential equation in the limit.

iii. The marching rate must be "stable". That is, the grid size should be such that the solution does not become unbounded anywhere. A relation between Δx and $\Delta\psi$ must be found to insure this condition.

The consistency of the present method may be shown by observing that the quantity $\mathcal{E}$, defined in Equation (3.40), approaches zero unconditionally as $(\Delta x, \Delta\psi)$ approach zero. The proof of convergence for quasi-linear difference equations is lengthy and is not presented here; however, the numerical scheme employed can be shown to be convergent with the method of Strang [65].

One of the important characteristics of explicit finite difference schemes is the stability of the solution. For a system of linear constant coefficient equations, it can be shown that the von Neumann stability criterion is the necessary and sufficient condition

for stability and convergence [63]. In variable-coefficient cases it is necessary for stability that the von Neumann conditions (derived as though the coefficients were constant) be satisfied at every point in the grid network. This is based on the observation that when instability occurs in practice, it often appears as a local disturbance in a region where the von Neumann condition is violated. John [in 63] has shown that for a general class of explicit difference equations for quasi-linear parabolic partial differential equations, the von Neumann condition is necessary for stability and that a slightly modified form of the von Neumann condition is sufficient.

On this basis the von Neumann stability criterion was derived, and this criterion was checked at each point in the grid network since the system of governing equations are quasi-linear. An outline of the von Neumann analysis for the difference equations used is given below.

A linear, constant coefficient parabolic partial differential equation with periodic boundary conditions has a solution of the form

$$u(x,y) = \sum_k A_k(x) e^{\hat{i}ky}$$

Assuming that in the limit the difference equation has the same type of solution, let

$$F_{n,m} = \sum_k A_k \lambda_k^n e^{\hat{i}km\Delta y} \tag{3.49}$$

Equation (3.49) is substituted into the general difference equation, Equation (3.39), and since it is also assumed that all Fourier coefficients decay exponentially, the k^{th} term is examined:

$$\lambda_k = 1 - \gamma(\xi_{n,m+1/2} + \xi_{n,m-1/2})(1 - \cos k\Delta y) + \hat{i}\gamma(\xi_{n,m+1/2} - \xi_{n,m-1/2})\sin k\Delta y \tag{3.50}$$

For $F_{n,m}$ to be bounded, the von Neumann criterion is

$$|\lambda_k| < 1$$

After some manipulation, the restriction on the grid size relation, γ, is obtained

$$\gamma \leq \frac{\xi_{n,m+1/2} + \xi_{n,m-1/2}}{\xi^2_{n,m+1/2} + \xi^2_{n,m-1/2} - 2\xi_{n,m+1/2}\xi_{n,m-1/2} \cos k\Delta y}$$

and the most restrictive condition occurs when the quantity on the right is a minimum, which is the case when $\cos(k\Delta y) = -1$. Then, the final form of the stability criterion which governs the interior grid size is

$$\frac{\Delta x}{(\Delta\psi)^2} \leq \frac{1}{\xi_{n,m+1/2} + \xi_{n,m-1/2}} \qquad (\xi = \rho u \varepsilon_m) \qquad (3.51)$$

It is further observed that if ξ is a constant, C, throughout the domain of interest, Equation (3.51) reduces to the form $C\Delta t/(\Delta x)^2 = 1/2$ which is the well-established stability condition for the linear "heat equation" with the difference scheme of Equation (3.39).

Since Equation (3.51) is valid only at the interior grid points, a stability condition for the boundary is derived in the same manner with the result

$$\frac{\Delta x}{(\Delta\psi)^2} \leq \frac{1}{2\xi_{n,o}} \qquad (3.52)$$

The above stability conditions were derived for the general difference equation. When applied to the governing system of equations, they are seen to be different by a constant K where

$K = 1$ for the momentum equation

$K = 1/Sc$ for the species equation

$K = 1/Pr$ for the energy equation

It was found, during the analysis of truncation error of linear equations, that when the stability criterion is multiplied by a factor of 1/3, a higher order of accuracy could be obtained, i.e., $\xi = K_1[\theta(\Delta x)^2] + K_2[\theta(\Delta\psi)^4]$. This is not strictly correct for quasi-linear equations, but if ξ is a "slowly varying" function, considerable improvement in accuracy can still be obtained by making use of the above result. Therefore, with the above modifications the final form of the stability conditions are

$$\frac{1}{6}\frac{(\Delta\psi)^2}{K\xi_{n,o}} \geq \Delta x \leq \frac{1}{3}\frac{(\Delta\psi)^2}{K(\xi_{n,m+1/2} + \xi_{n,m-1/2})} \tag{3.53}$$

This results in six conditions, the most restrictive of which is utilized, depending on the magnitude of the dimensionless quantities Pr, Sc and Le.

Thus, Equations (3.41) through (3.48) together with the stability condition, Equation (3.53), constitute the numerical solution to the flow field. The only remaining point is the formulation of the quantity ε_m, and this will be discussed in Chapter IV.

CHAPTER IV

TURBULENT MOMENTUM AND MASS TRANSPORT

General Considerations

Although the first portion of this chapter could have been included in the literature survey, it is felt that the presentation of the analysis would be more continuous if it were included in this section.

To this point the consideration of the analytical treatment of the turbulent mixing problem has dealt primarily with the question of solving the questions of motion. While being necessary, this is not the area of greatest difficulty. The major difficulty associated with these problems is the mathematical representation of turbulent transport processes. The present understanding of the turbulence phenomenon is such that turbulent processes within a shear flow cannot be treated locally. Rather, the most that can be expected is some prediction of the "mean" flow properties.

There are essentially two distinct approaches previously taken in the analysis of mixing problems. The more recent approach [66,67,68] is to introduce additional conservation equations which describe the Reynolds stress. This approach is appealing since it guarantees conservation of the turbulent quantities. Unfortunately, the resulting equations contain second and higher order correlations and, thus, to apply this approach, empirical relations are required for the third and higher order correlations. Furthermore, due to its complexity, this approach has not been applied to compressible free shear layer

flows. Therefore, solutions of practical problems of current interest have been attained only by employing the more commonly used approach of utilizing an eddy viscosity model along with assumed constant Sc, Pr and hence Le. The eddy viscosity models that have been proposed for free mixing flows are summarized in Table I.

Classical Eddy Viscosity Models

The famous mixing length theory for turbulent shear was formulated by Prandtl [7] who hypothesized that the mean value of the fluctuating velocity component in a turbulent flow field is equal to the product of the local mean velocity gradient and a characteristic mixing length, ℓ. The quantity ℓ is defined as a distance in the flow field such that a fluid element conserves its longitudinal velocity as it moves across this distance. In the case of free mixing, the mixing length is assumed to be constant across the mixing layer and also assumed to be proportional to the local width of the mixing zone. Thus, Prandtl's mixing length theory gives the following relation for the Reynolds stress in the longitudinal direction

$$\tau_t = -\overline{(\rho v)'u'} \approx c^2 b^2 \left|\frac{\partial u}{\partial y}\right| \frac{\partial u}{\partial y} \tag{4.1}$$

where c is an experimentally determined constant and b is the width of the mixing layer. Using the concept of eddy viscosity in Equation (3.16)

$$\varepsilon_m = c^2 b^2 \left|\frac{\partial u}{\partial y}\right| \tag{4.2}$$

Based on a similar mixing length concept, Taylor [in 1] derived a vorticity transport theory where the vorticity of the fluid element is assumed to be conserved across the mixing length. In both of these

mixing length concepts, the eddy length scale was assumed to be much smaller than the local width of the mixing layer. The complexity of Taylor's model for axi-symmetric flows has prevented its utilization; and for the case of two-dimensional flows, except for a numerical constant, the vorticity theory results in the same expression for turbulent shear as obtained from Prandtl's mixing length theory.

Prandtl [10] later proposed another model for the turbulent eddy viscosity based on the hypothesis that the eddy scale was of the same order as the width of the mixing layer. This model was based on the assumption that the eddy viscosity is related to the local mean velocity gradient and was expressed as

$$\varepsilon_m = cb(U_{max} - U_{min}) \tag{4.3}$$

where c is an empirical constant and U_{max} and U_{min} are the maximum and minimum longitudinal velocities, respectively. Prandtl's second model predicts a constant eddy viscosity across the mixing layer since the width, b, is not a function of the lateral coordinate.

Equation (4.3) has been widely applied to a variety of free mixing problems due to its mathematical simplicity and the results it yields agree satisfactorily with experimental data for several flow configurations. It, therefore, forms the basis for most eddy viscosity models existing in the literature, and is used for a particular flow field by appropriately including the effects that may be of significant interest in that case. However, it is noted that the model fails completely when the velocities of the two streams are equal. Hence, it predicts that two streams of equal velocities flow along as segregated without turbulent mixing. This implication has

been shown to be incorrect by the experimental results of references [5] and [35].

The various eddy viscosity models available today are the result of attempts by several investigators to include the cases of equal velocities within the framework of Prandtl's original hypothesis for free turbulent flow. Ferri et al. [34] suggested the following model by simply extending the second Prandtl model to describe flows with density gradients

$$\rho\varepsilon_m = c\, r_{1/2}[(\rho u)_{max} - (\rho u)_{min}] \tag{4.4}$$

where $r_{1/2}$ is the half-radius. This model has yielded predictions of unreliable accuracy for axi-symmetric flows [35,58] but when applied to the planar case, good predictions were achieved [36]. However, the Ferri model fails when the mass flux of each stream is equal.

In order to circumvent such irregularities, Alpinieri [35] considered the eddy viscosity to be proportional to the sum of the mass flux and the momentum flux and for an axi-symmetric jet, proposed the relation

$$\frac{(\rho\varepsilon_m)_{C.L.}}{(\rho u)_j} = c\, r_{1/2}\left[\frac{\rho_e u_{CL.}}{\rho_j u_j} + \frac{\rho_e u_e^2}{\rho_j u_j^2}\right] \tag{4.5}$$

where $(\rho\varepsilon_m)$ is the "dynamic" turbulent viscosity at the center-line of the coaxial jet with the subscripts e and j referring to the properties of the external stream and the inner jet, respectively. The Alpinieri model is contrary in form to any other model and is viewed as essentially empirical, qualitatively as well as quantitatively [69].

Density differences may arise within the mixing region either due to compressibility effects, as in the case of heated jets and supersonic flows, or due to streams of different composition. Ting and Libby [70], employing a Mager transformation, postulated the following relation between the eddy viscosity for constant density mixing and that for variable density axi-symmetric flows

$$\varepsilon_m = \varepsilon^* \left(\frac{\rho_o}{\rho} \right)^2 \frac{1}{r^2} \int_o^r 2 \frac{\rho}{\rho_o} r dr \tag{4.6}$$

where ε^* is the eddy viscosity for incompressible flows and ρ_o is a reference density. As can be seen, the above relation is essentially a conversion of the incompressible eddy viscosity, ε^*, to one applicable for flows with density variations either due to compressibility or stratification. It should be recognized, however, that while this transformation admits possible practical applications, no definite form of ε^* or ρ_o is suggested and the results vary depending on the forms of ε^* and ρ_o used. A planar form of this model was utilized by Schetz [36] with the expression

$$\rho^2 \varepsilon_m = \varepsilon^* \rho^2_{C.L.} \left[\frac{1}{\psi} \int_o^\psi \frac{\rho}{\rho_{C.L.}} d\psi \right] \tag{4.7}$$

Donaldson and Gray [20] attempted to account for compressibility via modifying the Prandtl model, Equation (4.3), by employing an empirically determined constant which varied with Mach number at the half-radius. This resulted in the expression

$$\varepsilon_m = \varepsilon_p (0.66 + 0.34 \exp(-3.42 M^2)) \tag{4.8}$$

where ε_p denotes the Prandtl eddy viscosity model of Equation (4.3).

Schetz [69] proposed a model which was developed from an extension of Clauser's model for the wake region of a turbulent boundary layer to free shear layers. The specific functional expression for a given flow problem was derived from the general statement: "the turbulent viscosity is proportional to the mass flow defect (or excess) in the mixing region." [69, page 1] The model was expressed as

$$\rho\varepsilon_m = c\rho_e u_e \int_{}^{\infty} \left| 1 - \frac{\rho u}{\rho_e u_e} \right| dy \tag{4.9}$$

Similar to the Ferri model, the above expression fails when the mass defect (or excess) is zero. Also, the model has been shown [31] to fail for the case of the quiescent jet since the mass entrainment, and therefore, mass defect, increases in the downstream direction thus predicting continually increasing eddy viscosity. It has been demonstrated by Eggers [71] that for an accurate prediction of the flow field in quiescent supersonic jets, the eddy viscosity must remain very nearly constant.

There have been other models formulated for the turbulent transport mechanism, but these are either too complicated to be of practical use, i.e., von Karman model (Table I), or are not applicable to the present study, i.e., Zakkay model. Each of the eddy viscosity models presented in Equations (4.2) through (4.9) are deficient in certain respects. Of course, some of the deficiencies are relatively unimportant and any one of these models is acceptable provided that they are used within the flow region for which they have been verified.

Choice of Models for the Present Study

It should be mentioned that the eddy viscosity models cited have been used for extensive correlations but only in the similarity regions of symmetric jets, subject to specific flow conditions and configurations. It is important to note the distinction between the similarity region of a symmetric jet and the similarity region of the half-jet which is the case under study. The similarity region of a symmetric jet is that part of the flow field far downstream of the so-called potential core. The half-jet may be thought of as a symmetric jet with an infinite jet radius or height, resulting in a potential core of infinite length. The important point is the fact that the models in Equations (4.4) through (4.9) have been verified only in regions past the potential core of a symmetric jet. Thus, no statement may be made regarding their application to other jet mixing configurations. In fact, this is true for all available expressions for ε_m because of the lack of complete and accurate data used in studying any eddy viscosity model. Hence, the results obtained in this study apply to both the initial and fully developed regions of a half-jet and the potential core of a symmetric jet.

The fact that several models may be used to correlate the same experimental data is shown by the results obtained by Ragsdale and Edwards [72,73] in their analytical and experimental study with air-bromine system. In their analytical study, various expressions for eddy viscosity were compared on a consistent basis. It was concluded that modifications of Prandtl's second hypothesis, that introduce mass flux or momentum flux or both, produce expressions whose differences

are more apparent than real. It was shown that these various expressions predict essentially the same eddy viscosity as long as they are applied only within the range of conditions for which they have been experimentally verified. It was concluded that this was perhaps because the initial turbulence present in the streams contributes significantly to the mixing process and may dominate the situation for nearly equal stream velocities.

The effect of free stream turbulence was also considered by Hokenson and Schetz [74] in their study of turbulent mixing with pressure gradients. The results of their investigation demonstrated that the empirical constant in the modified Clauser model of Equation (4.9) must reflect the turbulence intensity and therefore is not a universal constant. It was also observed that this empirical constant was approximately independent of the longitudinal distance from the initial station, and that if adequate information (i.e., turbulence intensity) is known at the initial station, a numerical evaluation of the flow field could reasonably be assumed within the framework of the generalized Clauser eddy viscosity.

To correlate the data obtained in the experimental phase of the present investigation, four models of the turbulent momentum transport mechanism were chosen; namely, Prandtl's mixing length hypothesis (Equation (4.2)), Ferri's differential mass flux model (Equation (4.4)), Alpinieri's momentum flux model (Equation (4.5)) and Schetz's extension of the Clauser model (Equation (4.9)). As stated earlier these models have been shown, within certain limitations, to correlate data in the "far field" or similarity region of symmetric jets. Since the region of interest for the present analysis is the

initial mixing region, the primary objective was to examine the validity of these models in the so-called "near field". It is also of passing interest to note that, to the author's knowledge, the Alpinieri model has never been applied to the case of two-dimensional mixing problems in any region of flow. Minor modifications necessary to compare the models on a consistent basis within the framework of the present analysis, is discussed in the next section.

Modification and Correlation of Models

The form of the governing equations, Equations (3.26) through (3.30), require that the turbulent transport mechanism be specified in the form (or units) of "dynamic" turbulent viscosity; i.e., as the counterpart of μ in the laminar case. To avoid confusion in terms of notation, $(\mu_t)_P$, $(\mu_t)_F$, $(\mu_t)_A$ and $(\mu_t)_S$ will be used to denote the Prandtl, Ferri, Alpinieri and Schetz models, respectively.

To be consistent with the governing equations, the Prandtl model is expressed in terms of the von Mises variables

$$(\mu_t)_P = \rho\varepsilon_m = c_1^2 b^2 \rho^2 u \left| \frac{\partial u}{\partial \psi} \right| \tag{4.10}$$

and with the aid of Equation (3.35) is put in finite difference form

$$(\mu_t)_P = c_1^2 b_{n-1}^2 \rho_{n,m}^2 u_{n,m} \frac{u_{n,m+1} - u_{n,m-1}}{2\Delta\psi} \tag{4.11}$$

In the Ferri and Alpinieri models, the eddy viscosity is expressed in terms of the half-radius based on either the velocity or the mass flux. The half-radius is defined as the distance from the axis of symmetry at which the axial velocity (or mass flux) is equal to the average of the maximum and minimum velocities (or mass flux), i.e.,

$$r \quad \text{at which } U = 0.5(U_{max} + U_{min})$$

or $$r \quad \text{at which } \rho U = 0.5((\rho U)_{max} + (\rho U)_{min})$$

Although this has some physical meaning in the similarity region of a symmetric jet, it has no meaning in the initial region of a half-jet. Therefore, rather than a width such as the half-radius being used, the actual width of the mixing region will be utilized. Since there is always an uncertainty as to the physical boundaries of the mixing region in any experimental study, the width will be defined as the distance in which the velocities are within 5 percent of the free stream values, i.e., referring to Figure 2, if

$$b = Y_1 - Y_2$$

then
$$Y_1 = Y \quad \text{at which} \quad |U - U_p|/U_p = 0.05 \tag{4.12}$$
$$Y_2 = Y \quad \text{at which} \quad |U - U_s|/U_s = 0.05$$

In the Alpinieri model the centerline velocity is replaced by the secondary stream, which is analogous to the condition in the potential core of the symmetric jet.

With the above modifications, the Ferri and Alpinieri models take the form

$$(\mu_t)_F = c_2 b[(\rho u)_{max} - (\rho u)_{min}] \tag{4.13}$$

$$(\mu_t)_A = c_3 b(\rho u)_s \left[\frac{\rho_p}{\rho_s} + \frac{\rho_p u_p^2}{\rho_p u_s^2}\right] \tag{4.14}$$

where the subscripts p and s refer to primary and secondary stream conditions, respectively.

The Schetz model when expressed in terms of the von Mises

variables reduces to

$$(\mu_t)_s = C_4 \int_{-\infty}^{\infty} \left| \frac{\rho_p u_p}{\rho u} - 1 \right| d\psi \qquad (4.15)$$

It was necessary to have a common frame of reference to be able to compare the different models on a consistent basis. The mixing zone width, defined in Equation (4.12) was chosen to be this common reference. The coefficients of each model were varied until the predicted growth of the mixing zone matched the experimental data for each of the four configurations of Table II. With each model predicting the same growth rate, the theoretical and experimental velocity profiles were compared as to the "goodness of fit" of each model.

It was also expected that the coefficients of a given model would vary from configuration to configuration and thus be a function of the flow field as was concluded by Hokenson and Schetz [74]. However, rather than use the turbulence intensity at the initial station, an attempt was made to correlate the coefficients (C_1 through C_4) with the initial mixing conditions such as the velocity ratio or the mass flux ratio. The results will be discussed in Chapter VI.

Remarks on the Turbulent Transport of Mass and Energy

In early analysis of mixing problems, it was often assumed that the turbulent Schmidt and Prandtl numbers were unity; an assumption which simplifies the governing equations considerably. However, recent experiments indicate that the Schmidt number may differ significantly from unity. Furthermore, the experimental data of Forstall

and Shapiro [5] show that the Schmidt number remains constant at approximately 0.7 throughout the mixing region, so that the eddy diffusivity ε_d is merely a constant times the eddy viscosity ε_m. For gaseous components in binary mixing, the values of Sc most frequently cited vary between 0.5 and 1.2. In the present investigation, the turbulent Schmidt and Prandtl numbers are considered as parameters and are retained constant in the entire mixing region. Using suitable values for Sc and Pr yields the values for ε_d and ε_h from calculated values of ε_m.

Hence, with the choice of the transport mechanism, the formulation of the problem is completed. The equations are solved numerically on an IBM 370/165 and the results are discussed in Chapter VI. A discussion and printout of the computer program is presented in the Appendix.

CHAPTER V

EXPERIMENTAL INVESTIGATION

General Considerations

The main objective of the experimental investigation was to examine the mixing of parallel two-dimensional coflowing supersonic gas streams. The primary emphasis was placed on obtaining pressure, velocity and species concentration profiles inside the mixing region.

The secondary stream design Mach number was chosen to be 1.3 for the following reasons:

i. to minimize disturbances at the nozzle exit, the pressure in the two streams was matched by presetting settling chamber conditions in each. To avoid pressure communication back to the repective chambers, both streams had to be supersonic, i.e., $M > 1$. Waves due to supersonic flow at Mach 1.3 (if any existed) would tend to be weak.

ii. an average run time of approximately thirty seconds was necessary to obtain various measurements. Due to the large number of runs needed to accurately define the specie profiles, the total pressure in the secondary settling chamber would have to be as low as possible to conserve the consumption of commercial bottled gas. High Mach numbers in the secondary stream would have forced the use of high total pressures to match exit conditions. Since flow rate is directly proportional to the total pressure, a design Mach number of 1.3 was chosen to keep the secondary stream mass flow rate relatively low.

iii. the contour of the supersonic portion on a Mach 1.3 nozzle was explicit enough to ensure relatively error free machining.

The primary stream design Mach numbers of 1.3 and 2.0 were chosen to obtain various velocity and mass flux ratios between the two streams. A summary of runs with various configurations and test conditions is shown in Table II.

Experimental Apparatus

The gas dynamics facilities in the mechanical engineering department were modified to utilize different species of gas for the mixing analysis (Figure 4). A block diagram of the system is also presented in Figure 5.

The existing facility consists of a two-stage positive displacement type compressor, feeding a series of high pressure air storage tanks. Air from the tanks is brought to the laboratory in two separate lines to a pair of on-off valves. The line pressures are stepped down to the desired levels by a pressure regulator in each stream before the air enters the settling chambers. Inside the two separate settling chambers are a series of flow straighteners and dampening screens. Thus, fairly uniform streams are introduced through converging sections into the test section. The test section is followed by a diffuser section; then the air is passed through a sound attenuator and exhausts into the atmosphere.

This system was modified by the addition of a storage tank that supplied the secondary stream with either argon or helium. The

existing dry air supply system was utilized for the primary stream. A two-dimensional test section was designed that permitted the use of interchangeable nozzle blocks.

Test Section

A photograph of the test section with the splitter plate and a set of nozzle blocks installed is shown in Figure 6. The designed test section consisted of a section which reduced the existing dimensions of the system to the desired dimensions of 8.5 by 0.5 inches for the primary and 4.5 by 0.5 inches for the secondary stream. This section was constructed out of steel and had a secondary function of supporting most of the length of the splitter plate. Erected between the reducer and the diffuser sections was the main frame also made from steel. The upper and lower portions of the frame were used to position and secure the primary and secondary stream nozzle blocks. Hard neoprene gasket material was used to seal the flanges. The frame was "sandwiched" between two one-inch aluminum side plates which when bolted together would give a test section width of one-half inch. Although a larger test section might have been desirable, the flow area (thus the flow rate) of the secondary stream was the governing factor in the test section dimensions. The frame and the side plates were sealed from the environment by linear "O-rings". The side plates had sections cut out to accomodate optical windows and the static pressure plate.

Since having the two streams an infinitesimally small distance apart when they came into contact with each other was physically impossible, the splitter plate was machined down to 0.015 inches at the tip.

A thinner plate would have caused strength problems since the splitter plate had to support the force due to the pressure difference between the streams.

To support the protruding portion of the splitter plate, a 1.25 inch wide by 0.25 inch deep groove was machined in the side plates. With the splitter plate in place, epoxy resin was poured into the groove and allowed to harden. Since the splitter plate was coated with silicone grease before this operation, it was easily removed when the resin had hardened. The excess resin was then sanded down smooth with the side plate surface. This method permitted the support of the "odd-shaped" portion of the splitter plate. The snug fit also served as a seal between the primary and secondary streams.

Nozzle Blocks

The contour of the nozzle blocks guiding the subsonic flow was an arbitrary shape which permitted smooth transition to sonic conditions at the minimum area. The contour providing the supersonic flow was determined from the two-dimensional method of characteristics. To get the shortest possible test section, a sharp-edged throat with a single wave reflection design was used. No allowance for the boundary layer was made in the nozzle design; however, the splitter plate had a taper of 0.007 inches per inch at the straight section. This made up for some of the boundary layer accumulation which is small in accelerated flows.

The nozzle blocks were cut out of 0.5 inch aluminum plates, and machined to the desired contour. The final polishing was done by

hand using fine grained emery cloth. Cushioned tape instead of O-rings was placed between the side plates and the nozzle blocks to seal the system.

The primary stream nozzles had a throat half-height of 2 inches. Thus, except for the reflected waves, the effect of the wall bounding the primary stream could be neglected. The secondary stream nozzle had a throat half-height of 0.5 inches. For this case the wall effects could not be ignored and limited the collection of data to the downstream location where the mixing region and the wall boundary layer interacted with each other. It should be recognized that the secondary stream dimensions were determined by the maximum feasible flow rate of the stream.

It was observed during calibration runs that the primary and secondary stream Mach 1.3 nozzles gave surprisingly clean (shock-free) flows. The primary stream Mach 2.0 nozzle, however, did display some wave patterns, but pressure measurements showed these waves to be weak.

The actual Mach numbers of the two streams were checked by three methods: 1) ratio of the settling chamber total pressure to probe total pressure, 2) ratio of the local static pressure to probe total pressure, and 3) measuring the wave angles on the schlieren photographs. With the air Mach 2.0 and 1.3 nozzles, the result was an average Mach number of 1.97 and 1.28 respectively. The secondary stream nozzle (designed for M=1.3) yielded an average Mach number of 1.27. A photograph of the air Mach 2.0 nozzle block is presented in Figure 7.

Gas Supply and Control System

The primary stream utilized air from the existing air storage system of the gas dynamics laboratory. This system consists of a Worthington two-stage compressor feeding a series of tanks capable of holding approximately 420 cubic feet of air at 300 psi. The air is passed through several oil and water traps and a regenerative type gas dryer before it goes into the storage tanks.

The secondary stream utilized argon (or helium) from a separate tank capable of holding approximately 50 cubic feet of gas at 150 psi pressure. This tank itself was supplied argon (or helium) from a series of commercial bottled gas manifolded together. A regulator was necessary to reduce the commercial pressure from a maximum of approximately 2500 psi to the desired 150 psi.

The pressures in the two settling chambers were controlled by Fisher pressure regulators. These regulators were activated by remote control with a single switch, and if necessary, the sequence of operation could be staggered with the bleed valve on each regulator.

The Schlieren System

A schlieren system was available to observe the behavior of the flow field. A xenon lamp was used as the monochromatic light source which converged on a 16 inch diameter parabolic mirror through a condensing lens and a knife edge. The parallel beam of light reflected from the mirror passed through the test section and was reflected off of another mirror and focused on a knife edge. The image was projected on a ground glass plate and by the use of a Graflex camera polaroid pictures of this image were taken. Figures 8 and 9 show two typical results

obtained. The shock free nature of the flow in the case where both streams are at Mach 1.3 should be noted.

Probe Drive Mechanism

Due to the small dimensions of the test section, it was necessary to have the total pressure probe very close to the primary stream wall during the start of the run. After steady flow conditions were established in the test section, the probe had to be passed through the free stream quickly in order to conserve run time. It then had to be slowed down in the neighborhood of the mixing region and traverse the mixing region at a relatively slow rate to obtain an accurate pressure profile. This was accomplished by the use of a variable speed reversible electric motor to drive the probe.

Eight holes were drilled at various intervals on top of the test section frame and the nozzle block to accomodate the probe shaft. The probe shaft was attached to a threaded rod which in turn was rotated by the electric motor. This mechanism was mounted on top of the test section and controlled from the instrument table. Provisions were made to accomodate a linear potentiometer and a pressure transducer on the mechanism frame. Limit switches were installed to automatically stop the probe drive once it reached either the upper or lower wall. The probe holes not in use were closed with a threaded brass plug which was screwed in until the tip was flush with the nozzle block surface. Photographs of the probe drive mechanism and the mounting on the test section are shown in Figures 10 and 11.

Static Pressure Plate

It was undesirable to obtain static pressure measurements with probes in such a small test section since the presence of the probe would influence the results. This could have been accomplished by installing pressure taps on the side walls if it were not for the schlieren windows. An alternative was to machine an aluminum plate, the exact size of the windows, which would be interchangeable with one of the windows. The pressure taps could then be drilled in this plate. This method was chosen since it allowed the determination of static pressure with the least amount of external disturbance in the flow field.

A total of ninety holes were drilled on the flow field side with each hole having a diameter of 0.030 inches. These holes were distributed among 13 axial stations ranging from 0.25 inches downstream of the nozzle exit plane to approximately 15 inches downstream. On the outside of the plate, these holes were enlarged to a diameter of 0.080 inches so that short pieces of stainless steel tubing could be pressed in. These tubes were sealed at the bases with epoxy resin. Vinyl tubing was used to connect the stainless steel tubing in the taps to the monometer board. A photograph of the static pressure plate is shown in Figure 12.

Gas Analysis System

Since one of the main objectives of the experimental program was to obtain species concentration profiles, gas samples were withdrawn from the flow field and collected in a series of vacuum bottles. These samples were subsequently analyzed on a Victoreen Model 4000 Gas chromatograph. A photograph of the gas chromatograph together with the columns used is shown in Figure 13.

The fundamentals of gas chromatography can be found in reference [75]. The chromatograph measures the volumetric concentration of each constituent of the sample. The components are separated when passed through a column consisting of a length of stainless steel or copper tubing packed with a solid phase such as charcoal. Since each component progresses through the column at different rates, the travel time (or elution time) identifies each component qualitatively. Thermal conductivity detectors measure the quantity of each of the separated gases relative to the carrier gas and concentrations are printed out on a strip chart recorder.

Measuring Devices

Total Pressure Measurements

Total pressure profiles in the mixing region were obtained by introducing a probe into the stream. The pressure registered via the probe was transformed into an electrical output using a MB Electronics Model 151-BAA-1 pressure transducer. Power was supplied to the transducer by a CEC-3-140 DC power supply. The output was recorded on a CEC-5124A 20 channel recording oscillograph. This strip chart recorder made traces on light-sensitive tape which was 6 inches wide. Thus, the voltage output from the transducer had to be scaled down by means of an external attenuation circuit so that a full scale deflection registered 180 psia pressure. With this calibration, probe pressures could be read to within $\pm$ 0.75 psia.

The probes had to be small enough so that the least amount of disturbance would be introduced into the flow field and thus give

accurate pressure readings. Yet they had to be strong enough to withstand the bending moments due to high speed flow. For this purpose stainless steel tubing of 0.060 inches OD (0.036 inch ID) was used. A length of this tubing was bent at a 90 degree angle and welded into a short piece of 0.25 inch diameter stainless tubing which in turn screwed into the probe shaft on the drive mechanism. The length of the "sting" was determined by the location of the probe holes in the test section frame relative to the static pressure taps since total pressure profiles were needed at the point where static pressure data were taken. It was found that three different "sting" lengths of 0.2, 0.5 and 0.75 inches were needed. After the desired lengths were cut, a 0.005 inch thick shim stock was inserted into the end of the sting and compressed to form a slit 0.005 by 0.040 inches. This design yielded satisfactory results in terms of accuracy and strength. A photograph of the probes is shown in Figure 14.

The pressures of the two settling chambers were monitored both visually on pressure gauges and also on the recording tape by the use of two Giannini Model 46139 pressure transducers.

Total Temperature Measurements

Total temperatures were monitored only in the two settling chambers using chromel-alumel alloy themocouples, the output of which was recorded on the recording tape. The reference junction was held at 32°F by immersing it in an ice bath. A full scale deflection of six inches on the recording tape corresponded to temperature readings between 32-92 °F, which was the temperature range of interest.

Static Pressure Measurements

A thirty-tube illuminated mercury manometer was used to measure static pressures. A pressure differential of approximately 60 inches of mercury could be measured on this manometer. By using atmospheric pressure as reference and setting the zero at the mid-point, pressure measurements in the range of 0-30 psia were obtained.

Since there were ninety pressure taps available and only thirty manometer tubes, a manifolding system had to be devised. This was accomplished by connecting each manometer tube to a six inch length of brass pipe at one end and welding shut the other. Three brass stop-cock valves were mounted in each piece of pipe and a pressure tap connected to each valve. Thirty of these manifolds were mounted on the manometer board. Vinyl tubing was used to make the connections and each connection was sealed with enamel paint (Glyptal). No leakage problems were encountered. Thus, each manometer tube was capable of reading one of three pressure taps depending on which valve was turned on.

A Graflex camera using 4 by 5 Polaroid plate film was used to record the pressure measurements. From the photographs, the pressures could be read to within 0.1 inches of mercury allowing pressure measurements to within $\pm$ 0.05 psia.

Concentration Measurements

1) Probe design

In order to reduce the number of runs necessary for the accurate determination of concentration profiles, gas sample rakes made up of three probes each were designed. The tips of the probes were made from 0.040 inch OD by 0.009 inch wall stainless steel tubing. The tips were

then immediately expanded to 0.040 inch ID to prevent the flow inside the probe from choking. As was done in the case of the pressure probes, the tubing was bent at a 90 degree angle and mounted inside a 0.25 inch diameter by 1.0 inch long stainless steel tubing which in turn screwed into the probe shaft on the drive mechanism. The nominal distance between the probe tips was 0.1 inches.[1] Each of the three probes was connected to a 2.5 cubic inch volume evacuated sample bottles by means of vinyl tubing. A photograph of the gas sampling rakes and a sample collection bottle is shown in Figure 15.

2) Chromatograms

The column used in the gas chromatograph was a 6-foot length of Varian 5-A molecular sieve. The column was conditioned by drying it in the chromatograph oven set at 750 °F for 24 hours. During the conditioning time the carrier gas was allowed to flow through the column at a rate of 40 ml/minute. A Varian Model 02-001126-00 thermal conductivity cell using two pairs of 30 ohm tungsten-rhenium filaments was used to measure the amount of each constituent in the mixture. The output from the conductivity cell was recorded by a Honeywell Model Electronik-194 strip chart recorder.

In the Series I tests where argon-air mixtures were being analyzed, helium was used as the carrier gas; argon was used as the carrier gas to analyze helium-air mixtures. For both series of tests, the injection ports, the column and the thermal conductivity cell were maintained at 86 °F.

---

[1]The spacing between the sample probes was determined from the recommendations of reference [17]. With the above design no interference problems were encountered.

The Series II tests of helium-air mixtures presented no problems since the molecular sieve column separated oxygen, nitrogen and helium into distinct bands and the mass fractions could be calculated from peak areas. However, argon cannot be separated from oxygen when column temperatures are above approximately -95 °F [76, 77]. If an acetone-dry ice bath was used to attain this temperature then nitrogen would not be eluted and thus be irreversibly adsorbed in the column. Another alternative was to separate nitrogen from the oxygen-argon mixture at room temperature, then immerse the column in the dry ice-acetone bath and inject the sample again. For a single chromatogram of a mixture, the turn-around time using this technique was estimated to be over 30 minutes. It was necessary to have three or more chromatograms of the same mixture to obtain a statistical average of the mass fractions of the constituents. This, together with the large number of samples collected, made the above method impractical.

An indirect method of calibration was devised to avoid this problem. It was assumed that air behaved as a single species.[1] As a measure on the validity of this assumption, self-diffusion coefficients obtained by kinetic theory considerations [78] were examined. It was found that in the temperature and pressure range of interest, the self-diffusion

[1]Air is conventionally treated as a single component in evaluation of transport properties for low density systems (i.e., pressures on the order of one atmosphere) [62]. Example calculations of binary and ternary diffusion in air (i.e., considering it as a single specie and as a mixture) may be found in reference [62]. As is usually expected, the two methods are in good agreement.

coefficients were within 5 percent of each other. Thus, for diffusion purposes, the nitrogen and oxygen molecules were practically indistinguishable. Then, if the mass fraction of nitrogen in the mixture was known, the mass fraction of oxygen could be computed since for every 0.79 moles of nitrogen there are 0.21 moles of oxygen. Knowing the mass fractions of two of the three constituents, the third could be deduced.

Exact amounts of pure argon, oxygen and nitrogen were injected into the column. The values of the peak areas, calculated by the method of triangulation, were then plotted against the known weight injected. As expected the curves were linear and passed through the origin (no sample, no response).

When an exact amount of unknown sample was injected into the column at room temperature, two peaks would appear on the chromatogram; one of pure nitrogen and one of the argon-oxygen mixture. Using the calibration curves the weight of nitrogen could be determined from its peak area. Then a simple ratio would yield the weight of oxygen present in the mixture. The calibration curves would again be used, this time somewhat in reverse, to obtain the peak area corresponding to this weight. This area would then be subtracted from the "compound" argon-oxygen peak area to get the argon peak area and therefore its weight. Knowing the weights of each of the constituents of the mixture, the mass fractions could be calculated.

It was realized from the start that errors would be magnified when the concentration of argon in the mixture fell below approximately 10 percent, i.e., samples collected from cross-stream locations close to the primary stream. The accuracy of the overall data, discussed in

the next section, showed this error to be at an acceptable level.

To keep all other sources of error at a minimum, the following precautions were taken:

i. calibrations were frequently checked.

ii. injection port, column and detector cell temperatures together with the carrier gas flow rate were maintained at the same levels as used in calibration runs.

iii. fast recorder chart speed was used to make peak width measurements more accurate.

iv. signal attenuations were adjusted to obtain full scale peaks so that peak height measurements were accurate.

v. the mximum allowable filament current was used in the detector cell to increase the overall accuracy of the chromatograms.

vi. number of chromatograms per mixture were increased to get better statistical values.

Testing Procedure

Since all of the measurements, namely static and total pressure, concentration and schlieren photographs, could not be made during the course of one run, it was necessary to make different sets of runs. The data collection technique, repeated for each set of nozzle blocks, is summarized below:

1) The settling chamber total pressures necessary to match static pressures in the exit plane of the nozzles were calculated. Using air in both streams the regulators were adjusted to yield these pressures. The secondary stream air line was then shut off and the static

pressure plate was installed in the test section. With the secondary stream now utilizing argon (or helium), further adjustments were made in the chamber total pressures by observing the exit plane static pressures. The static pressure plate was removed and the schlieren window was installed, after which the flow field was observed for "cleanliness", i.e., the presence of unwanted expansion or compression waves. The repeatability of chamber pressures from run to run was within 3.5 percent for the primary and 1.5 percent for the secondary. Better repeatability (i.e., 1 percent) was obtained with the primary stream when Mach 1.3 nozzle block was used.

2) After a satisfactory flow field was established, a schlieren photograph was made. The static pressure plate was replaced and three runs made to determine the static pressure distribution. In between the runs the appropriate manifold valves were turned on.

3) The total pressure runs were made with the windows back in place so that the shock pattern due to the presence of the probe in the flow field could be viewed on the schlieren screen. The number of runs at each axial location depended on repeatability and the quality of the traces. As the pressure probe was traversing the flow field, the exact location of the probe tip had to be known. To accomplish this a linear potentiometer was connected to the travelling probe mechanism. Before each run, position calibration was done by getting a trace on the recorder tape while the probe tip was located at the lower wall. Thus, knowing a reference position and measuring the displacement of the potentiometer output trace obtained during a run, the position of the probe and the corresponding pressure at that point could be obtained.

At the begining of each run the probe was located next to the primary stream wall. The "blow-down" was started and allowed to reach a steady state after which the probe mechanism was activated. The probe was allowed to "sweep" the entire flow field, but as it approached the lower wall, the direction was reversed and the speed reduced so as to obtain a "fine-trace" through the mixing region.

4) A vacuum pump was connected to a manifold with three outlets; one outlet was connected to a 30 inch vertical mercury manometer, the second to the injection port of the gas chromatograph and the third to the sample bottle. Before each sample collection run, the sample bottles were evacuated, after which the system was purged with carrier gas so as to minimize the concentration of any possible residual sample from the previous run. Position calibration was done in the same manner as was done in total pressure measurements, by obtaining a trace with the outermost probe on the lower wall. The probe rake was then moved to the location where sample collection was desired by activating the drive mechanism. This location was determined from schlieren photographs; that is, most of the samples were collected from inside the mixing region with only a couple of measurements in the free streams. The "blow-down" was started and the flow of sample was established through the probes. After steady flow conditions prevailed, the probes were connected to the sample bottles and the bottle valves were opened. It was observed that spproximately 20 seconds of run time was required to obtain an "adequate[1]" quantity of sample. After each run the samples were normalized

[1] "adequate" quantity was determined by trial and error to be a sample at approximately 1/3 to 1/2 atmosphere pressure. This yielded a sample of high enough concentration after normalization to one atmosphere pressure for the required number of chromatograms (i.e., 3-6).

to one atmosphere pressure by the addition of carrier gas into the bottles. Then 1 ml. of each sample was injected into the gas chromatograph by means of a micro-volume gas sampling valve which is an integral part of the gas chromatograph. A slight vacuum had to be applied to the exhaust port of the sampling valve to "suck" in the sample which was at one atmosphere pressure.

Data Reduction

Two methods of reducing the data were considered. The first method was to assume uniform static pressure equal to an average test section pressure throughout the flow field. The second method was to use the average static pressure at each downstream station after making sure that the cross-stream variation was less than $\pm$ 5 percent. Either method could be used to reduce the data of Series I-B and II-B tests with practically the same results since the streamwise static pressure variation is very small (Figures 17 and 19). On the other hand, as may be seen in Figures 16 and 18, some static pressure variations were observed in the Series I-A and II-A tests. Both methods were used to reduce the data of Series I-A and II-A tests. It was observed that the two methods yielded reduced velocity data within 2-3 percent of each other, provided the streamwise static pressure variations were within 6-8 percent of the exit plane value. Hence, the results of the second method of data reduction are presented because retention of a true representation of conditions in the mixing region is desirable. It is noted, however, that an average test section static pressure was used in the mixing analysis of Chapter III.

Since the two streams had different specific heat ratios, concentration values were needed in conjunction with the pressure measurements. The total pressure data obtained were in the form of a smooth trace from the recorder, whereas concentration measurements were points spread throughout the mixing region. Total pressure and concentration measurements corresponding to a specific cross-stream location were obtained by plotting the total pressure and concentration profiles on the same graph, then drawing a smooth curve through the concentration values; thus, the species concentration and the total pressure corresponding to a specific cross-stream location were available.

The following equations were used to obtain the average specific heat ratios of the mixtures:

$$\overline{C}_p = \sum_i \alpha_i C_{pi} \tag{5.1}$$

where $\overline{C}_p$ = average C_p of the mixture (btu/lb-R)

α_i = mass fraction of species i (lb i/lb mixture)

C_{pi} = C_p of species i (Btu/lb-R)

$$\overline{W} = 1/\sum_i \frac{\alpha_i}{W_i} \tag{5.2}$$

where W = average molecular weight of mixture

W_i = molecular weight of species i

$$\overline{R} = \frac{\mathcal{R}}{\overline{W}} \tag{5.3}$$

where $\overline{R}$ = gas constant of mixture (Btu/lb-R)

$\mathcal{R}$ = universal gas constant (Btu/lb mole-R)

$$\overline{k} = \frac{\overline{C}_p}{\overline{C}_p - \overline{R}} \tag{5.4}$$

where $\bar{k}$ = average specific heat ratio of mixture.

Velocities were computed by first determining the Mach numbers through the Rayleigh pitot formula [79]:

$$\frac{P_{oy}}{P_x} = \left(\frac{k+1}{2} M^2\right)^{k/k-1} \Big/ \left(\frac{2k}{k+1} M^2 - \frac{k-1}{k+1}\right)^{1/k-1} \tag{5.5}$$

where P_{oy} = the measured probe pressure at (x,y)

P_x = the measured average static pressure at (x)

k = the average specific heat ratio a (x,y)

M = the local Mach number.

Since local values of static and total pressures in conjunction with mass fractions are used, the utilization of Equation (5.5) for mixtures is justified. In other words, no attempt is being made to relate any of the quantities along streamlines to the undisturbed portion of the flow.

Although the distribution of total temperature across the mixing zone is non-uniform even for streams of equal total temperatures, this non-uniformity is small if the Prandtl number is close to unity. For example, in air-air mixing, the variation of the total temperature is only about 0.1 percent for a Mach number of unity [1]. In his investigation of the supersonic mixing of hydrogen and air, Morgenthaler [80] observed that typical experimental profiles at Mach 2.0 indicated a 3 percent variation in total temperature.

On this basis the total temperature was assumed to be constant through the mixing region and the average of the total temperatures of the two streams was used for $\bar{T}_o$. The total temperatures of the two streams were never more than 10° apart with the average value being

approximately 535 R. Thus, static temperature profiles were determined through the relation

$$T = \bar{T}_o/(1 + \frac{k-1}{2} M^2) \tag{5.6}$$

For a mixture of n species, the local mass average velocity U is defined as [62]

$$U = \frac{\sum_{i=1}^{n} \rho_i U_i}{\sum_{i=1}^{n} \rho_i} = \sum_{i=1}^{n} \alpha_i U_i \tag{5.7}$$

It is noted that U is the velocity one would measure by means of a pitot tube (i.e., incompressible flow) and corresponds to the velocity as used for pure fluids. The local velocity of each species was calculated using the adiabatic flow equation

$$U_i = \sqrt{2C_{pi}(\bar{T}_o - T)} \tag{5.8}$$

Finally, densities were computed from the perfect gas law

$$\rho = \frac{P}{\bar{R}T} \tag{5.9}$$

The assumption of argon, helium, oxygen and nitrogen being perfect gases was valid since the pressures were much less than the critical pressure and the temperatures much greater than the critical temperature for all species during all test conditions.

It was desired to relate the reduced velocity and temperature data to a set of average initial conditions for each test configuration (i.e., an average primary stream velocity and temperature together with an average secondary stream velocity and temperature). This was

necessary because the theoretical analysis in Chapter III required initial profiles of velocity and temperature and with these profiles the mixing program "marched" downstream. Since the experimental system was not perfectly repeatable, each set of initial conditions varied somewhat from run to run. In addition to the above, in some of the experimental configurations as discussed earlier, there were slight variations in the static pressure which affected the velocity profiles. Eggers and Torrence [81], in their experimental investigation of compressible air jets encountered similar problems. They compensated for the above stated variations by suggesting a velocity modification of the type

$$\frac{V - U_s}{U_p - U_s} = \frac{V_p - U_{sx}}{U_{px} - U_{sx}} \tag{5.10}$$

where V = the new local velocity modified for pressure and free stream deviations

U_p = the average primary stream velocity at the nozzle exit plane

U_s = the average secondary stream velocity at the nozzle exit plane

V_p = the local velocity modified for static pressure changes

U_{px} = the primary stream velocity modified for static pressure changes

U_{sx} = the secondary stream velocity modified for static pressure changes

The above modification was adopted for the present analysis together with a temperature modification of the same type

$$\frac{T - T_s}{T_p - T_s} = \frac{T'_p - T_{sx}}{T_{px} - T_{sx}} \tag{5.11}$$

where T = the new local temperature (modified)

T_p = the average primary stream temperature at the nozzle exit plane

T_s = the average secondary stream temperature at the nozzle exit plane

T'_p = the local temperature

T_{px} = the local primary stream temperature

T_{sx} = the local secondary stream temperature.

It should be recognized that these modifications were adopted for the sake of consistency between the experimental data and the theoretically predicted profiles. Since both the experimental and theoretical results are presented in the form of excess velocity profiles (discussed in the next chapter) there are no consequences due to these modifications.

Accuracy of Results

Based on the chart and photograph resolutions of recorded data, repeatability of runs and calibration, the estimated accuracy of the measurements are:

Static pressures ..... $\pm$ 0.1 psia

Probe pressures ..... $\pm$ 0.75 psia

Total temperatures ..... $\pm$ 10°

Probe position ..... $\pm$ 0.025 inches.

The test section static pressures are on the order of 10 psia; the probe pressures range from 35-70 psia; the temperature range of

interest is on the order of 535 R and measurements are made in a region of approximately 2 inches. Thus, in terms of percentage errors:

Static pressures ..... ± 1%

Probe pressures ..... ± 2.5%

Total temperatures ..... ± 2%

Probe position ..... ± 1.5%

With the above values and the equations used to reduce the data, it is estimated that the velocity data are accurate to within 3 percent. This estimation does not include any uncertainty due to concentration measurements.

One means of assessing the overall accuracy of the data is to apply the principle of conservation of mass to the secondary stream. This would also indicate the degree of accuracy of the concentration measurements. The following equation was evaluated numerically for each axial station at which data were taken:

$$\dot{m}_c = \int_A \alpha_i \rho u dA \tag{5.12}$$

where ρu = local mass flow per unit area evaluated from experimental data

α_i = local mass fraction of the secondary stream constituent

A = area of the flow field over which α_i is nonzero.

If the data were correct, $\dot{m}_c$ would be equal to the secondary stream flow rate which can be approximated from settling chamber conditions (for uniform, one-dimensional, isentropic flow)

$$\frac{\dot{m}}{A_t} \frac{\sqrt{T_o}}{P_o} = \text{const.} \tag{5.13}$$

where the constant depends on whether argon or helium is being used. Differences between $\dot{m}$ and $\dot{m}_c$ are due to experimental error. A comparison between these two mass flow quantities is an essential criterion in assessing the accuracy of concentration measurements because of uncertainties in obtaining representative samples from flowing streams.

The application of this criterion to the data presented herein is reported in Table III. Large errors in concentration measurements taken from binary streams may occur; the probe design, sampling technique and the local turbulence level in the flow field have a significant effect upon the results [35,81]. The actual physical mechanism which causes unrepresentative sample collection is not known, but satisfactory results were obtained with the probe and sampling technique used in this investigation. As can be seen in Table III, the overall error is less than 10 percent for all cases, and 75 percent of the cases have an error of 6 percent or less. Similar sampling problems were found in references [35,81,82,83,84,85] where errors of up to $\pm$ 25 percent were encountered. Therefore, it is concluded that the accuracy of the data is well within acceptable limits. Furthermore, it is deemed that the error involved in the method of determining argon mass fractions in argon-air mixtures is negligible as compared to the uncertainties of the samples themselves.

CHAPTER VI

DISCUSSION OF THEORETICAL AND EXPERIMENTAL RESULTS

Schlieren Photographs

Schlieren photographs were made to observe the quality of the supersonic flow for each of the four test configurations. Figure 8 shows the flow field with primary stream of air at a Mach number of approximately 2.0 and the secondary stream of argon at a Mach number of about 1.3. Here, the wave patterns are distinct and although the mixing zone is not too clearly visible, the waves may be observed to bend as they pass through the mixing zone. The "left-running" wave emanating from the left middle of the photograph is the typical "lip shock" resulting from two supersonic streams coming into contact with each other. Static and total pressure measurements confirmed these waves as being weak and the local wave angles in the primary stream indicated a Mach number on the order of 1.97.

There is considerable difference between the flow fields depicted in Figures 8 and 9. In Figure 9 both streams are at a Mach number of 1.3 again with air in the primary and argon in the secondary streams. The possibility of the flow being subsonic due to the absence (or non-visibility) of the "lip wave" and other waves was discarded with total pressure measurements. When a total pressure probe was injected into the flow field, weak oblique shock waves were also observed around the probe tip. Due to the cleanness of the flow, the mixing zone is more distinct than in Figure 8.

Similar qualitative results were obtained when helium was utilized in the secondary stream. The small width of the test section

was a factor in the quality of the schlieren photographs since the quality of the image is a function of the width over which the initially parallel light beams are diffracted.

Static Pressure Variations

The mixing analysis of this study involved the use of the boundary layer form of the conservation equations, from which it was deduced that the transverse pressure gradient ($\partial P/\partial y$) was negligible. It was further assumed that the streamwise pressure gradient ($\partial P/\partial x$) could also be neglected. The validity of these assumptions are now analyzed in light of the experimental data obtained. The static pressure measurements are plotted in Figures 16 through 27 with the average static pressure at the exit plane of the nozzles used as a reference pressure and with the physical coordinates non-dimensionalized with respect to the exit height of the secondary stream, i.e., slot height.

For all four test conditions, the streamwise pressure distribution is plotted along three lateral locations; along the plane of the splitter plate ($y/a = 1.0$), and one-half slot height above and below the plane of the splitter plate ($y/a = 1.5$ and $y/a = 0.5$). It may be observed in Figures 16 through 19 that the static pressure increases monotonically after a certain axial location. This is a typical characteristic of confined (ducted) flows. The axial location at which this steady increase is observed usually corresponded to approximately the downstream location where the mixing zone interacted with the wall boundary layer. When both streams are at Mach 1.3, Series I-B and II-B tests (Figures 17 and 19), the static pressure variation is within

2-3 percent of the average exit plane value for about 12 slot heights. In Series I-A and II-A tests, where the primary stream of air is at Mach 2.0 and the secondary stream of argon or helium is at Mach 1.3 (Figures 16 and 18), higher variations of up to 10 percent for regions within 12 slot heights are observed. When the streamwise static pressure variations and the schlieren results are considered together, it is concluded that, for the configurations involving the Mach 2.0 nozzle block, the variation of the static pressure can be attributed to the weak waves present in the flow field.

A further check on the magnitude of the streamwise pressure gradient was also made by comparing it to one of the convective terms (i.e., ρu^2) in the momentum equation.[1] The results are presented below in terms of the parameter θ, where θ is defined as

$$\theta = \frac{\partial}{\partial x}\int_0^{y^*} \rho u^2 dy \Big/ \frac{\partial}{\partial x}\int_0^{y^*} P dy$$

x/a	θ
1.0	55
3.0	42
5.0	39
7.0	36
9.0	32

The above values are from the data of Series II-A tests. Similar results were obtained with the Series I-A test data.

Therefore, if only the region upstream of the point of

[1] These values were obtained by getting intermediate printed output from the computer program.

interaction of the mixing region and the confining walls is considered, the assumption of constant axial pressure distribution is well justified for one configuration and at least acceptable for the other.

The transverse pressure variations for the Series I and II test at various axial locations are presented in Figures 20 through 27. For Series I-B tests involving both streams at the same Mach number of 1.3, the variation is within $\pm$ 5 percent for all stations up to x/a = 12. The same is essentially true for Series I-A tests except that at about x/a = 12 (Figure 23) the variation increases up to about 8 percent. This again is attributed to the waves present in the flow field when the Mach 2.0 nozzle block is utilized. The same trend may be observed in the helium tests (Series II). With a Mach 1.3 primary stream, static pressure variations are on the order of $\pm$ 4 percent. With a Mach 2.0 primary stream, pressure variations of up to 9 percent at about x/a = 5.5 (Figure 26) may be seen.

Even though there is some variation of the static pressure in the lateral direction, this variation is due to the presence of weak waves in the supersonic flow field, and the assumption of negligible transverse pressure gradient seems to be justified.

Growth of the Mixing Region

The growth of the shear layers for each of the four test conditions is presented in Figure 28. There is always some uncertainty in locating the edges of the mixing zone. The range of uncertainty[1] for each case is shown on the curves in Figure 28.

[1]The range of uncertainty is the maximum lateral distance in which the velocities change from 5 percent of their free stream values to the free stream values.

The largest growth is observed in the Series II-B tests where helium with a velocity of about 3500 ft/sec is mixing with air flowing at 1300 ft/sec. The least growth rate is observed in the case of argon (U = 1150 ft/sec) mixing with air (U = 1350 ft/sec), i.e., Series I-B tests. Thus, with the two other configurations showing the same trend of increased mixing zone growth with an increase in the velocity difference, it is concluded that as the velocity difference between the two streams increases so does the growth rate of the mixing region. This is consistent with the well-established fact [1] that the growth rate is a maximum when one stream exhausts into a quiescent medium.

Although curve (a) in Figure 28 corresponds to the test condition with the largest mass flux difference, curve (d) does not correspond to the case of the smallest mass flux difference. Therefore, the same reasoning that holds for velocity differences does not hold for mass flux differences.

The curves have been started at approximately 2 slot heights downstream of the exit plane due to the lack and uncertainty of data at previous locations. It is also noted that if the curves are extrapolated to determine the intercept, none of the curves pass through the origin. This is attributed to two possible reasons; the first is the fact that the growth of the mixing zone might be non-linear in this region. The second and more probable reason might be that this initial thickness is due to the accumulation of boundary layers on both sides of the splitter plate. It is the opinion of the author that the above phenomenon is due to a combination of the two

possibilities rather than due to solely one. Of course, experimental error could also have a significant effect.

Correlation of Velocity Data

A step function velocity profile as the initial profile input to the mixing program could not be expected to satisfactorily predict the mixing in the near field since the profiles are expected to be non-similar and there is the possibility of a "wakelike" profile stemming from the boundary layer accumulation on the splitter plate. Thus, it was necessary to input measured profiles rather than assumed or calculated profiles; and this was accomplished by starting the mixing program with experimental profiles at $x/a = 0.57$. At this axial location, no "wakelike" profiles were observed in any of the test conditions. As described in the Appendix, the input consisted of velocity, static temperature and mass fraction profiles in equal intervals of Δy.

The constants in Equations (4.10), (4.13), (4.14) and (4.15) were varied until the theoretical and experimental mixing zone growth rates matched. However, difficulties were encountered in Prandtl's mixing length model as it predicted a highly non-linear growth rate for the mixing zone in the region of interest, i.e., $2 \leq x/a \leq 10$. No evident reason can be given for this behavior. It is speculated that the dynamic eddy viscosity (ε) is a very weak function of the transverse coordinate. References [35] and [57] tend to support this speculation. The Prandtl model is a strong function of the transverse coordinate since it involves the gradient of the longitudinal velocity. Hence, the behavior may be related somewhat to the above speculation. The mixing length model was thus eliminated from further analysis.

The remaining three momentum transport models (Schetz, Ferri and Alpinieri) were correlated, as stated earlier, in the "very" near field, $2 \leq x/a \leq 10$. The reason for using only a portion of the data was to see how well the models could predict available mixing data in the region $x/a \geq 10$.

Four different empirical constants were determined for each of the three models, i.e., one for each test condition. Since the eddy viscosity is semiempirical in nature, it is too much to expect a single correlation to be valid for all conditions encountered. These constants were then examined to see if any trend could be observed. In other words, it was desired to relate the coefficients to initial mixing conditions. The only flow property that depicted any trend in values of the empirical constants was found to be the ratio of the mass flux per unit area of the secondary stream to the primary stream. Figure 29 shows the values of the coefficients for the turbulent eddy viscosity models as a function of the mass flux ratios of the two streams. The "asymptotic" characteristic of coefficients for the Ferri and Schetz models as the mass flux ratio approaches unity may be related to the fact that the two models fail when the mass fluxes of the two streams are equal. No reason can be given for the same trend shown by the Alpinieri model. It is also recognized that more test data areneeded in the region of unity mass flux ratio (both less than and greater than) as well as large values of mass flux ratio to validate the proposed relation between the empirical coefficients and the mass flux ratios.

The velocity profiles predicted by each model as well as the experimental velocity profiles for each of the four test conditions

are presented in Figures 30 through 49. The profiles are presented in the form of the dimensionless excess velocity

$$\phi = \frac{U - U_s}{U_p - U_s} \tag{6.1}$$

and the dimensionless transverse coordinate y/a at five axial stations. Only sample experimental points are plotted showing the trend of the data to avoid a cluster of points in obscuring the plots.

With all three of the eddy viscosity models predicting nearly the same growth rate for the mixing zone, the Schetz model is observed to be superior in predicting the velocity profile compared to the Ferri and Alpinieri models as may be seen in Figures 32, 39, 43, 47 and 49. The Ferri model tends to under predict the velocity profiles in the region $x/a \geq 8$, i.e., past the region of correlation (Figures 34, 38, 44 and 49). The Alpinieri model falls in between the predictions of the Ferri and Schetz models. The better correlation obtained with the Schetz model may be explained by the fact that this model takes into account the velocity and density profiles in the shear layer. By integrating these profiles at each axial station an "average" value for the eddy viscosity is obtained. On the other hand, the Ferri and Alpinieri models predict a turbulent eddy viscosity by means of free stream properties and a representative width for the mixing zone.

Although the Alpinieri and Ferri models correlate the data presented somewhat satisfactorily, certain limitations are inherent in their formulations. For example, in both cases, the mixing zone width b is based on velocity difference; thus as the velocity

difference between two streams becomes very small, the mixing zone width becomes undefined. As discussed earlier, the Ferri model also fails when the mass flux difference between the two streams approaches zero. Although the Schetz model also fails when the mass flux gradients in the flow field disappear, the former problem is circumvented since this model is not based on a mixing zone width.

Thus, it is concluded that on the basis of formulation characteristics and the satisfactory correlation of the experimental data, the Schetz extension of the Clauser integral model for the turbulent momentum transport mechanism is superior to Prandtl's mixing length, Ferri's differential mass flux and Alpinieri's momentum flux models in terms of predicting the velocity profiles in the initial region of a confined half-jet. It should be added, however, that the Ferri and Alpinieri models may also be utilized in the initial region with fairly good results. Although the empirical constant in all three of the models requires adjusting for different flow configurations, it is anticipated that the application of a given eddy viscosity model to a sufficient quantity of data will produce a relationship in terms of the mass flux ratios of the two streams, which will enable calculation of the constant for initial mixing conditions.

Correlation of Mass Fraction Data

As may be recalled from the discussion of Section 4.5 involving the turbulent transport of mass, the approach taken in this study is to formulate and correlate a turbulent momentum transport mechanism and then to use a suitable value of the turbulent Schmidt number to determine the species mass fraction profiles. Thus, the

correlation technique requires the employment of the mixing zone growth to determine the empirical constant in the eddy viscosity model and then the employment of the mass fraction profiles to obtain the most appropriate value of the turbulent Schmidt number.

After the eddy viscosity models were correlated according to the procedure discussed in the previous section, turbulent Schmidt numbers of 0.5, 0.7 and 1.0 were used in the theoretical analysis. It was observed that a value of 0.5 for the Schmidt number overpredicted the mass fraction profiles and a value of 1.0 was seen to be too high, i.e., underprediction. Then small changes in the neighborhood of the value 0.7 were made. It was seen that the velocity profiles were insensitive to these small changes in the value of the turbulent Schmidt number. However, the mass fraction profiles were observed to be fairly sensitive to changes in the Schmidt number and a final value of 0.7 was chosen for the Schmidt number as yielding the best overall results. It is noted that similar observations were made in references [5] and [35]. Whether the turbulent Prandtl number or turbulent Lewis number is 0.7 or 1.0 cannot be determined from the data herein. However, to be consistent with the assumption of constant total temperature throughout the mixing region, a value of 1.0 was assumed for the turbulent Prandtl number. This determined the value of the turbulent Lewis number on the order of 1.4. It should be emphasized that the turbulent Schmidt number is sufficient to determine the uniqueness of the concentration profiles along with the empirical constant for the eddy viscosity model.

The helium and argon mass fraction profiles are presented in

Figures 50 through 69 for all of the configurations tested. It was assumed and later validated in Chapter V that air behaved as a single species. Thus, knowing the secondary stream (helium or argon) mass fraction profile, the air species profile may be obtained through the relation

$$\alpha_{air} = 1 - \alpha_{argon\ (or\ helium)} \tag{6.2}$$

Then the individual profiles of oxygen and nitrogen may be deduced by the method employed in Chapter V.

All theoretical mass fraction profiles were obtained with a value of 0.7 for the turbulent Schmidt number. The Alpinieri and Schetz models in conjunction with the prescribed value of the Schmidt number yielded equally good results in terms of predicting the mass fraction profiles in Series I-A, I-B and II-A tests (Figures 50 through 64). The Schetz model was observed to correlate the mass fraction data better than the Alpinieri model for the Series II-B tests; especially for axial locations greater than approximately 8 slot heights downstream. Here the Alpinieri model tended to overpredict the profiles (Figures 68 and 69). This is not too surprising since the same trend may be observed in the excess velocity profiles (Figures 48 and 49). The Ferri model was seen to underpredict the mass fraction profiles consistently. This is similar to the results obtained for the velocity profiles with the Ferri model. The underprediction of the species profiles could be overcome somewhat by decreasing the value of the Schmidt number. However, the same value of 0.7 was used for all models so that a consistent comparison could be made.

Remarks on the Similarity of Profiles

Although the main emphasis of this study is in the initial region of mixing where the profiles are expected to be non-similar, it was of interest to see if any of the tests yielded similar profiles and if so, to predict the onset of similarity. For this purpose, the excess velocity and mass fraction profiles were plotted in terms of the conventional similarity variable y/b. No similarity features were observed for the Series I-A, I-B and II-A tests. However, for the data of Series II-B tests, an approach to similarity was detected in the mass fraction profiles. The similarity plots for the Series II-B tests are presented in Figures 70 and 71. It may be seen that the velocity plot of Figure 70 shows no semblence of similarity; but in Figure 71 it may be seen that the mass fraction data for $x/a = 8.44$ and $x/a = 12.17$ lie almost on top of each other. From this it is concluded that when profiles approach similarity, the speciesmass fraction profiles exhibit similarity features earlier than the velocity profiles. For the flow conditions of Series II-B tests, it is estimated that the mass fraction profiles are similar at approximately 12-15 slot heights downstream.

CHAPTER VII

SUMMARY OF RESULTS AND CONCLUSIONS

An investigation of the turbulent mixing in the initial region of a half-jet composed of dissimilar gas streams has been made. An iso-energetic, non-reacting and isobaric binary system with various velocity and mass flux ratios was studied both experimentally and theoretically.

The flow problem was formulated as an initial value problem using the turbulent boundary layer equations in conjunction with phenomenological models for the turbulent eddy viscosity. The eddy diffusivity was obtained form the eddy viscosity model by considering the turbulent Schmidt number as a parameter. The analytical solution was obtained using an all-explicit forward marching finite difference scheme with the stability of this scheme being ensured by satisfying the von Neumann stability criterion.

In the experimental phase of the study, a two-dimensional test section was designed and built to be used in conjunction with the existing blow-down wind tunnel facilities. Quantitative data in the form of total and static pressure measurements, total temperature and mass fraction measurements were collected. These data were used to correlate and complement the analytical study.

The results of this study may be summarized as follows:

1) Constant pressure mixing in the initial region of a half-jet may be obtained in confined supersonic flows with careful construction of contoured nozzle blocks. The experimental study may be

extended to fully developed mixing zones by using larger transverse dimensions and longer test sections than used in this investigation. The experimental results also apply to the initial regions of two-dimensional symmetric jets for which data are found to be quite scarce in literature.

2) Large errors in concentration measurements taken from binary systems may occur; the probe design, sampling technique and local turbulence level in the flow field have a significant effect upon the results. Satisfactory results were obtained with the probe design and sampling technique used in this investigation.

3) Several phenomenological models for the turbulent momentum transport were investigated on a consistent basis. It is concluded that Schetz modification to the Clauser integral model correlates the velocity data in the near field very well, provided the empirical constant is properly adjusted for each flow configuration. There is no universal constant that will correlate all possible flow conditions simply due to the fact that eddy viscosity is semiempirical in nature.

4) In the analysis of different models for eddy viscosity, it was speculated that the dynamic turbulent viscosity $(\mu)_t$ is a very weak function of the lateral coordinate. This may be a reason why the mixing length model does not correlate the data presented. This conclusion supports previous work done in fully developed mixing zones.

5) In correlating the mass fraction profiles, it was observed that a constant value of 0.7 for the turbulent Schmidt number gave good results for all flow conditions tested. Therefore, in analyzing turbulent mixing problems involving streams of different composition, it is

sufficient to model a turbulent eddy viscosity and then retain the turbulent Schmidt number as a parameter to obtain the eddy diffusivities.

6) The value of the turbulent Schmidt number being less than 1.0 suggests that mass appears to diffuse more readily than momentum. This is consistent with previous work reported in the literature.

7) When using turbulent momentum transport mechanisms based on the mixing zone thickness to analyze the initial region of a half-jet, it is proposed that the physical width of the mixing zone be utilized rather than a symbolic half-radius which is applicable to symmetric jets. Satisfactory correlation results were obtained with the Alpinieri model with the proposed definition of the mixing zone thickness.

8) The empirical constant in a given eddy viscosity model may be related to initial mixing conditions such as the mass flux ratios of the two streams. If a relation between the empirical constant and the mass flux ratio can be validated by large quantities of data, then the constant can be calculated for a given set of free stream conditions.

9) Boundary layer form of the conservation equations is observed to be valid for constant pressure confined supersonic mixing. The consistency of the boundary layer equations was also checked numerically. It was observed that axial derivatives of the longitudinal velocity were 2-3 orders of magnitude smaller than the corresponding transverse derivatives.

Large quantities of data are needed in the study of turbulent mixing problems, especially in the initial region. As stated earlier, other flow conditions than the ones investigated in this study are

necessary to obtain a firm relationship between the empirical constants and the initial flow variables. This study has dealt with iso-energetic streams; studies involving streams of different thermal levels are needed so that solutions and transport models may be applicable to a broader range of flow conditions. The correlations obtained in this study are for the initial region. It would be interesting to see if these correlations are also valid for "far field" calculations, i.e., fully developed mixing zones. Finally, validity of turbulent transport models in the presence of strong pressure gradients should be investigated in the initial region.

TABLES

Table I. Most Prominent Models Proposed for Eddy Viscosity.

AUTHOR	YEAR	PLANAR	AXI-SYMMETRIC	EXPRESSION
Prandtl	1926	X	X	$\varepsilon = \ell^2 \frac{\partial u}{\partial y}$
Von Karman	1930	X	X	$\varepsilon = K^2 \frac{(\partial u/\partial y)^4}{(\partial^2 u/\partial y^2)^2}$
Taylor	1932	X	X	$\varepsilon = \ell_w^2 \left(\frac{\partial u}{\partial y} \right)$
Prandtl	1942	X	X	$\varepsilon = \ell^2 \sqrt{\left(\frac{\partial u}{\partial y} \right)^2 + \ell_1 \left(\frac{\partial^2 u}{\partial y^2} \right)^2}$
Prandtl	1942	X	X	$\varepsilon = Kb(U_{max} - U_{min})$
Ting-Libby	1960		X	$\rho^2 \varepsilon = \frac{2\rho_c \varepsilon_o}{r^2} \int_0^r \frac{\rho}{\rho_c} r'dr'$

Table I (Continued)

AUTHOR	YEAR	PLANAR	AXI-SYMMETRIC	EXPRESSION
Ting-Libby	1960	X		$\rho^2\varepsilon = \rho_c^2\varepsilon_o$
Ferri	1962	X	X	$\rho\varepsilon = K\, r_{1/2}[(\rho u)_{max} - (\rho u)_{min}]$
Bloom-Steiger	1963		X	$\rho\varepsilon = K\delta r_{1/2}(U_{max} - U_{min})$
Alpinieri	1964		X	$\frac{(\rho\varepsilon)_c}{\rho_j u_j} = K\, r_{1/2}\left[\frac{\rho_e u_c}{\rho_j u_j} + \frac{\rho_e u_e^2}{\rho_j u_j^2}\right]$
Zakkay	1964		X	$\varepsilon = K\, r_{1/2}\, U_c$
Donaldson-Gray	1966		X	$\varepsilon = \varepsilon_o(K_1 + K_2 \exp(-K_3 M^2))$
Schetz	1968	X	X	$\rho\varepsilon = K\rho_e U_e \int_o^\infty \left\lvert 1 - \frac{\rho u}{\rho_e u_e} \right\rvert dy$

Table II. Test Conditions and Configurations.

	SERIES I-A (Argon-Air)	SERIES I-B (Argon-Air)	SERIES II-A (Helium-Air	SERIES II-B (Helium-Air)
M_p	2.0	1.3	2.0	1.3
M_s	1.3	1.3	1.3	1.3
a (in) (slot ht.)	0.54	0.54	0.54	0.54
P_{op} (psia)	98±3	41±1	92±3	41±1
P_{os} (psia)	37±0.5	46±0.5	35±0.5	46±0.5
T_o (°R)	535±5	535±5	535±5	535±5
U_p (ft/sec)	1710	1300	1710	1300
U_s (ft/sec)	1100	1100	3500	3500
$\lambda = \frac{U_s}{U_p}$	0.644	0.846	2.040	2.69
$\beta = \frac{(\rho U)_s}{(\rho U)_p}$	0.761	1.385	0.243	0.331

Table III. Comparison of Calculated and Measured Mass Flow Rates.

x/a	Series I-A $\dot{m}_c/\dot{m}$	Series I-B $\dot{m}_c/\dot{m}$	Series II-A $\dot{m}_c/\dot{m}$	Series II-B $\dot{m}_c/\dot{m}$
0.57	0.925	0.938	0.980	0.962
2.54	0.905	0.936	0.991	0.931
4.06	1.045	0.938	1.050	0.974
5.56	0.944	0.946	1.020	0.990
8.44	-----	-----	0.974	1.020
12.17	0.918	1.042	1.320*	1.070
17.70	0.895	0.950	-----	-----
23.26	-----	0.951	-----	-----

*Interaction with the wall and strong shock patterns were observed on schlieren photographs.

FIGURES

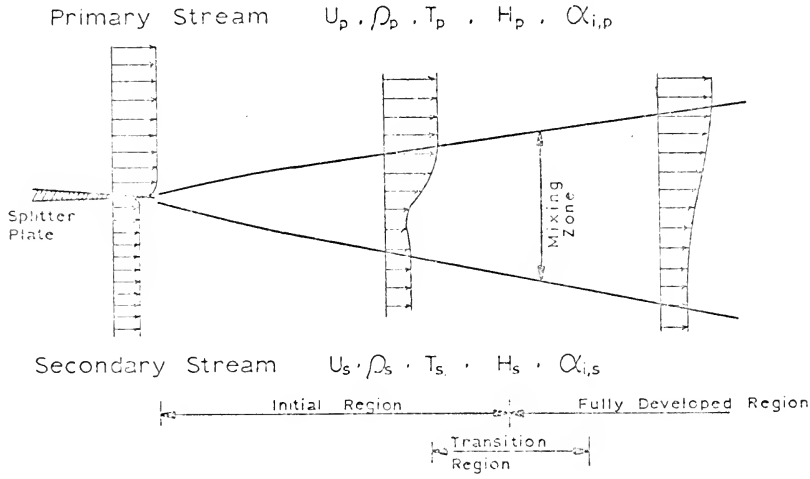

Figure 1 . Schematic of the Mixing Region Resulting from the Contact of Two Parallel Semi-Infinite Streams.

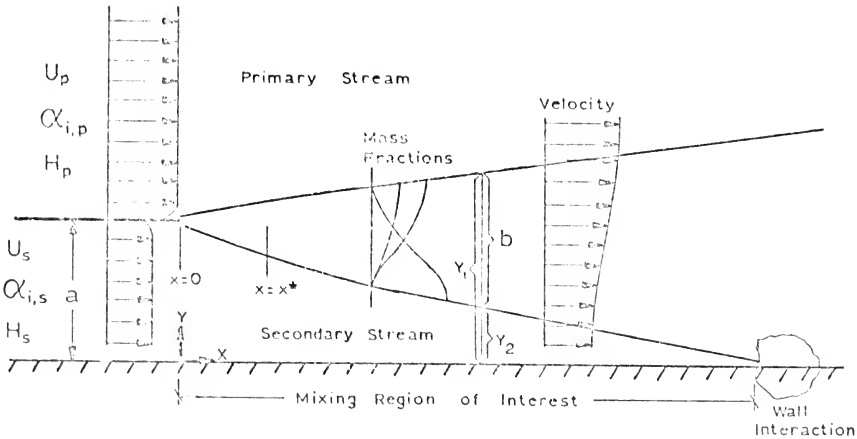

Figure 2 . A Typical Geometry of the Problem Under Consideration.

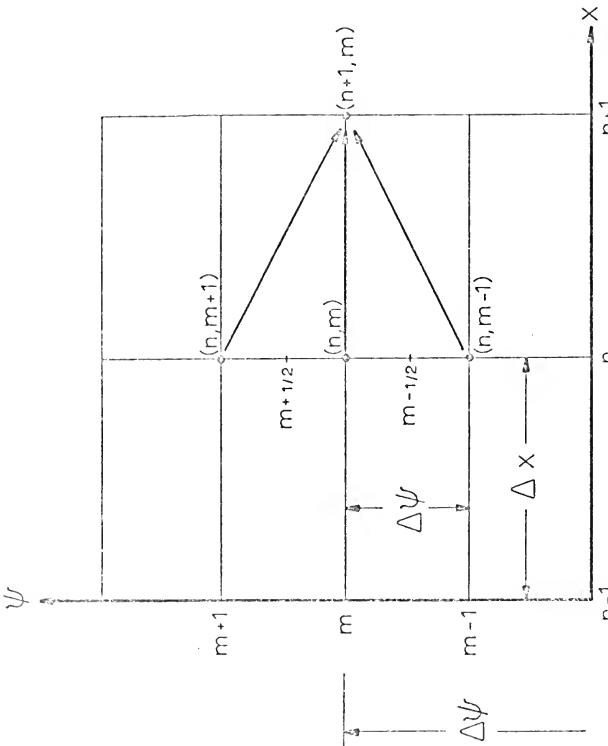

Figure 3 . The Grid Network Utilized in the Finite Difference Scheme.

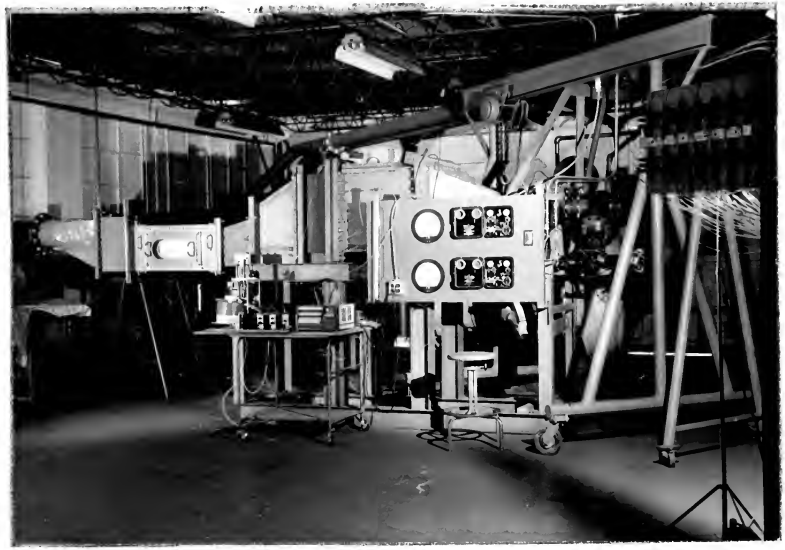

Figure 4 . Test Section Installed in Blowdown Wind Tunnel Facility

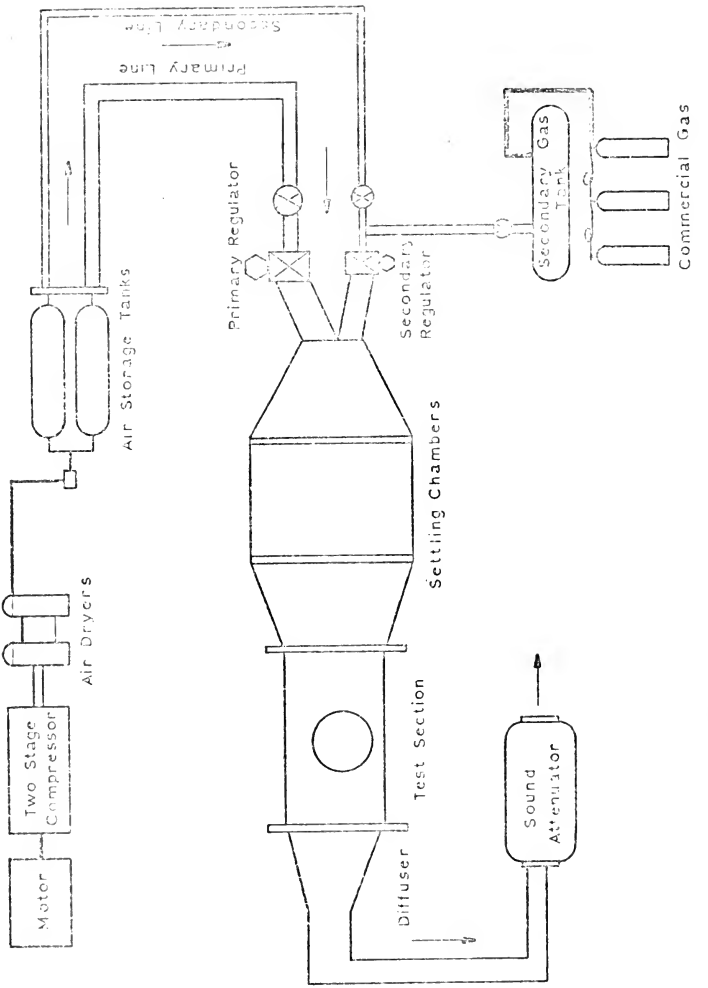

Figure 5 . Schematic Diagram of the Gas Dynamics Facilities Used in the Experimental Phase of the Investigation.

Figure 6 . Close-Up of Test Section with Two Mach 2.0 Nozzle Blocks.

Figure 7 . Close-Up of the Air Mach 2.0 Nozzle Block.

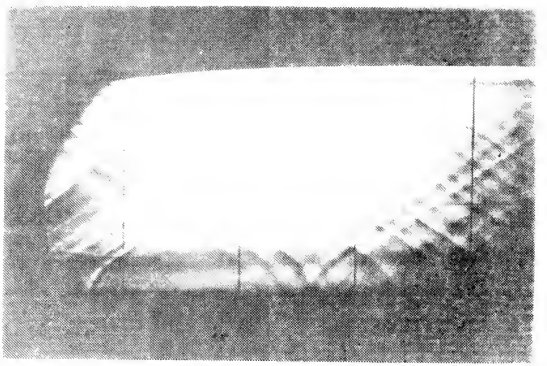

Figure 8 . Schlieren Photograph of Mixing Flow with Mach 2.0 Air and Mach 1.3 Argon.

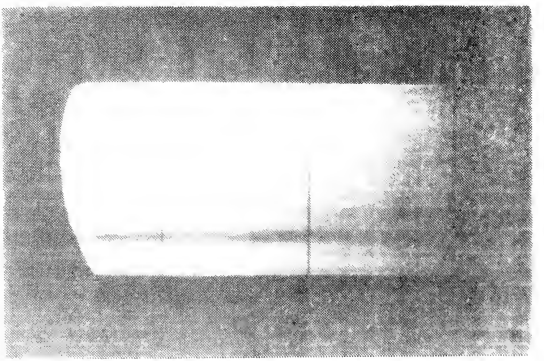

Figure 9 . Schlieren Photograph of Mixing Flow with Mach 1.3 Air and Mach 1.3 Argon.

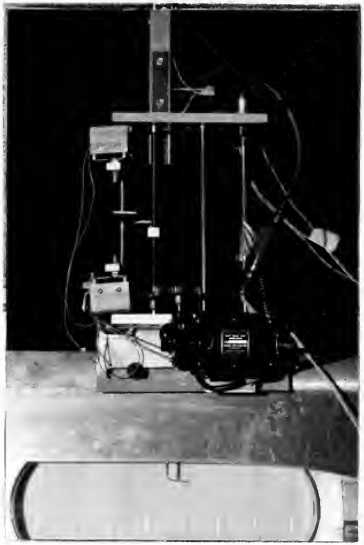

Figure 10 . Probe Drive Mechanism Mounted on the Test Section

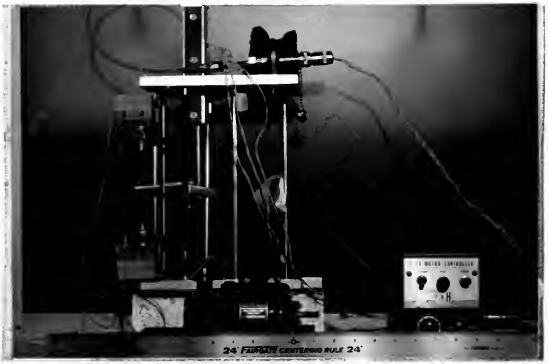

Figure 11 . Close-Up of the Probe Drive Mechanism with the Control System

Figure 12 . Close-Up of Static Pressure Plate

Figure 13 . Gas Chromatograph with a Molecular Sieve 5-A Column in Front

Figure 14 . Total Pressure Probes.

Figure 15 . A Sample Bottle with Species Sampling Rakes.

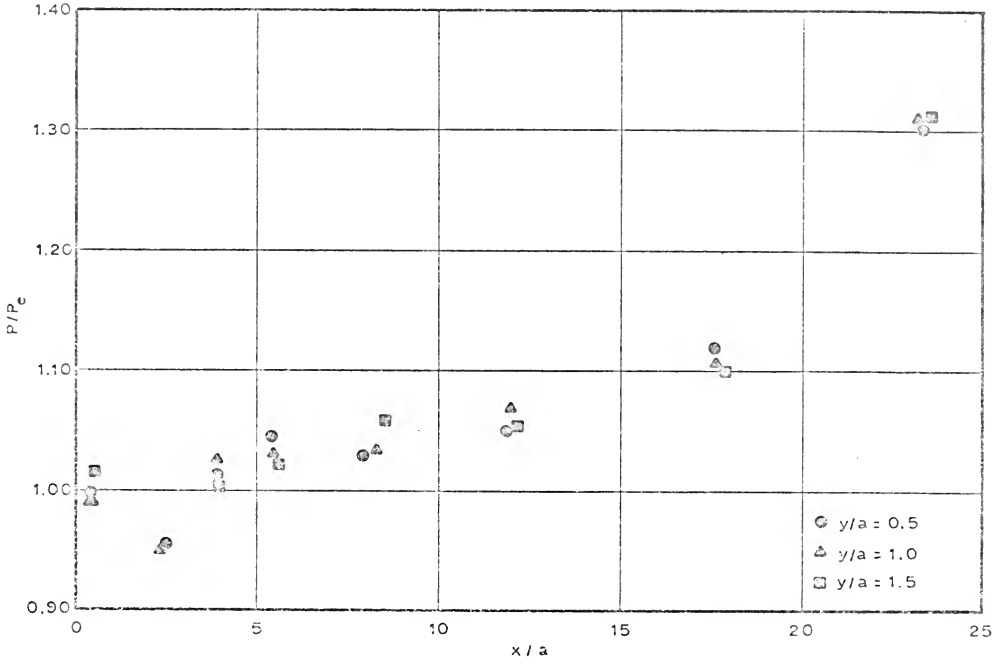

Figure 16 . Streamwise Static Pressure Variation for Series I-A Tests.

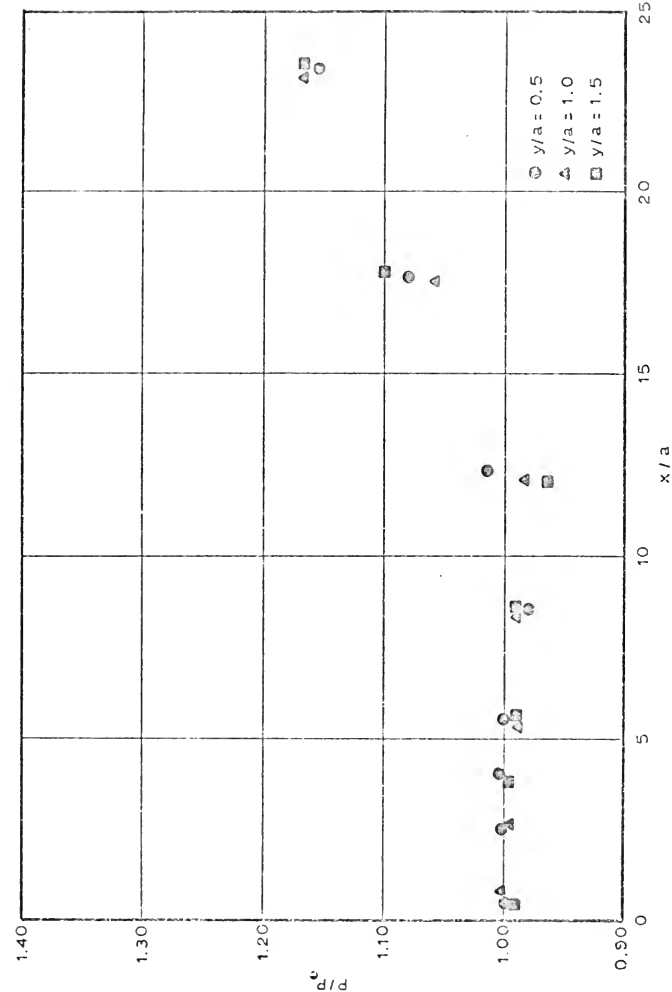

Figure 17 . Streamwise Static Pressure Variation for Series I-B Tests.

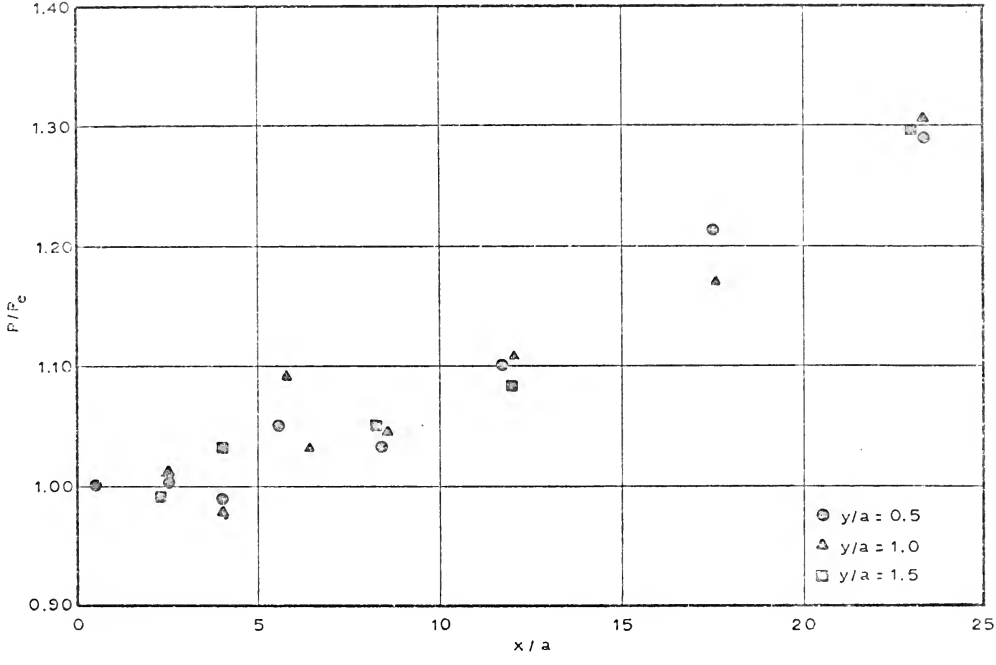

Figure 18 . Streamwise Static Pressure Variation for Series II-A Tests.

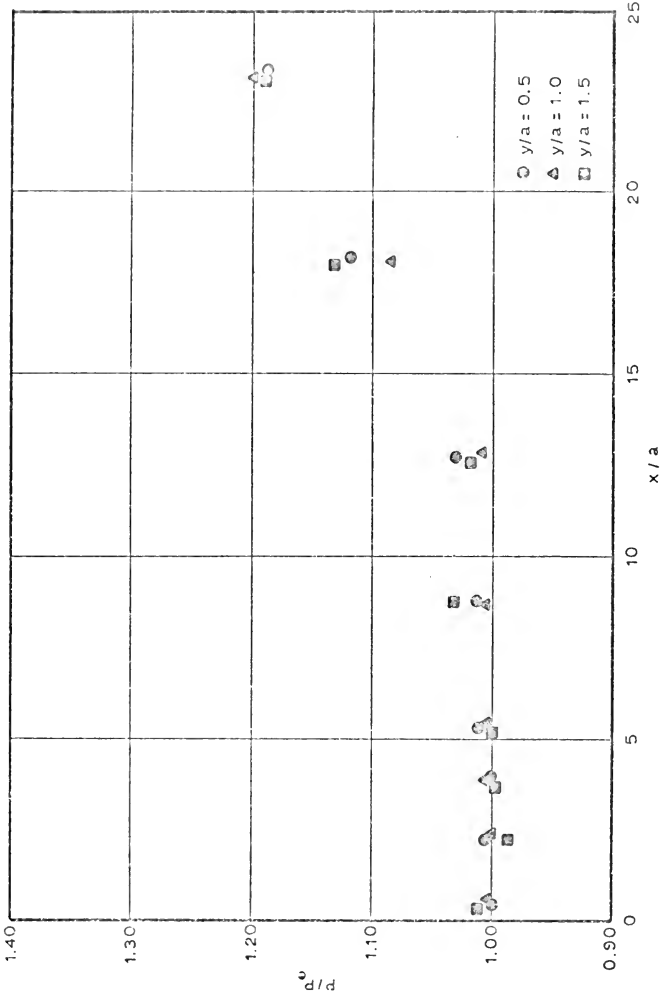

Figure 19 . Streamwise Static Pressure Variation for Series II-B Tests.

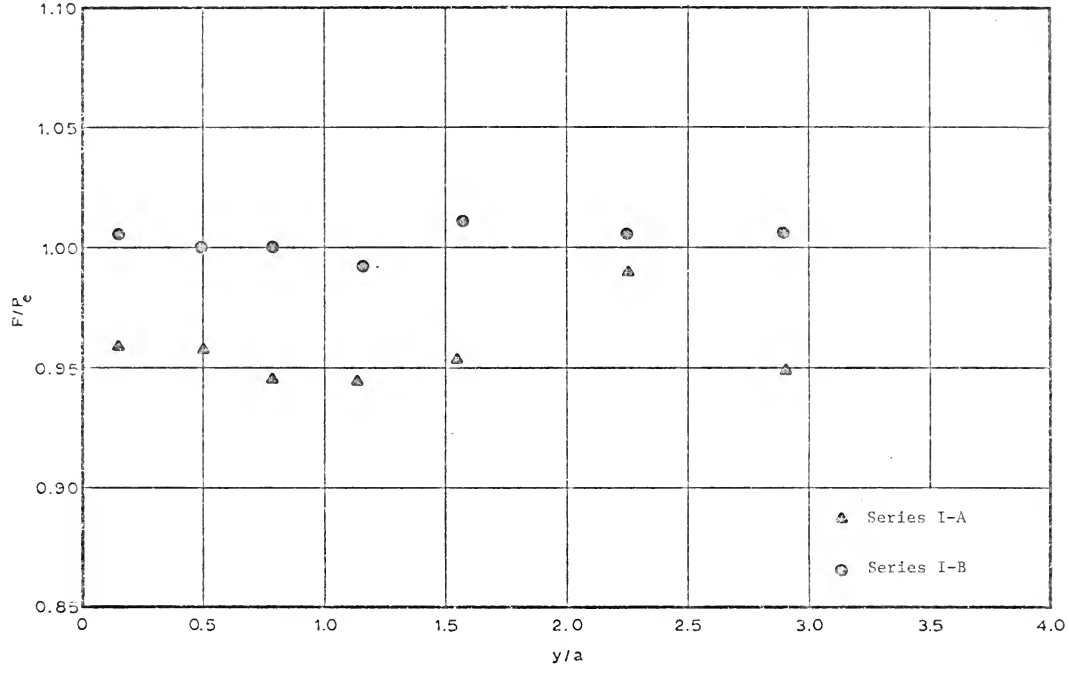

Figure 20 . Transverse Static Pressure Variation for Series I Tests.
x/a = 2.54 .

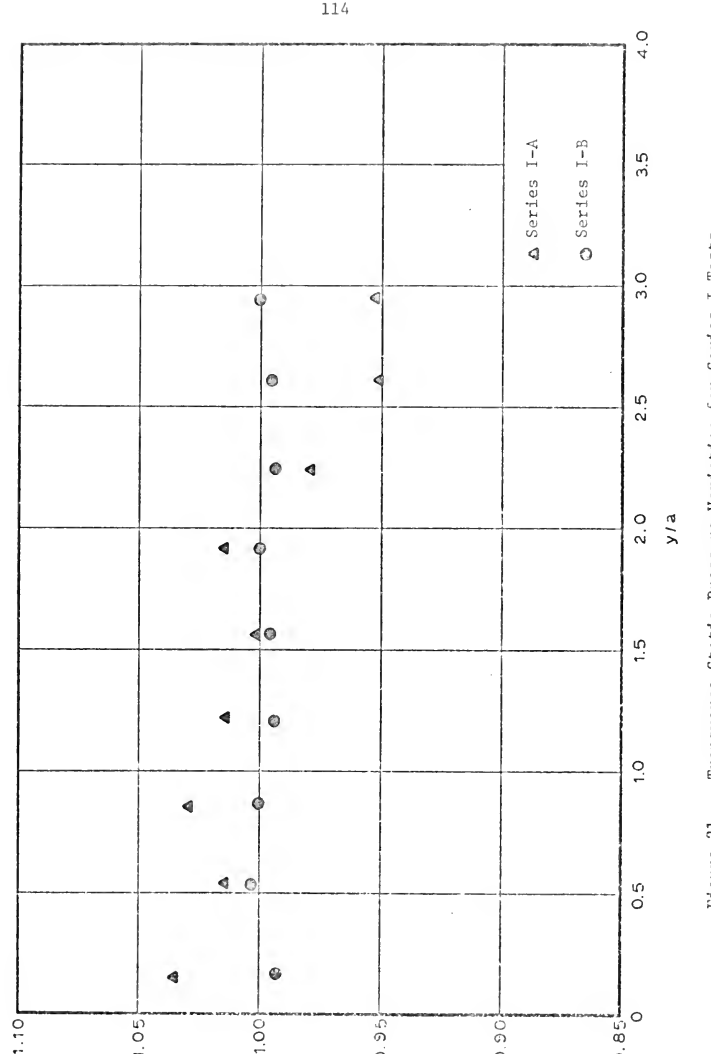

Figure 21 . Transverse Static Pressure Variation for Series I Tests .
x/a = 4.06 .

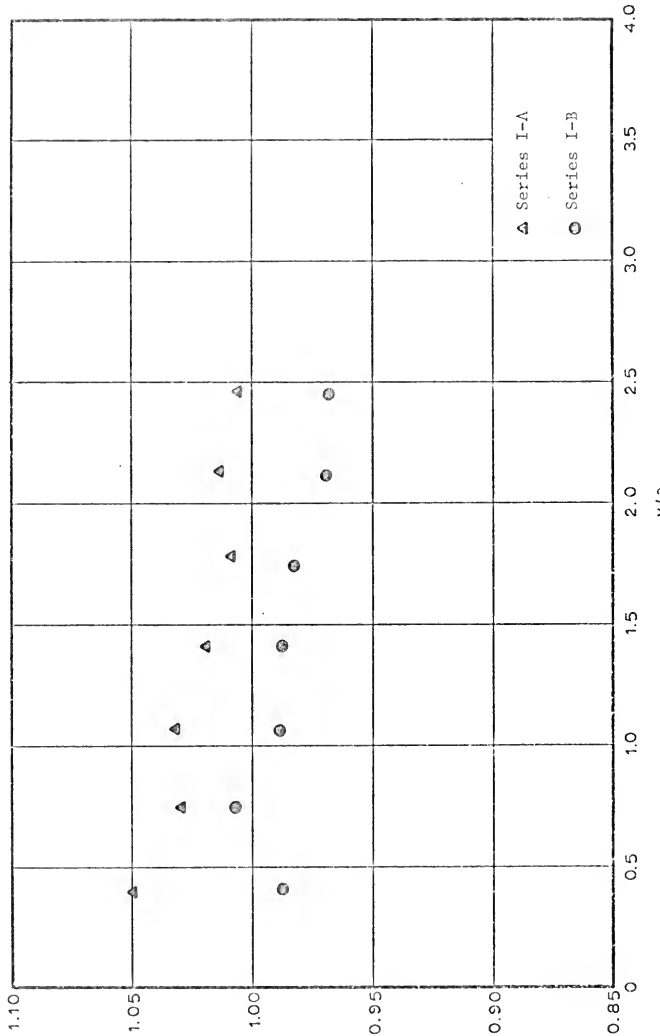

Figure 22 . Transverse Static Pressure Variation for Series I Tests.
x/a = 5.56 .

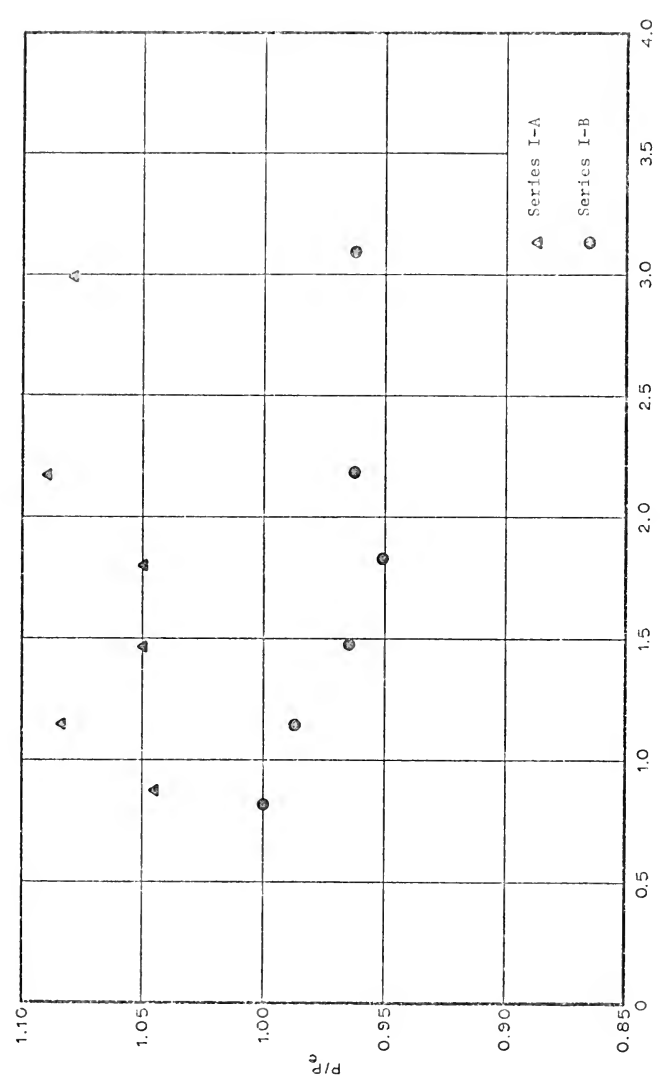

Figure 23 . Transverse Static Pressure Variation for Series I Tests.
x/a = 12.17 .

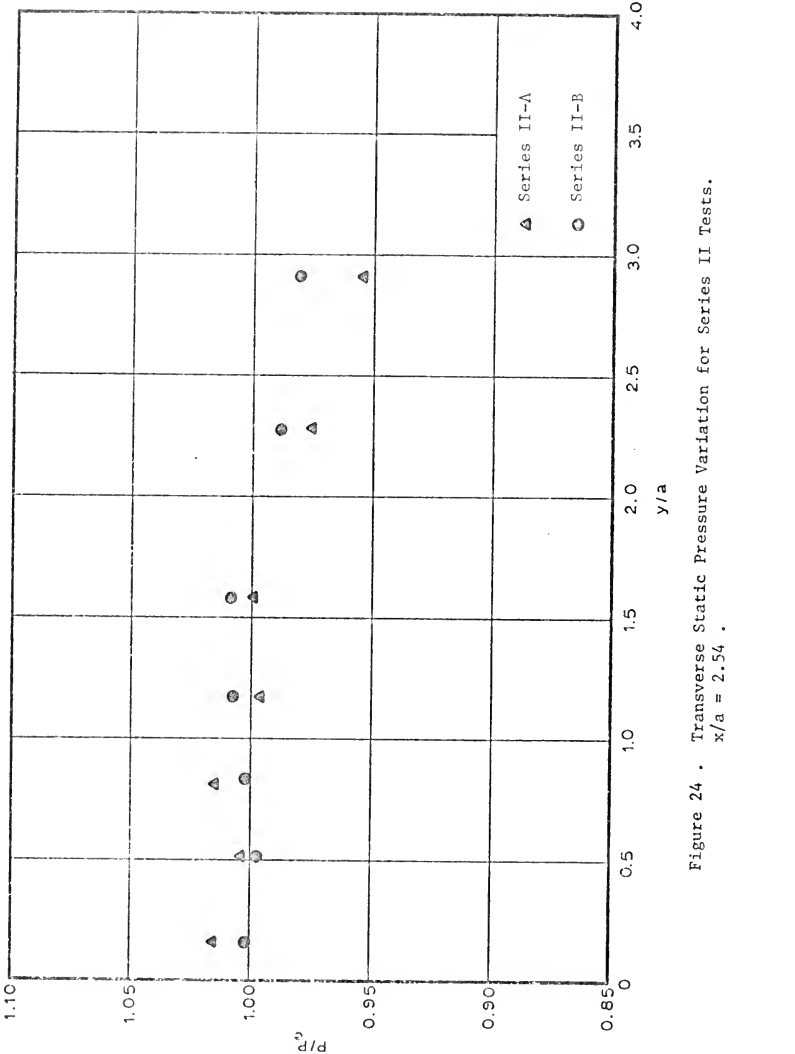

Figure 24 . Transverse Static Pressure Variation for Series II Tests.
x/a = 2.54 .

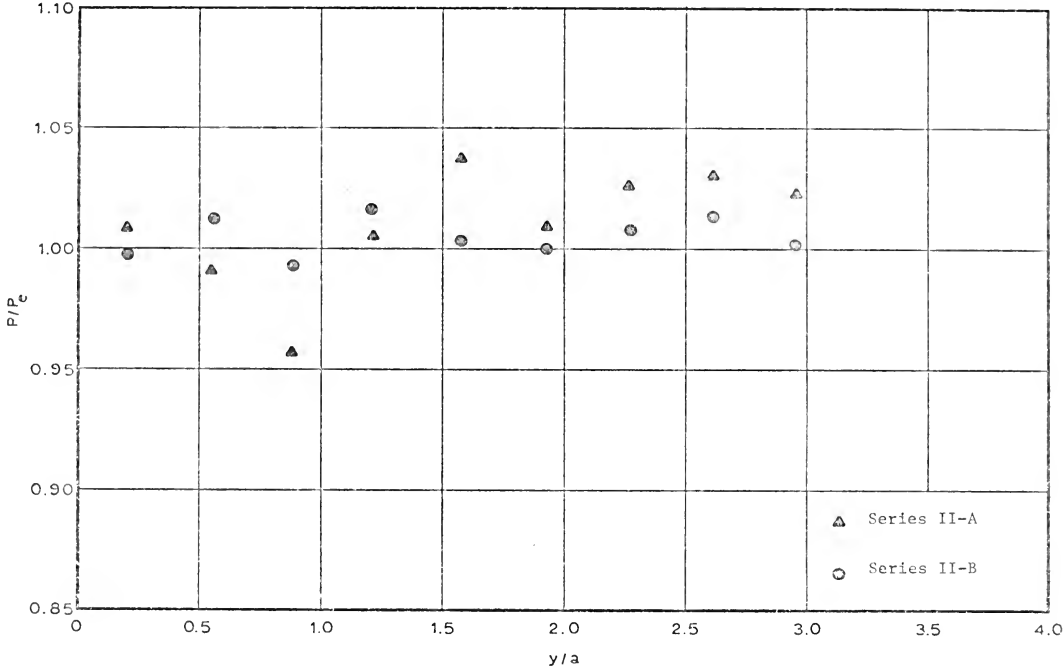

Figure 25 . Transverse Static Pressure Variation for Series II Tests.
x/a = 4.06 .

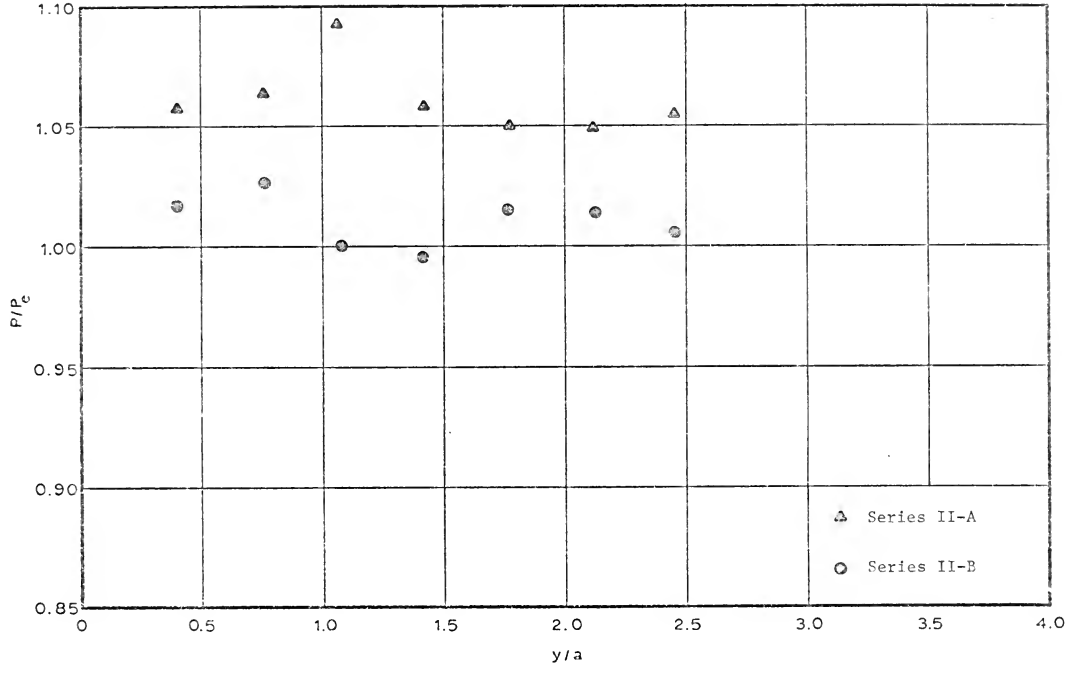

Figure 26 . Transverse Static Pressure Variation for Series II Tests.
x/a = 5.50 .

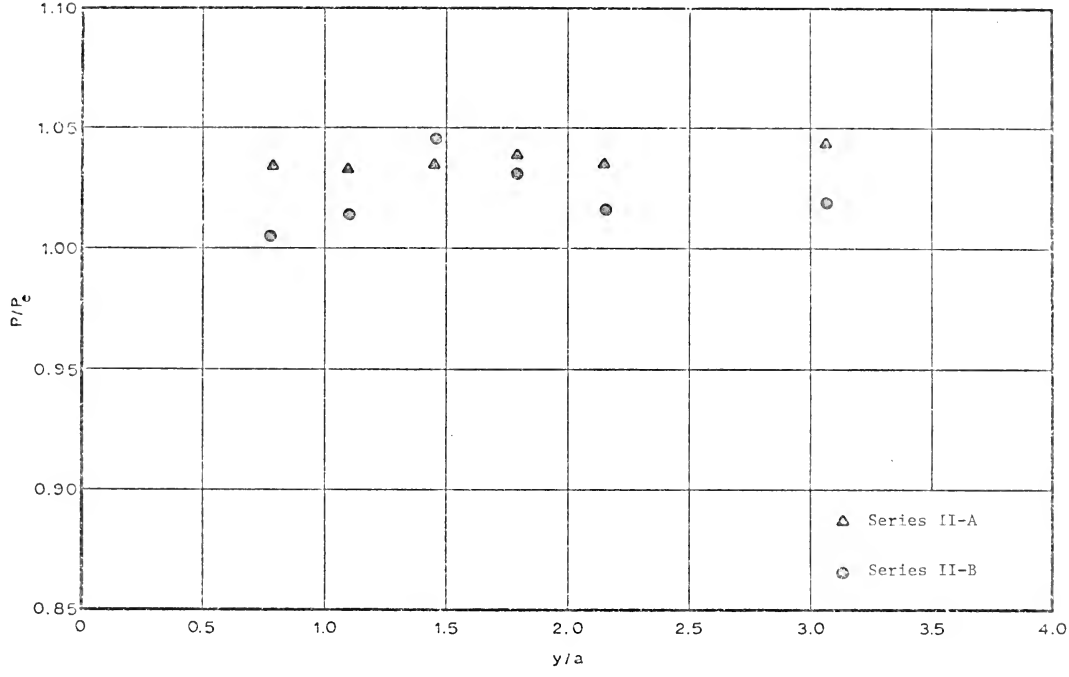

Figure 27 . Transverse Static Pressure Variation for Series II Tests.
x/a = 8.44 .

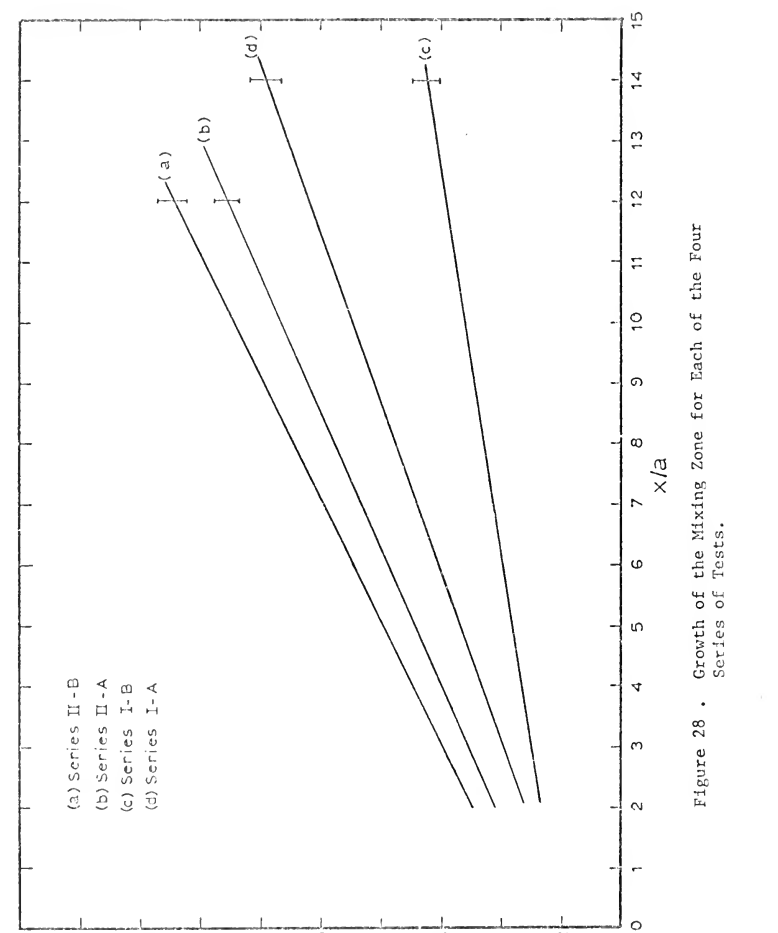

Figure 28 . Growth of the Mixing Zone for Each of the Four Series of Tests.

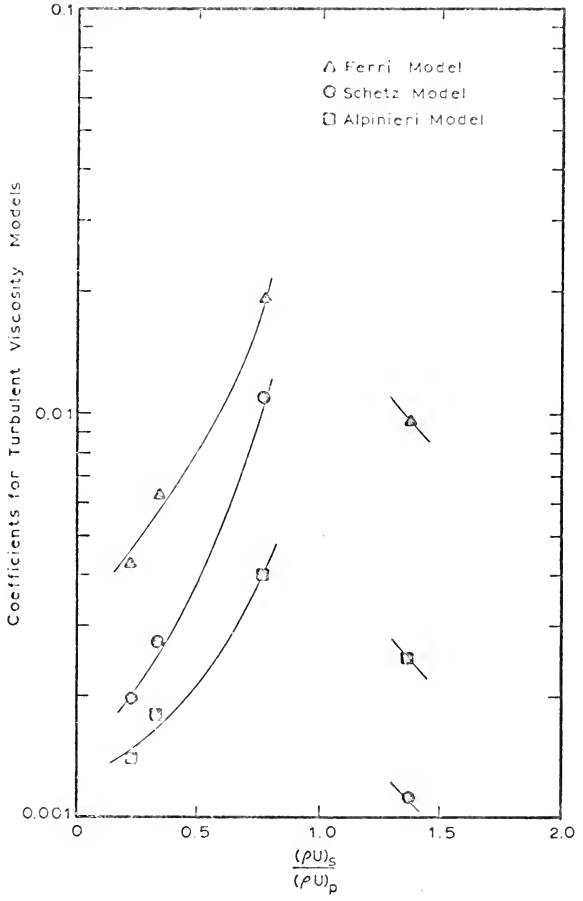

Figure 29 . Empirical Coefficients for the Turbulent Viscosity Models as a Function of the Mass Flux Ratios of the Two Streams.

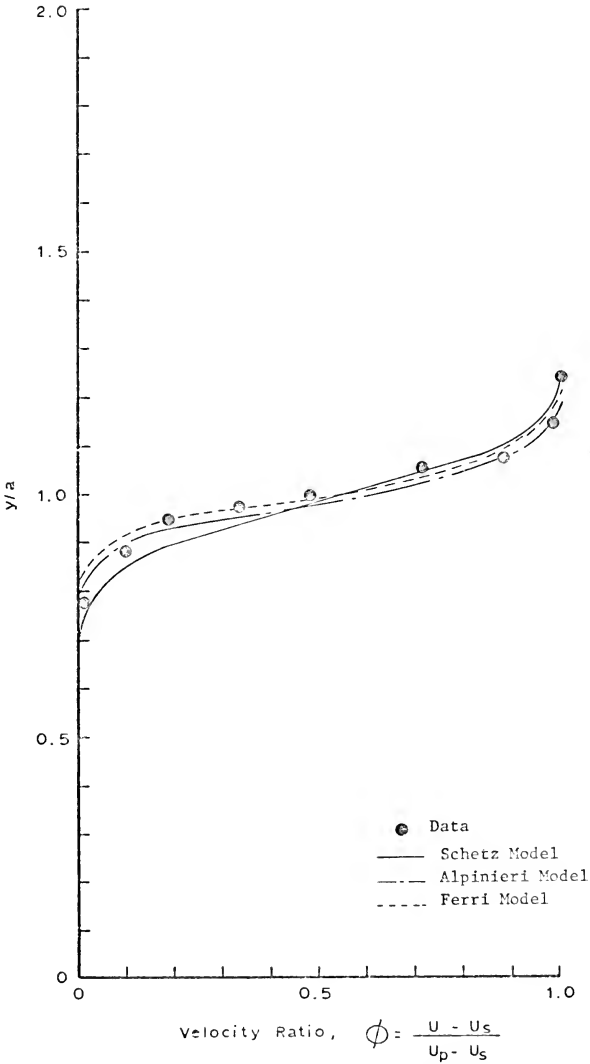

Figure 30 . Dimensionless Excess Velocity Profile at x/a=2.54 for Series I-A (Argon-Air) Tests.

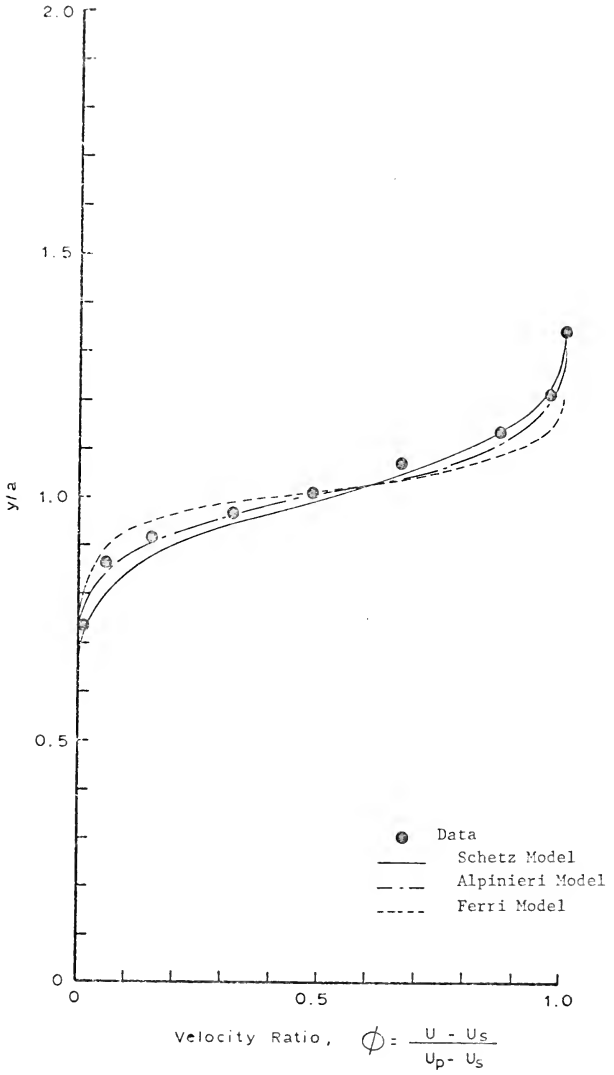

Figure 31 . Dimensionless Excess Velocity Profile at x/a=4.06 for Series I-A (Argon-Air) Tests.

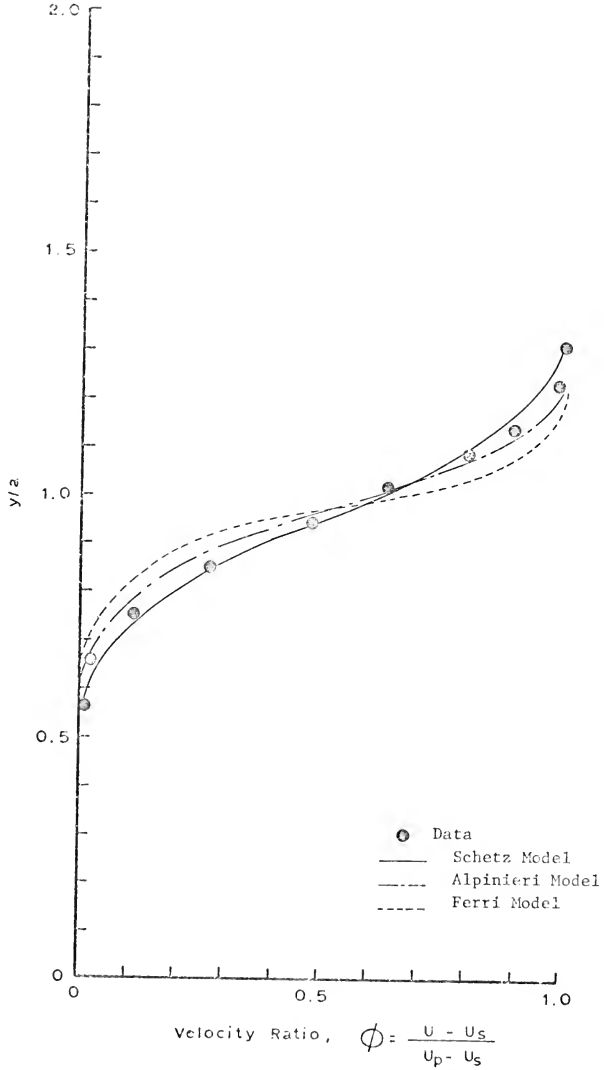

Figure 32 . Dimensionless Excess Velocity Profile at x/a=5.56 for Series I-A (Argon-Air) Tests.

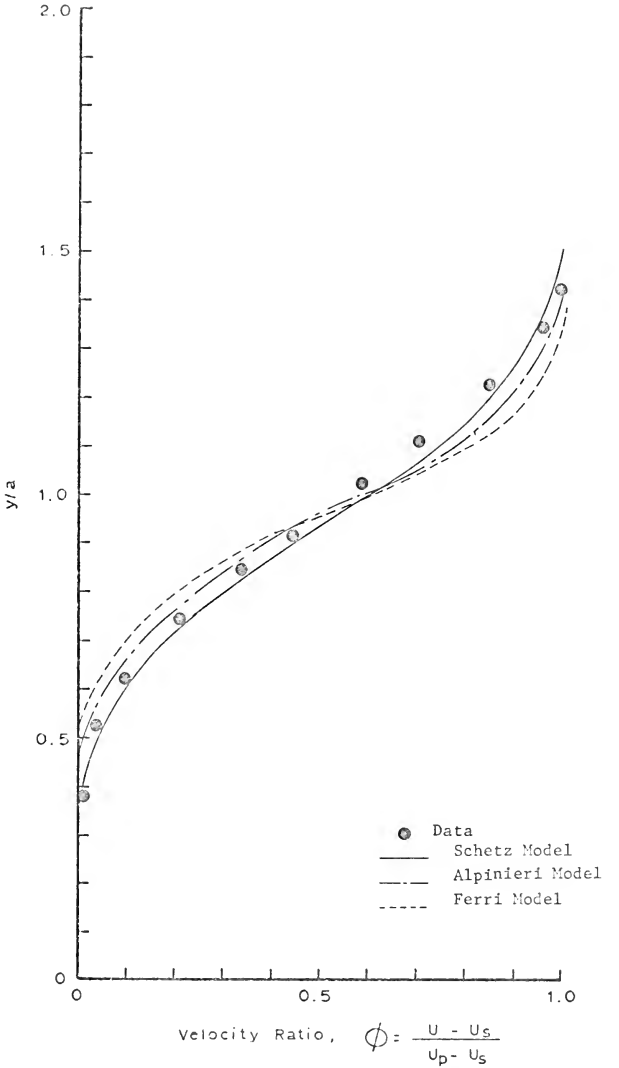

Figure 33 . Dimensionless Excess Velocity Profile at x/a=12.17 for Series I-A (Argon-Air) Tests.

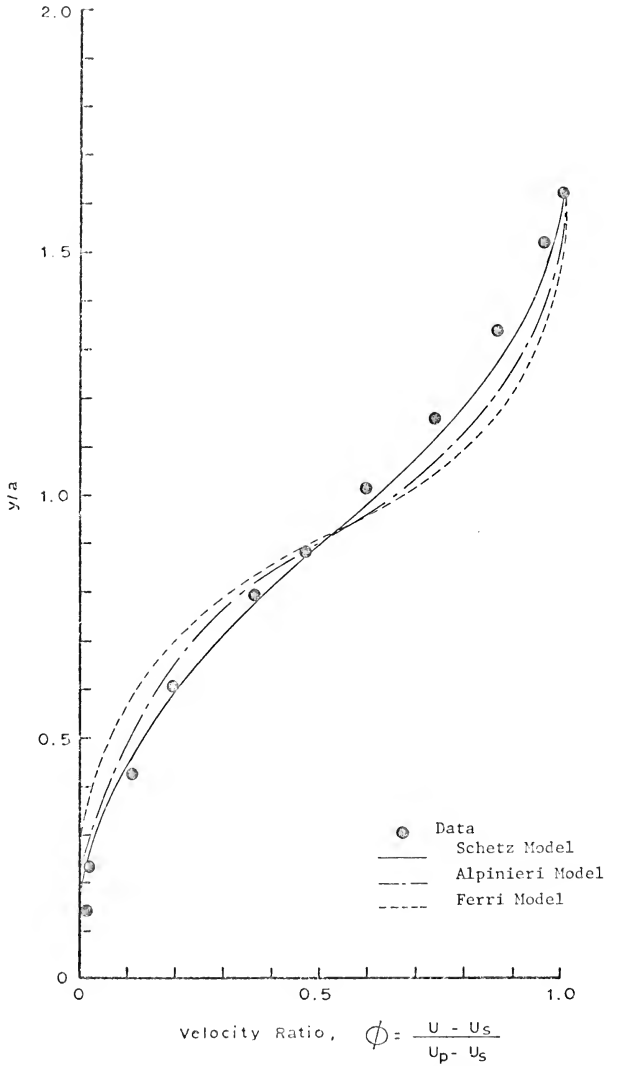

Figure 34 . Dimensionless Excess Velocity Profile at x/a=17.7 for Series I-A (Argon-Air) Tests.

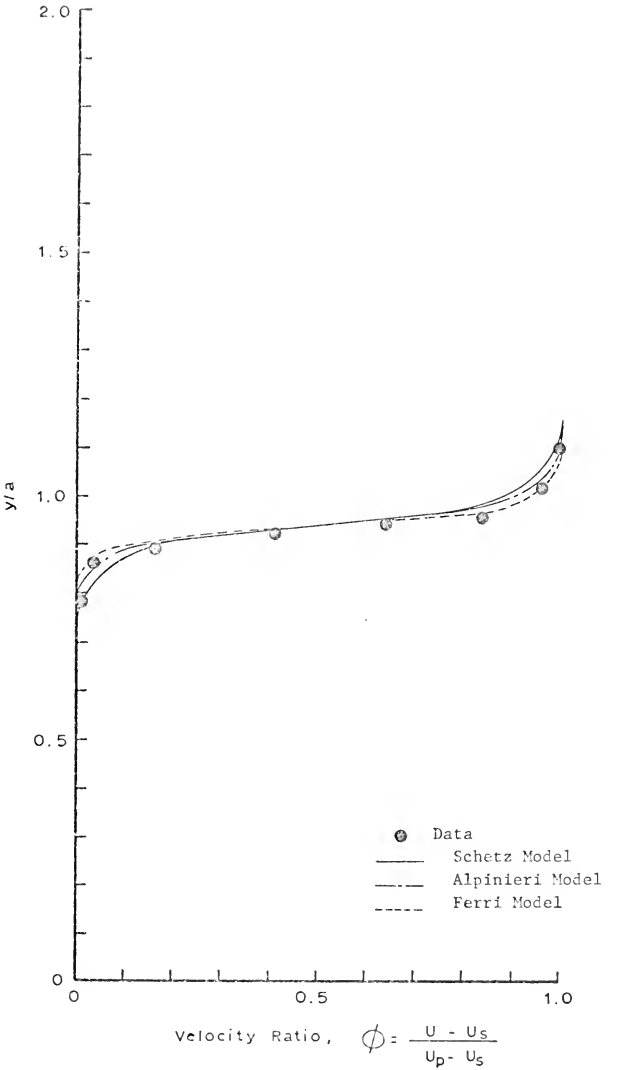

Figure 35 . Dimensionless Excess Velocity Profile at x/a=4.06 for Series I-B (Argon-Air) Tests.

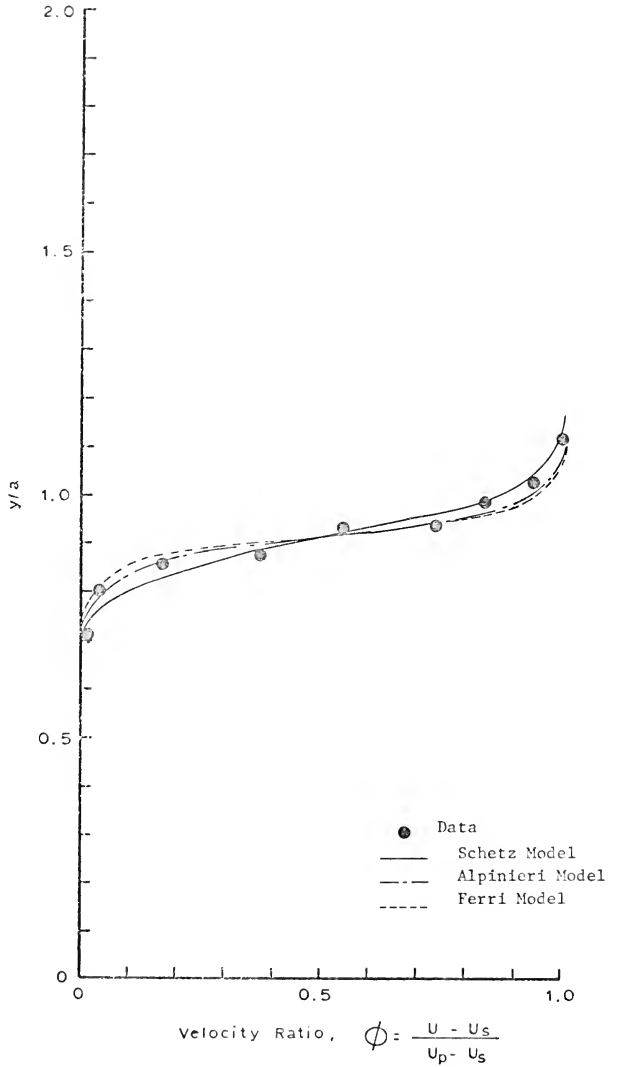

Figure 36 . Dimensionless Excess Velocity Profile at x/a=5.56 for Series I-B (Argon-Air) Tests.

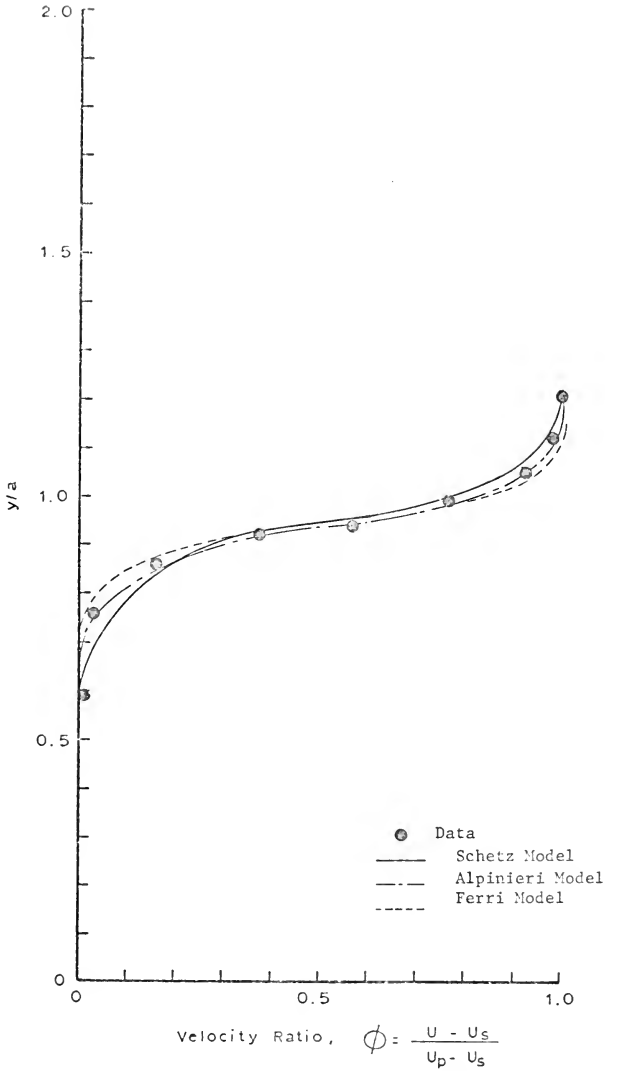

Figure 37 . Dimensionless Excess Velocity Profile at x/a=12.17 for Series I-B (Argon-Air) Tests.

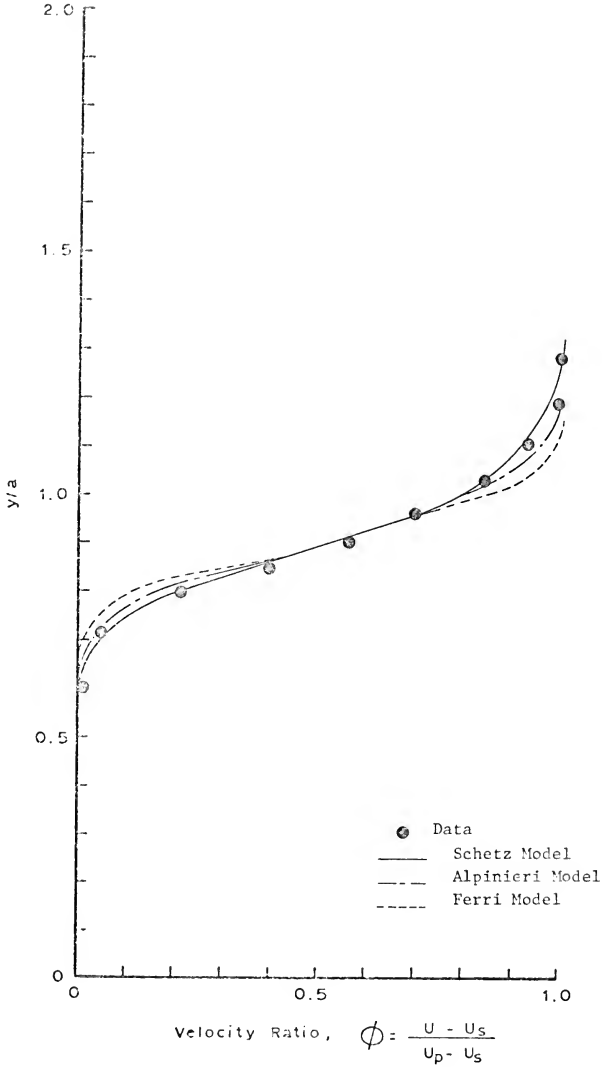

Figure 38 . Dimensionless Excess Velocity Profile at x/a=17.7 for Series I-B (Argon-Air) Tests.

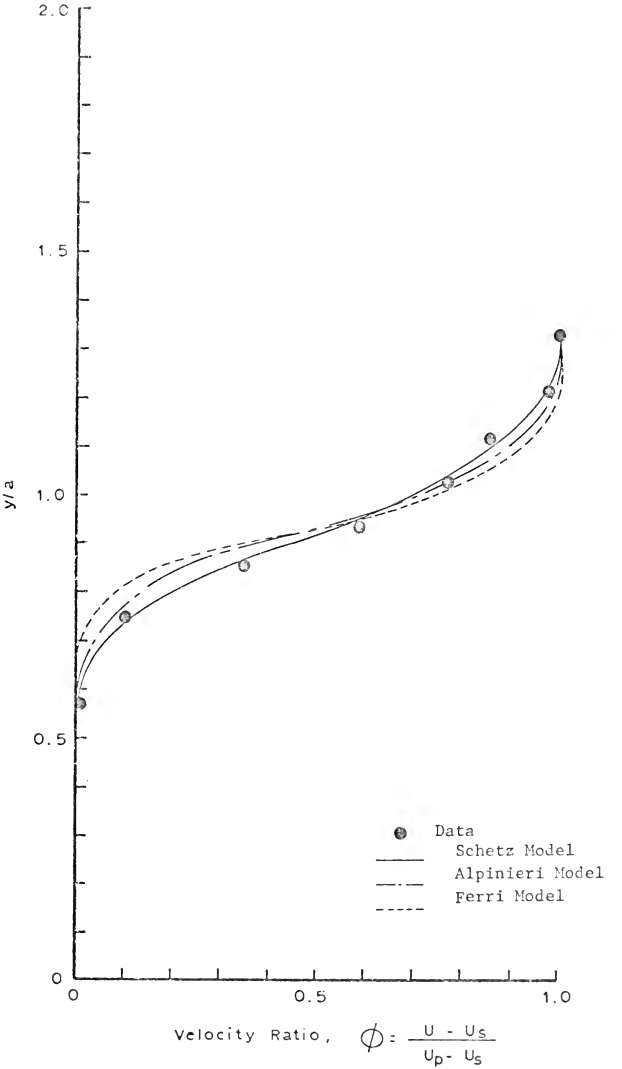

Figure 39 . Dimensionless Excess Velocity Profile at x/a=23.26 for Series I-B (Argon-Air) Tests.

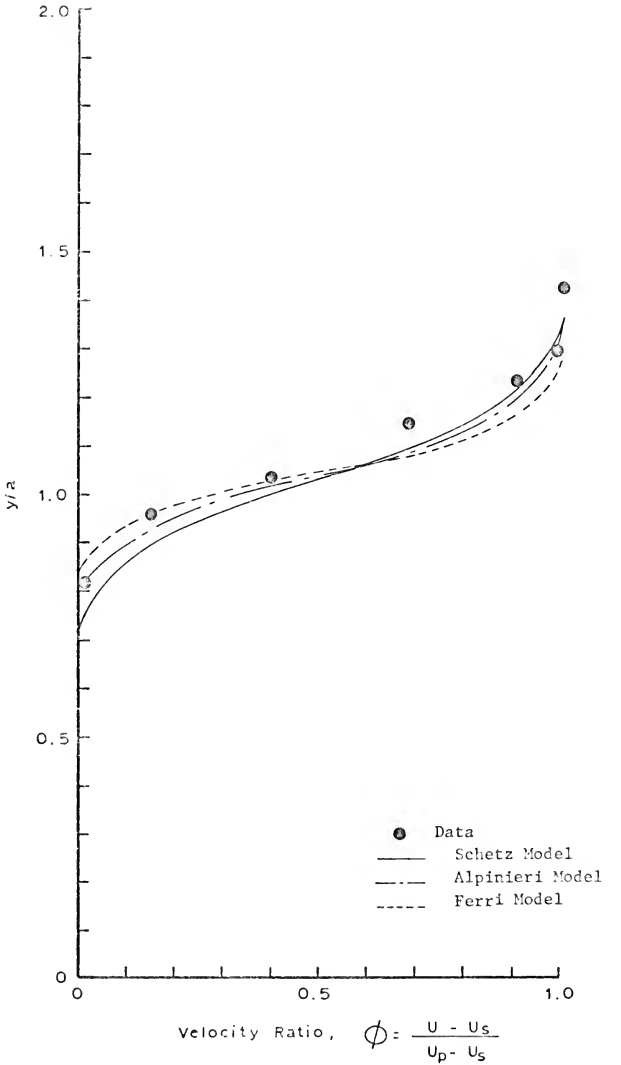

Figure 40 . Dimensionless Excess Velocity Profile at x/a=2.54 for Series II-A (Helium-Air) Tests.

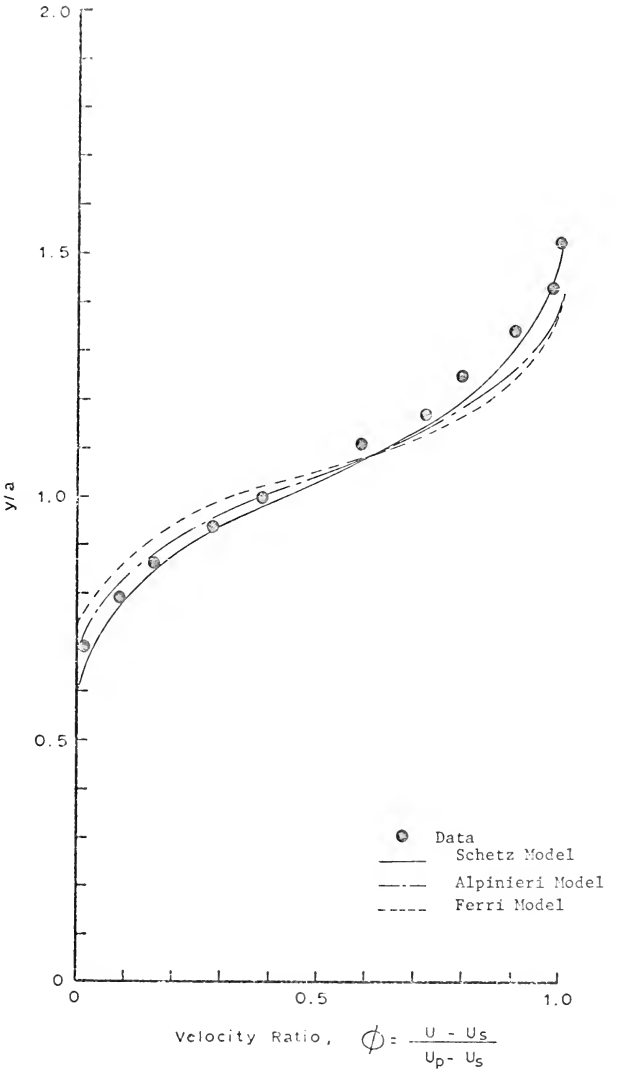

Figure 41 . Dimensionless Excess Velocity Profile at x/a=4.06 for Series II-A (Helium-Air) Tests.

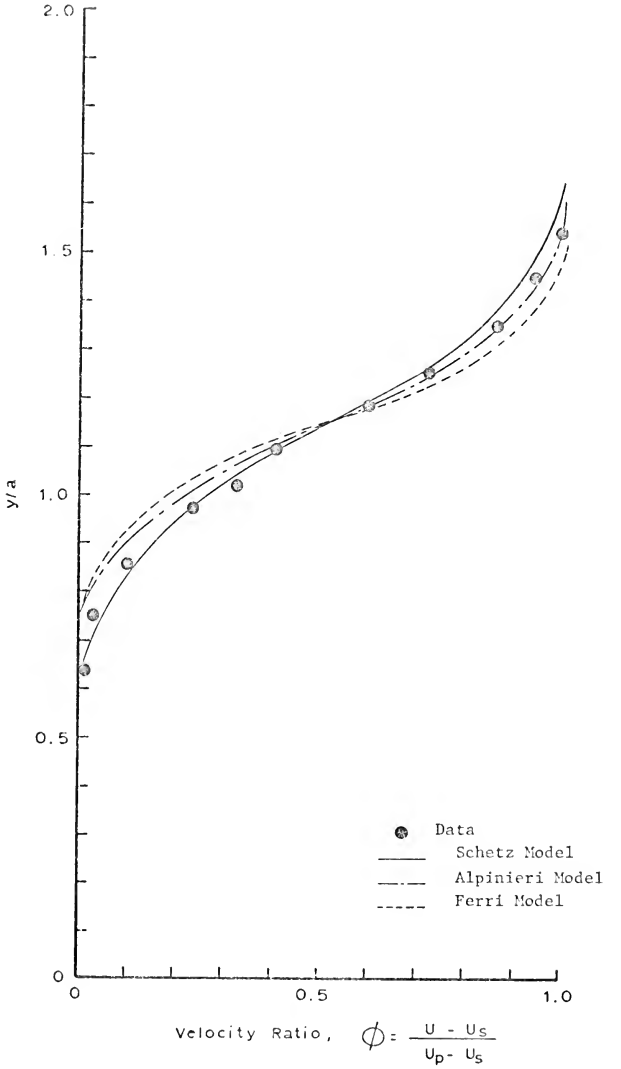

Figure 42 . Dimensionless Excess Velocity Profile at x/a=5.56 for Series II-A (Helium-Air) Tests.

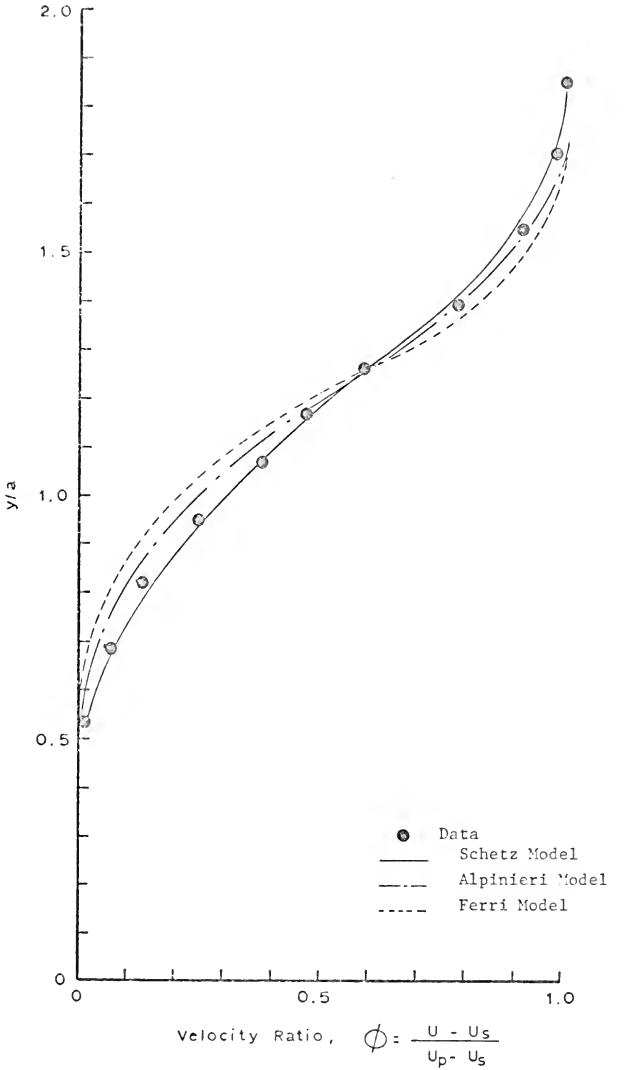

Figure 43 . Dimensionless Excess Velocity Profile at x/a=8.44 for Series II-A (Helium-Air) Tests.

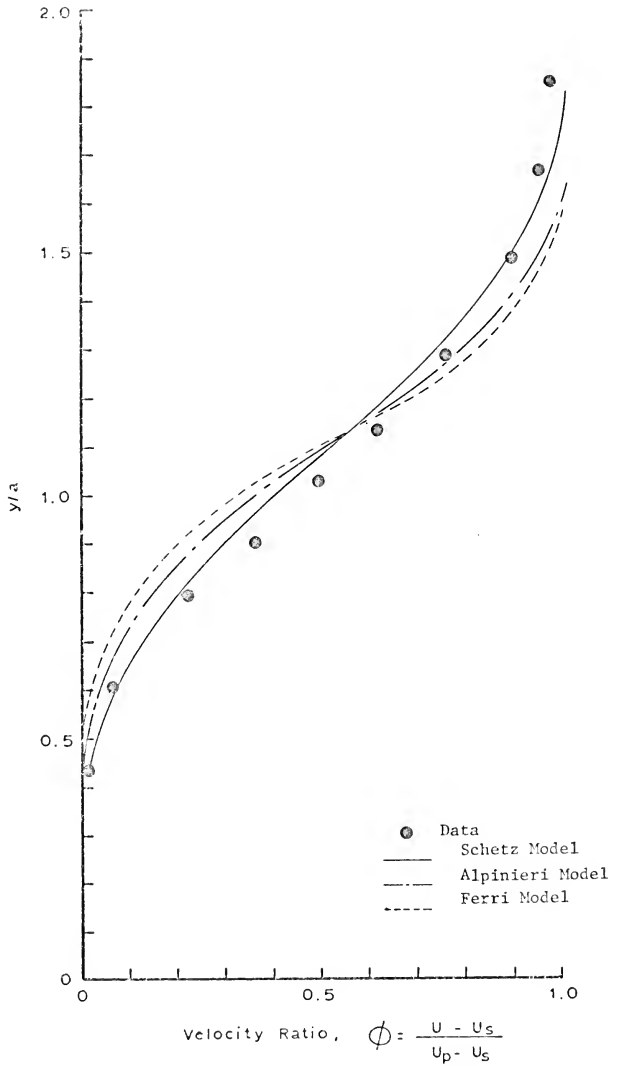

Figure 44 . Dimensionless Excess Velocity Profile at x/a=12.17 for Series II-A (Helium-Air) Tests.

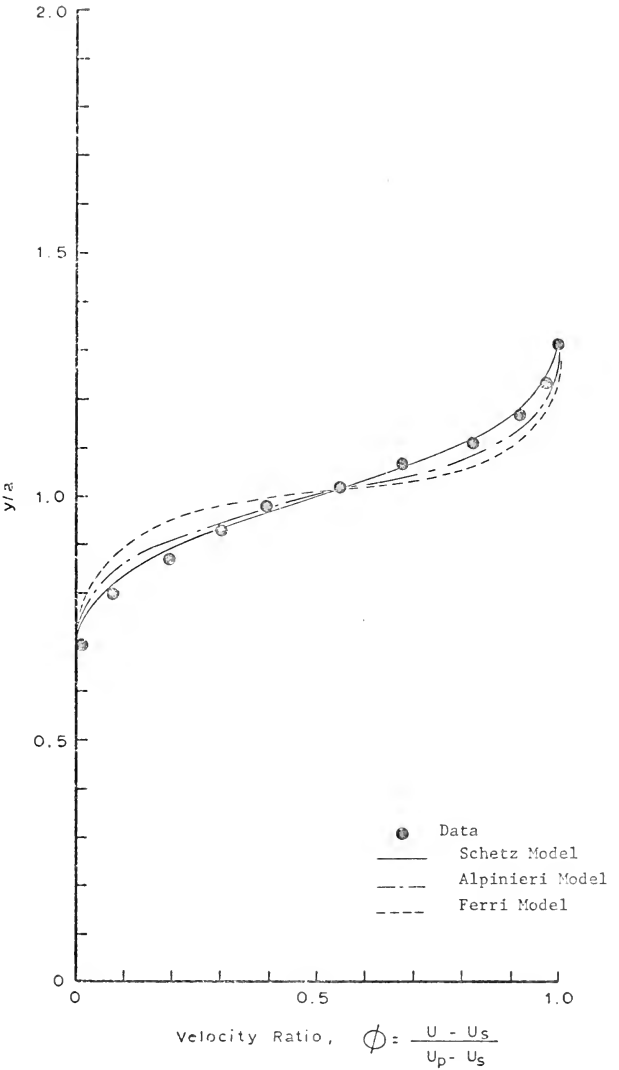

Figure 45 . Dimensionless Excess Velocity Profile at x/a=2.54 for Series II-B (Helium-Air) Tests.

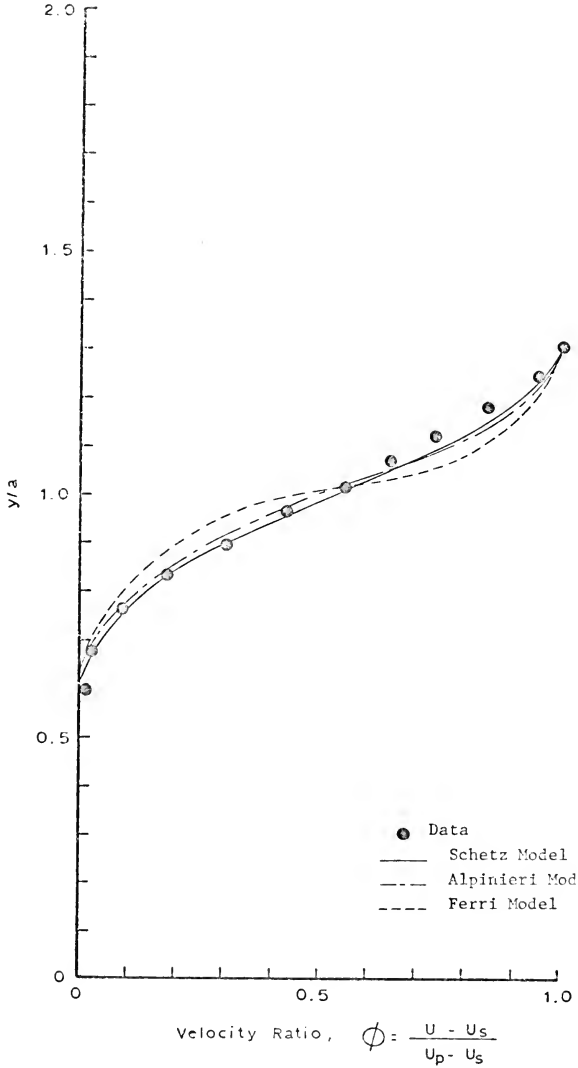

Figure 46 . Dimensionless Excess Velocity Profile at x/a=4.06 for Series II-B (Helium-Air) Tests.

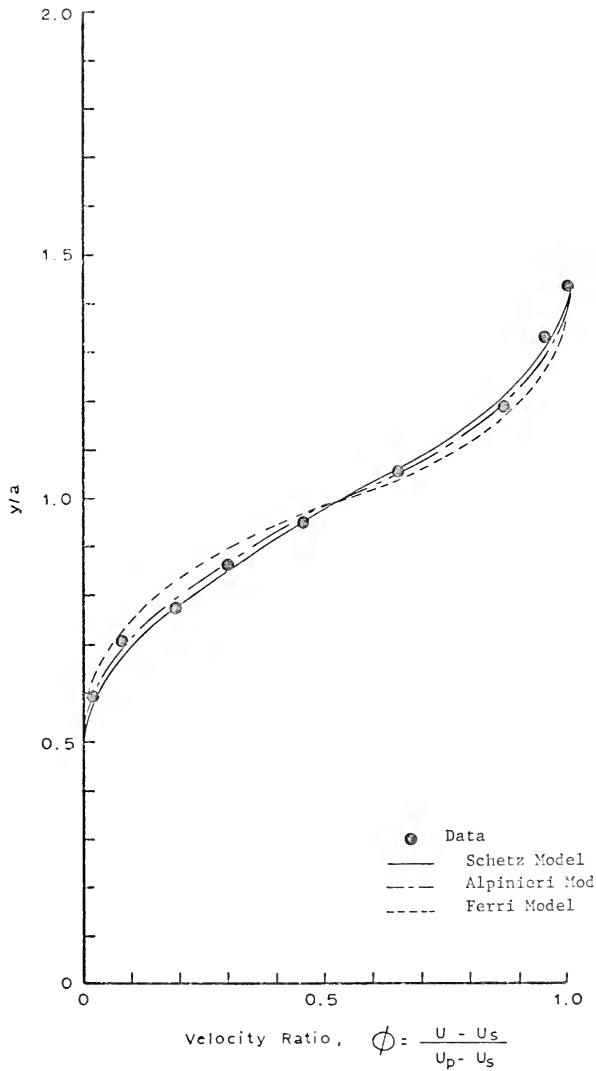

Figure 47 . Dimensionless Excess Velocity Profile at x/a=5.56 for Series II-B (Helium-Air) Tests.

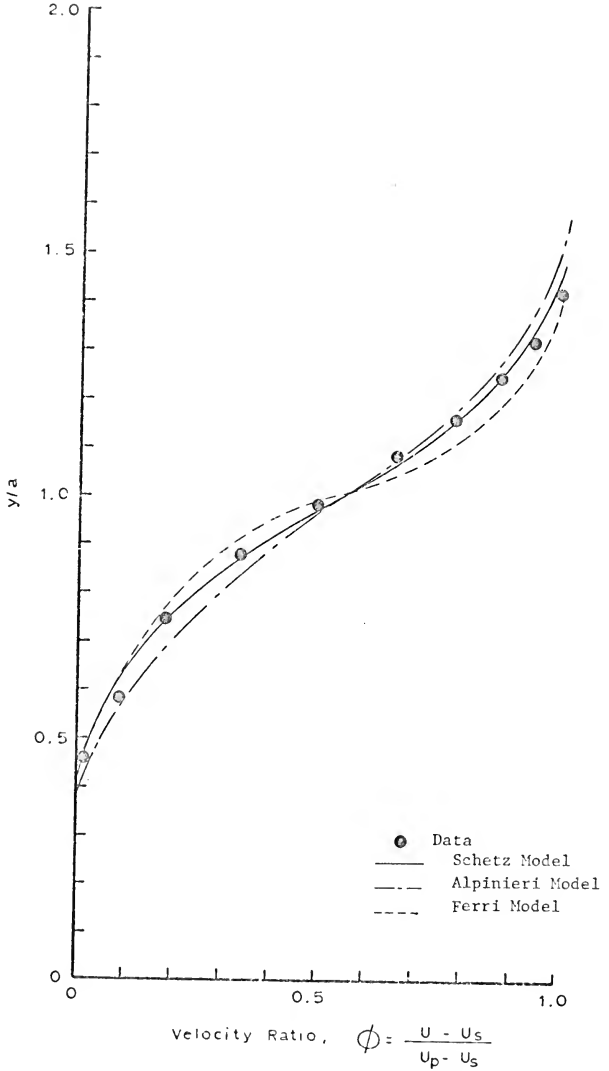

Figure 48 . Dimensionless Excess Velocity Profile at x/a=8.44 for Series II-B (Helium-Air) Tests.

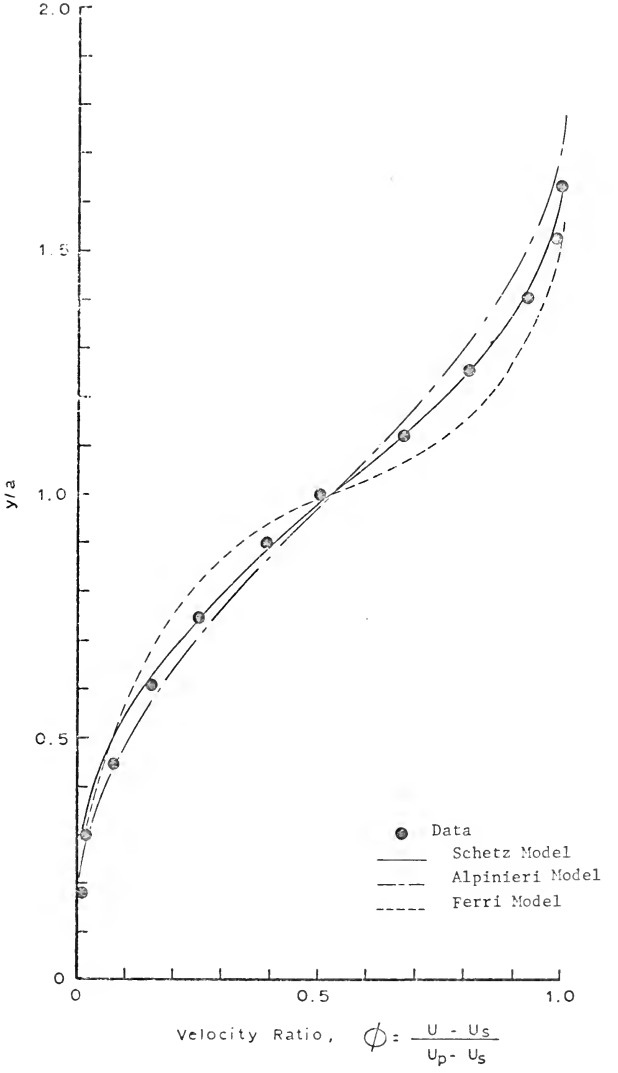

Figure 49 . Dimensionless Excess Velocity Profile at x/a=12.17 for Series II-B (Helium-Air) Tests.

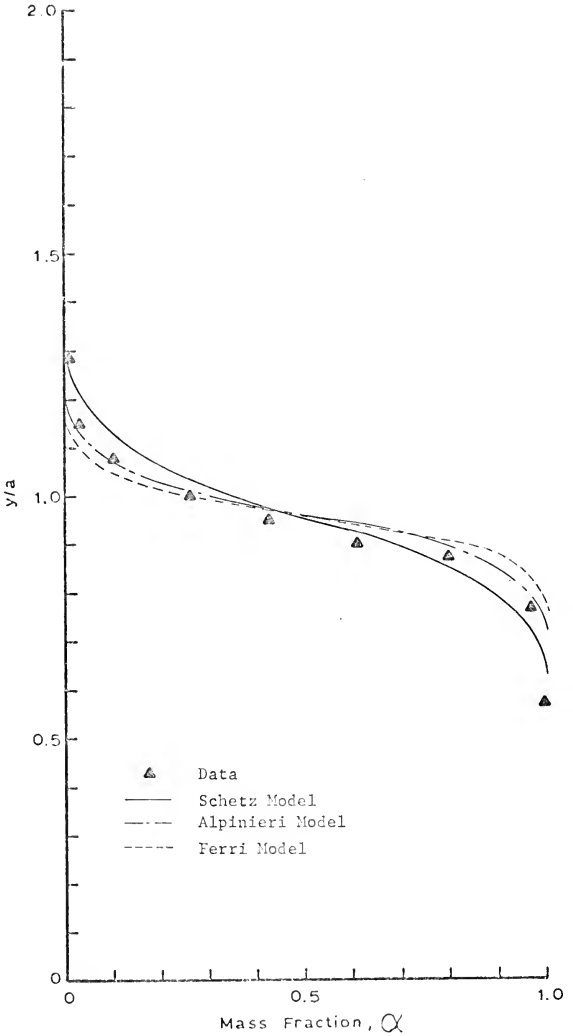

Figure 50 . Argon Mass Fraction Profile at x/a=2.54 for Series I-A Tests.

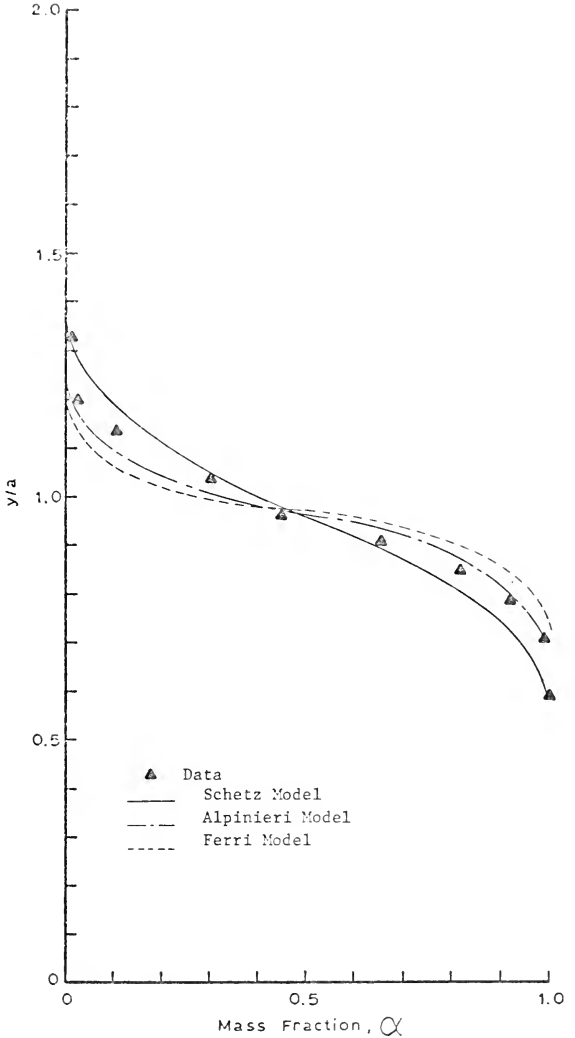

Figure 51 . Argon Mass Fraction Profile at x/a=4.06 for Series I-A Tests.

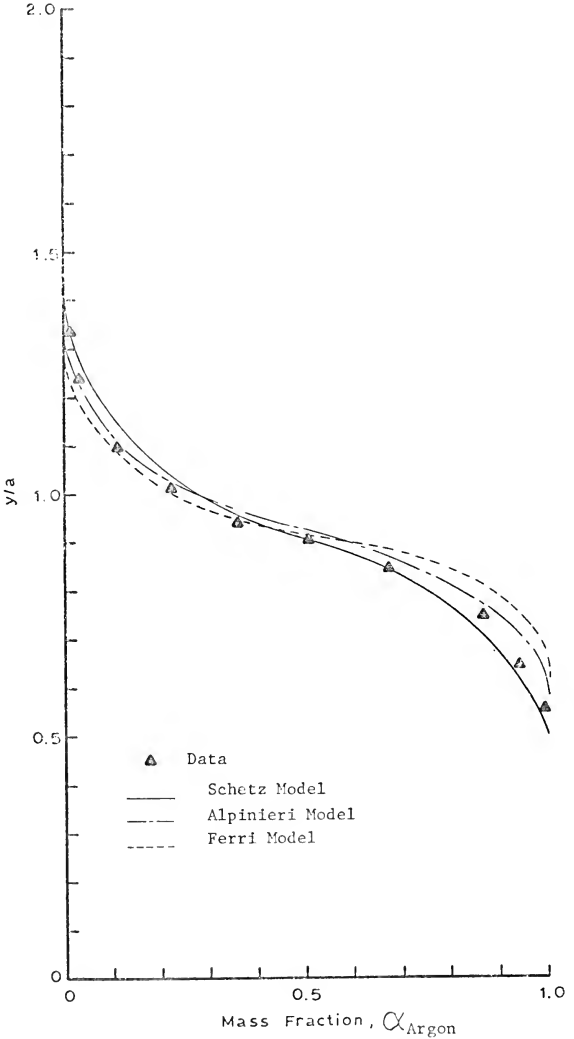

Figure 52 . Argon Mass Fraction Profile at x/a=5.56 for Series I-A Tests.

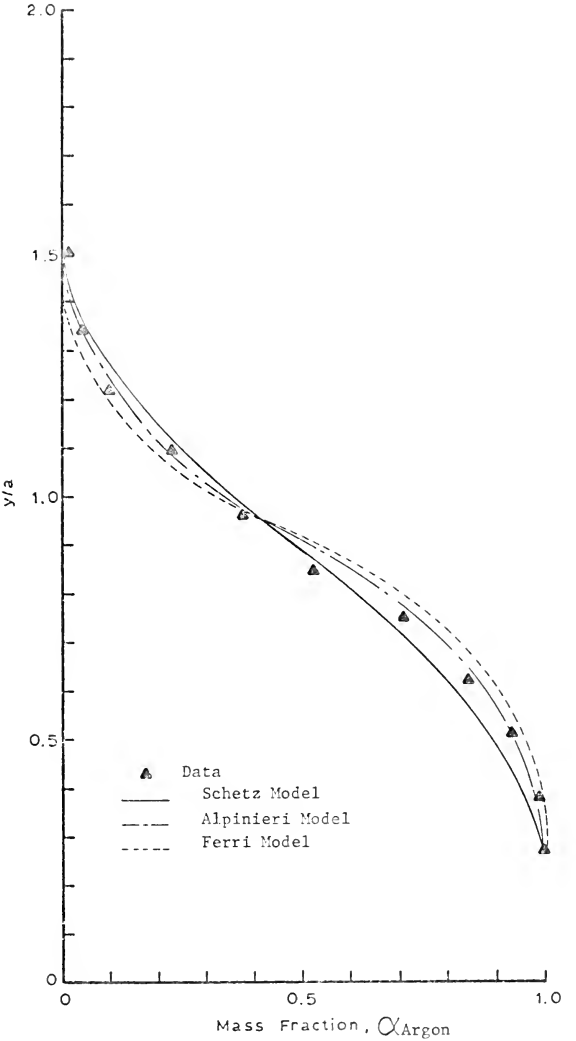

Figure 53 . Argon Mass Fraction Profile at x/a=12.17 for Series I-A Tests.

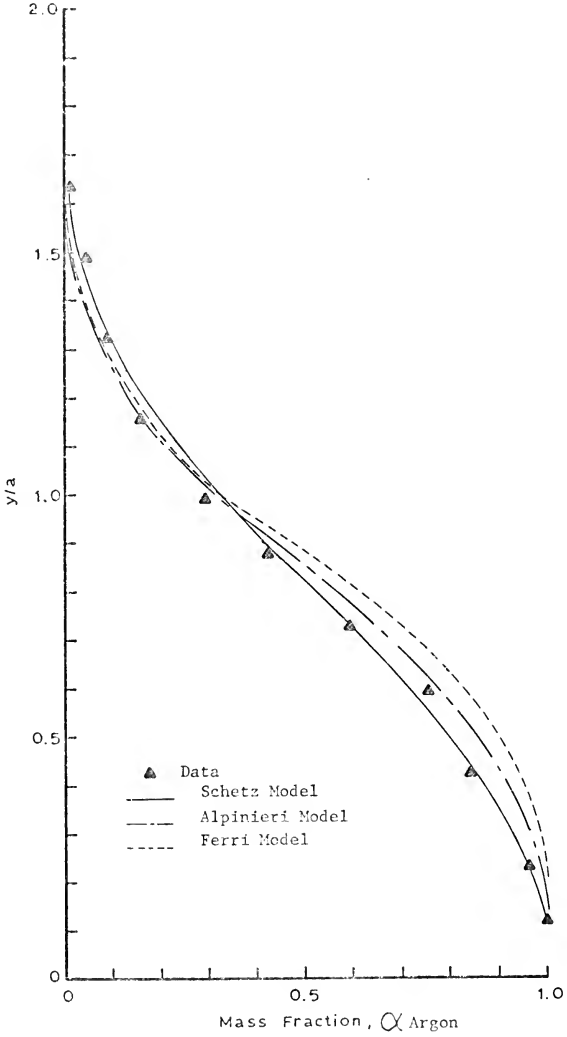

Figure 54 . Argon Mass Fraction Profile at x/a=17.7 for Series I-A Tests.

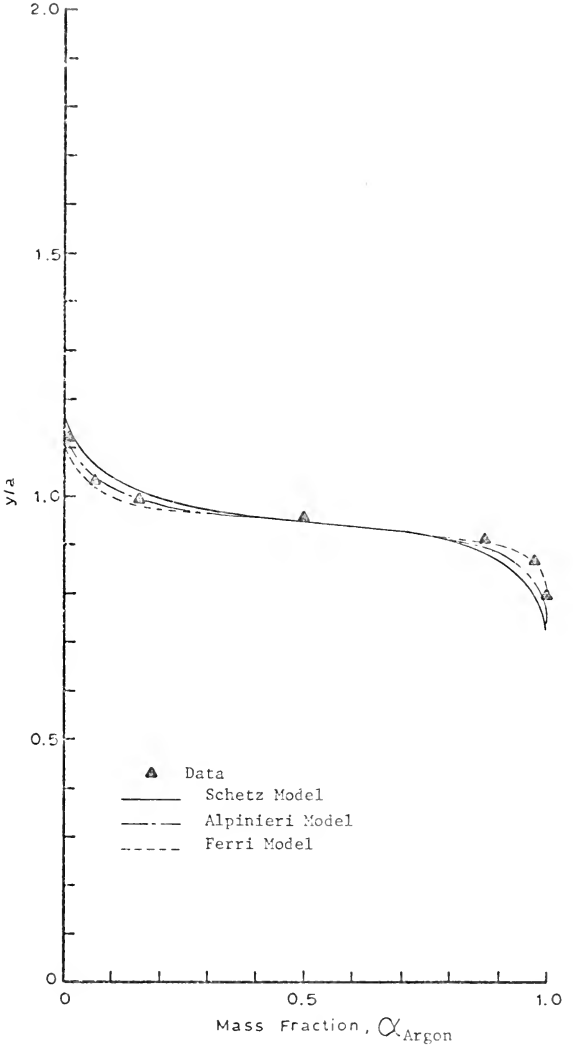

Figure 55 . Argon Mass Fraction Profile at x/a=4.06 for Series 1-B Tests.

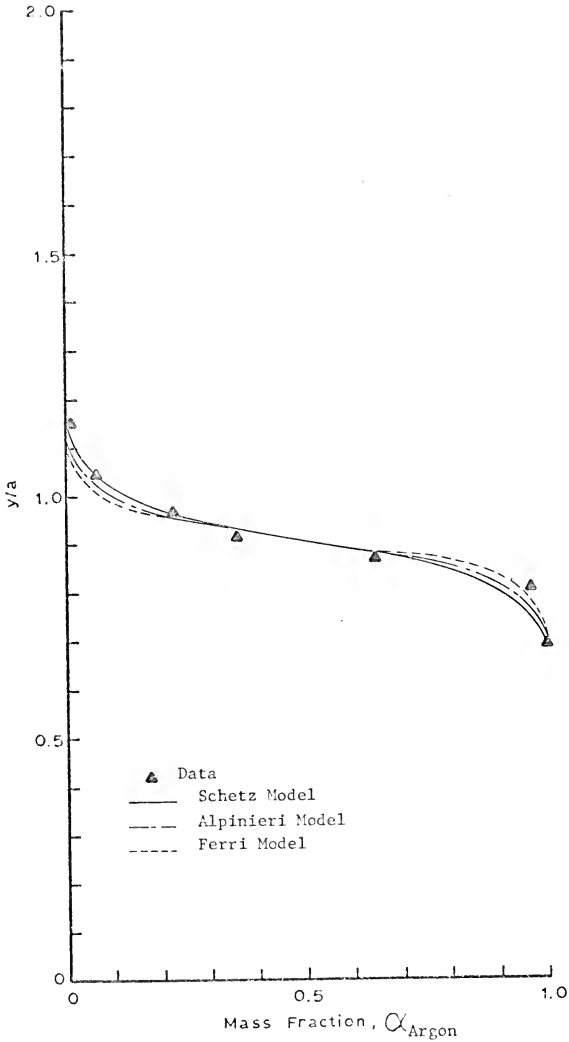

Figure 56 . Argon Mass Fraction Profile at x/a=5.56 for Series I-B Tests.

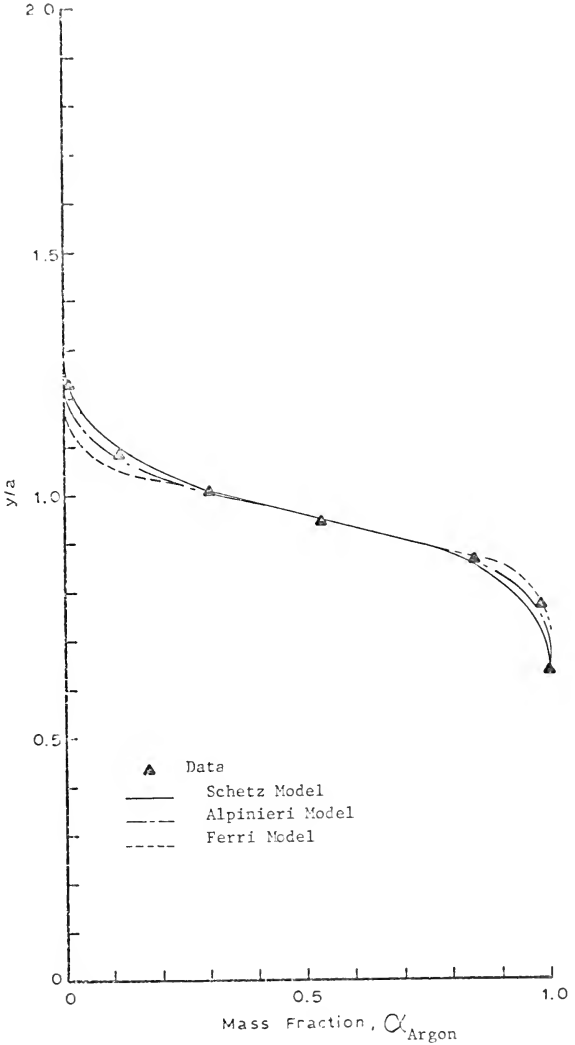

Figure 57 . Argon Mass Fraction Profile at x/a=12.17 for Series I-B Tests.

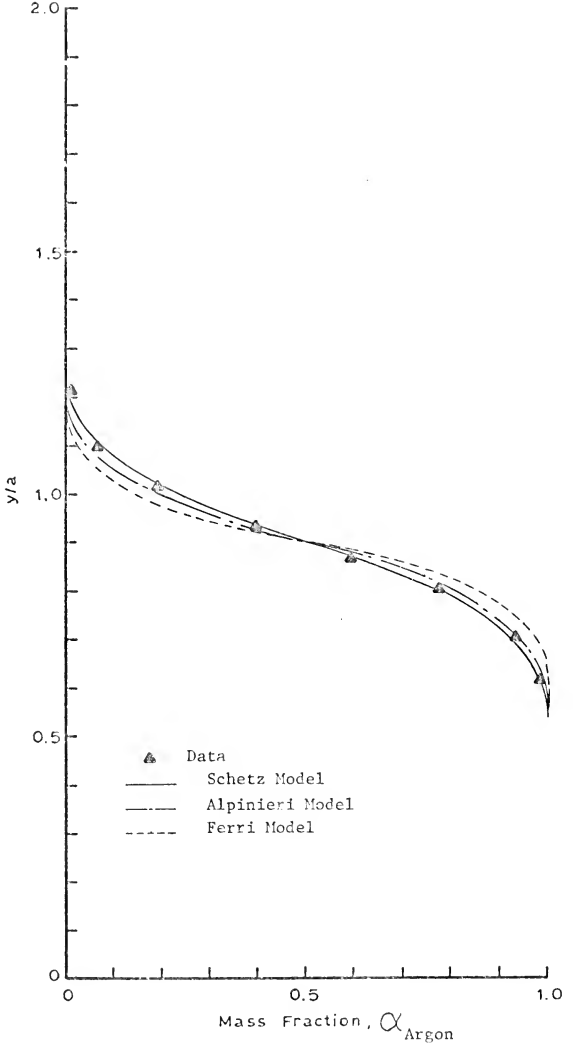

Figure 58 . Argon Mass Fraction Profile at x/a=17.7 for Series 1-B Tests.

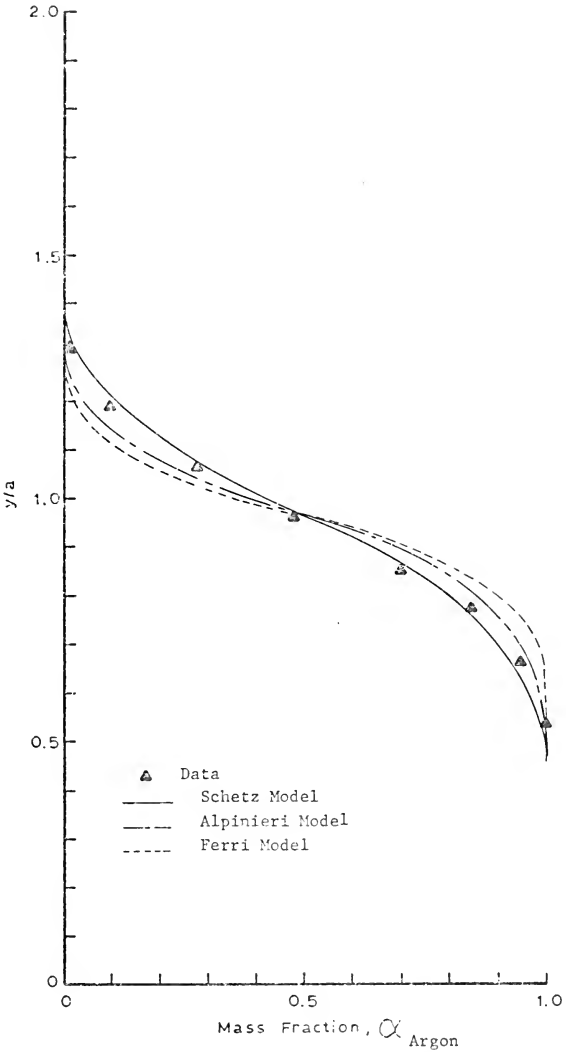

Figure 59 . Argon Mass Fraction Profile at x/a=23.26 for Series I-B Tests.

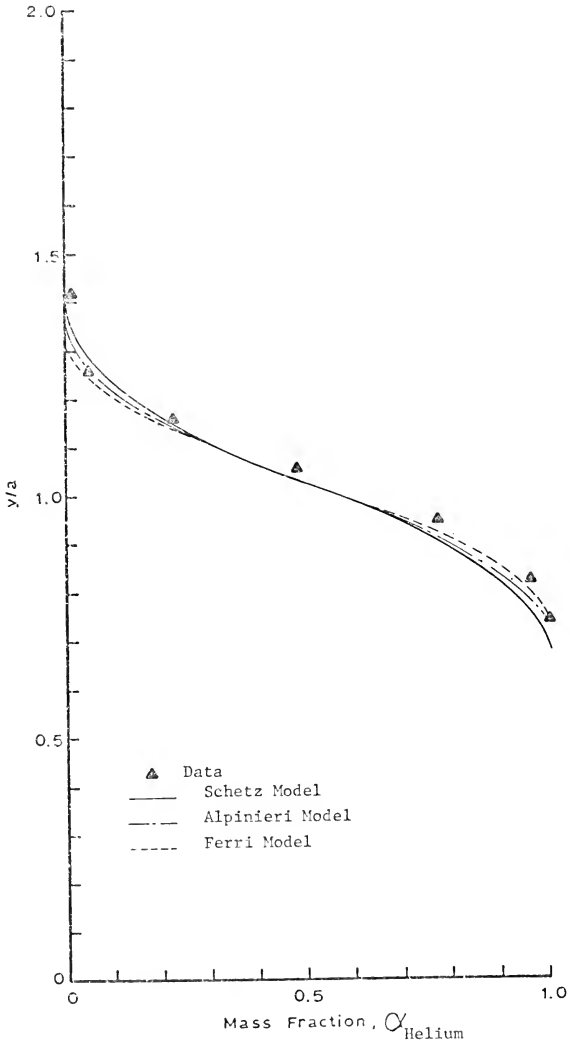

Figure 60 . Helium Mass Fraction Profile at x/a=2.54 for Series II-A Tests.

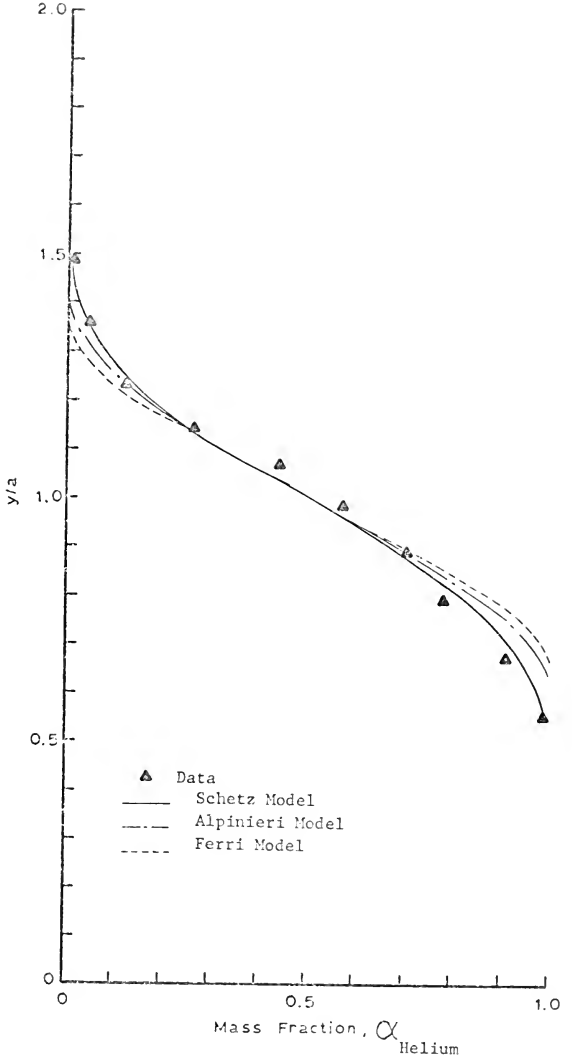

Figure 61 . Helium Mass Fraction Profile at x/a=4.06 for Series II-A Tests.

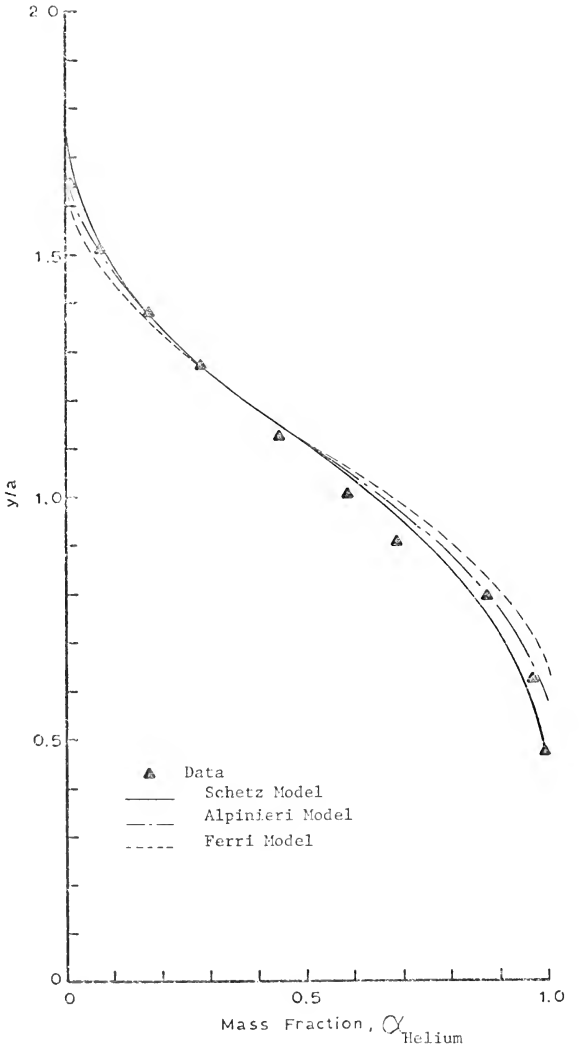

Figure 62 . Helium Mass Fraction Profile at x/a=5.56 for Series II-A Tests.

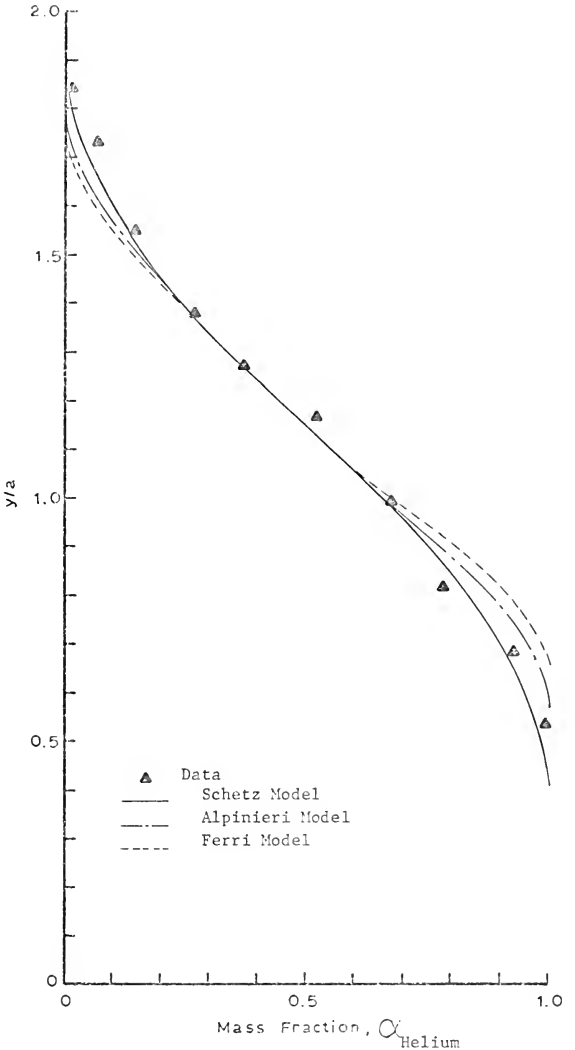

Figure 63 . Helium Mass Fraction Profile at x/a=8.44 for Series II-A Tests.

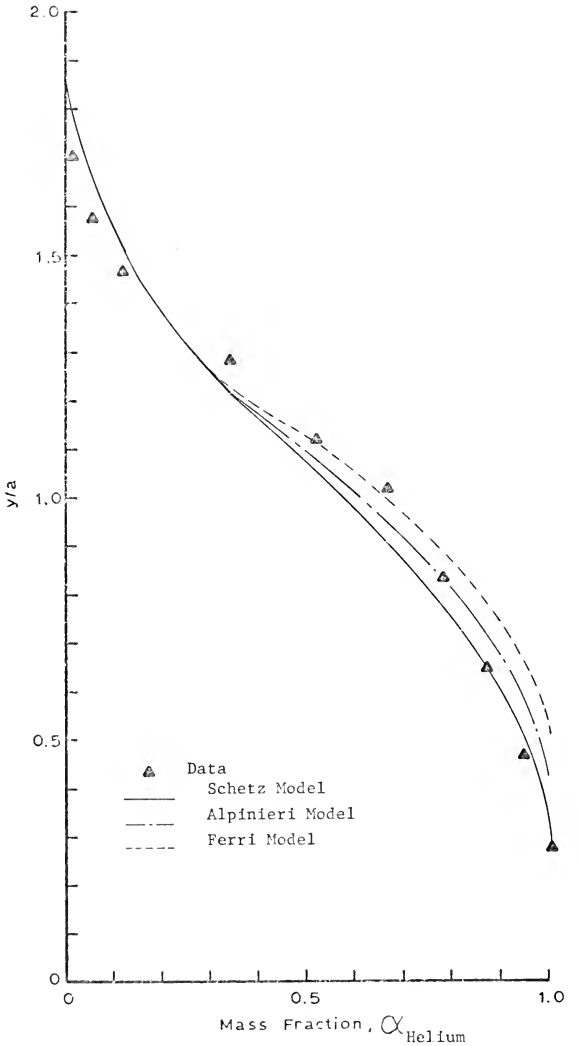

Figure 64 . Helium Mass Fraction Profile at x/a=12.17 for Series II-A Tests.

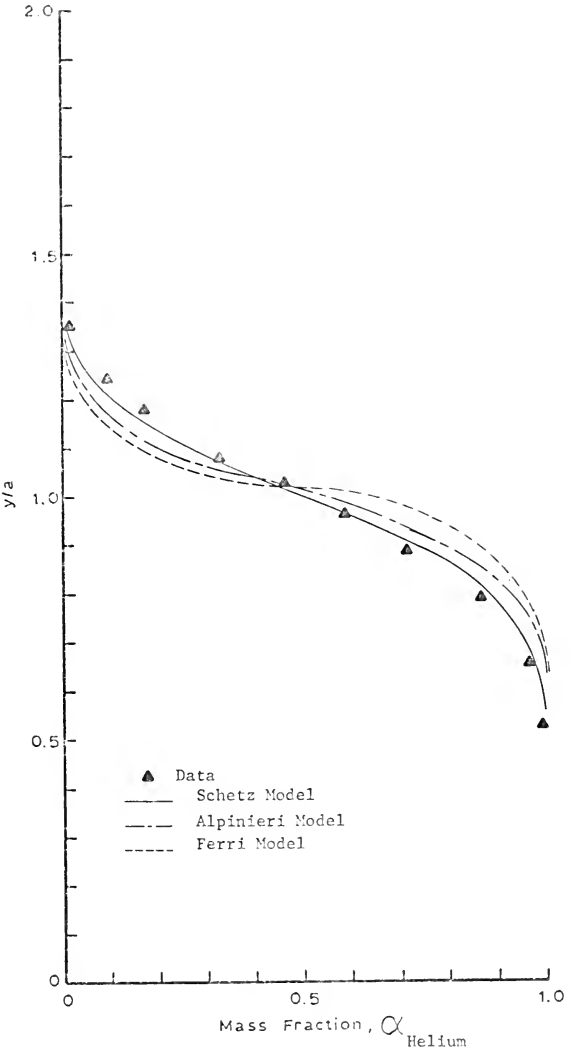

Figure 65 . Helium Mass Fraction Profile at x/a=2.54 for Series II-B Tests.

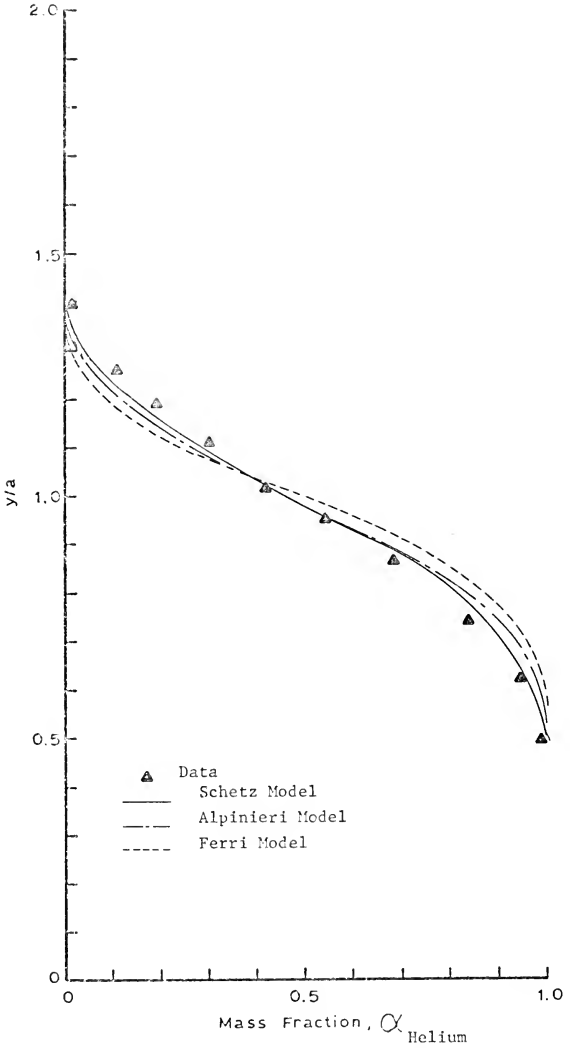

Figure 66 . Helium Mass Fraction Profile at x/a=4.06 for Series II-B Tests.

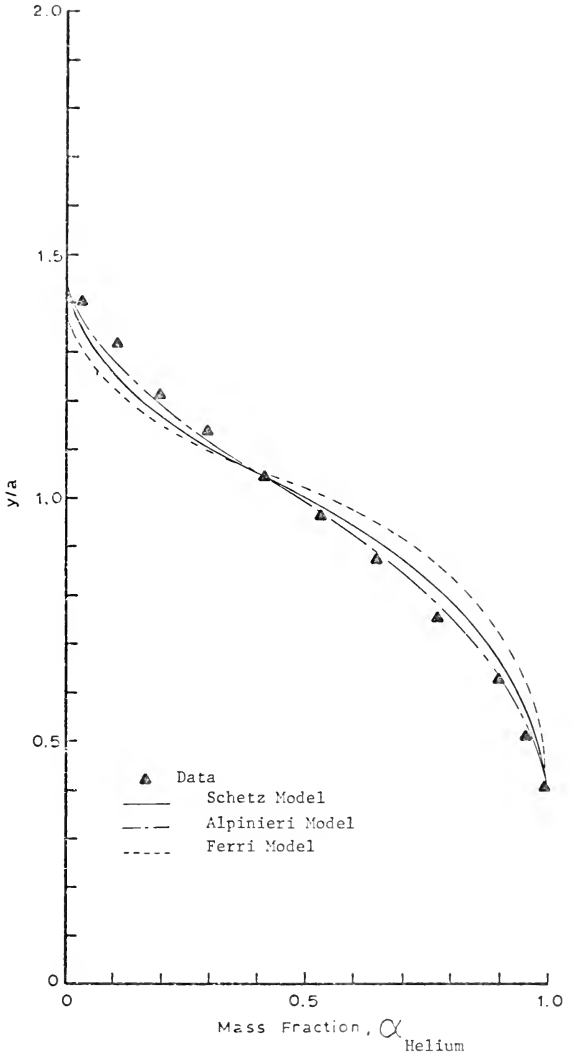

Figure 67 . Helium Mass Fraction Profile at x/a=5.56 for Series II-B Tests.

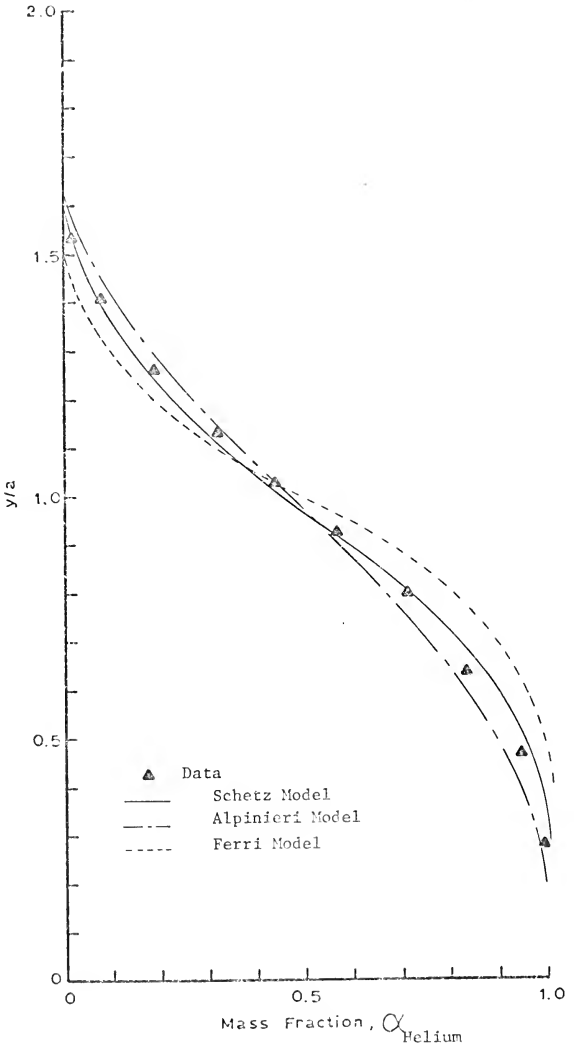

Figure 68 . Helium Mass Fraction Profile at x/a=8.44 for Series II-B Tests.

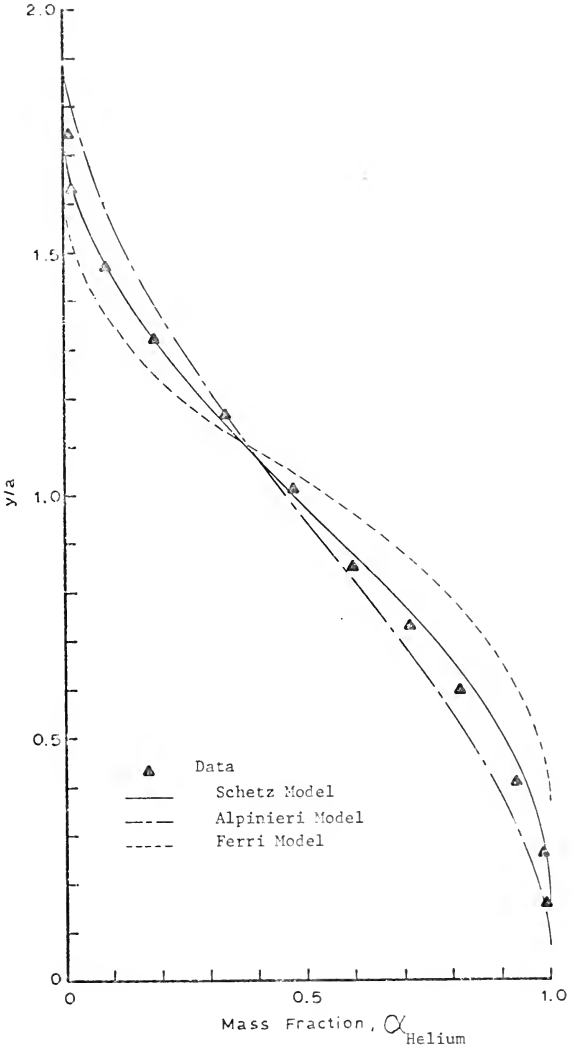

Figure 69 . Helium Mass Fraction Profile at x/a=12.17 for Series II-B Tests.

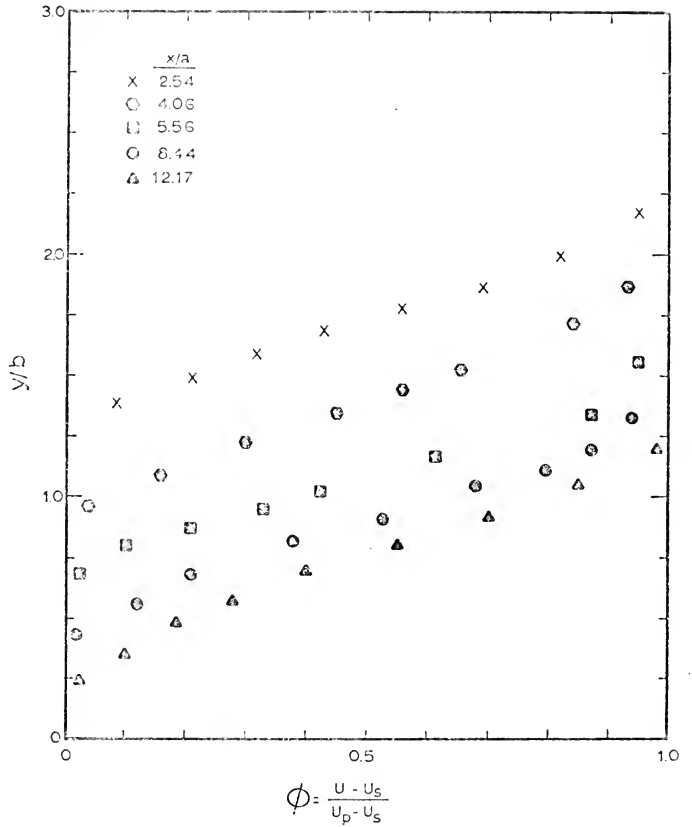

Figure 70 . Velocity Similarity Plot for Series II-B Tests

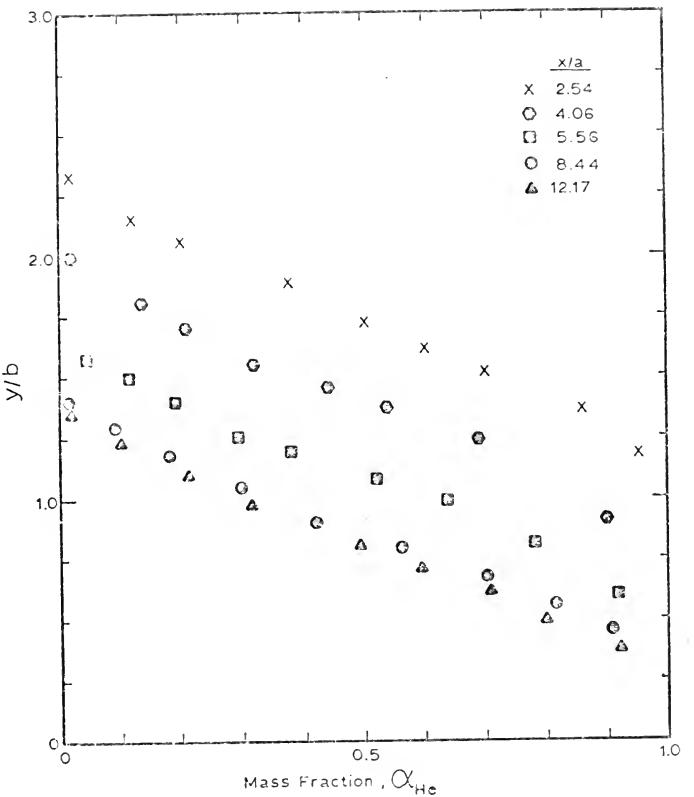

Figure 71. Mass Fraction Similarity Plot for Series II-B Tests

APPENDIX

APPENDIX

Description of the Program

The computer program consists of five routines for which the flow diagrams are shown in Figures 72 through 76. The function of each routine may be summarized as follows:

1) The MAIN routine is used for input, defining constants, initialization and to link the rest of the subroutines together.

2) Subroutine PRELIM computes the parameters necessary to implant the finite difference scheme and also controls output.

3) Control passes from subroutine PRELIM to subroutine SHEAR which computes the thickness of the mixing zone. Then multiple entries are utilized to enter the same subroutine depending on the model for the turbulent eddy viscosity.

4) Once the parameters and viscosity are computed, control is passed to subroutine SOLVE which solves the explicit finite difference equations (3.41) through (3.43) and (3.45) through (3.47).

5) After a step in the streamwise direction is taken by solving the difference equations, subroutine SUPP is entered. SUPP is a complementary subroutine to SOLVE. It takes the values of calculated total enthalpy, velocity and mass fractions from SOLVE and computes static mixture and species enthalpies, mixture specific heats, molecular weights, densities and temperatures at each new grid point.

The program terminates and calls for new initial profiles when it has "marched" to the specified streamwise location, XMAX.

Input to the program is a finite number ($\leq$ 100) of grid points in the lateral to flow (ψ) direction. The input grid points are initial velocity, static temperature and specie mass fraction profiles in equal intervals of $\Delta\psi$.

All major variables used in the program are defined at the beginning of the Fortran listing. It is hoped that these definitions in conjunction with numerous comment cards in the program enable the reader to follow the Fortran program with relative ease.

As the program executes the computations, additional points in the lateral direction are added one at a time to the grid whenever it is necessary. The criterion for adding points to the mesh is

$$\left| \frac{\Omega_{n,MPSI} - \Omega_{n,MPSI-1}}{\Omega_{n,MPSI}} \right| > 0.001 \qquad (A.1)$$

where Ω denotes enthalpy, velocity or the element mass fractions and MPSI is the total number of ψ grid points.

The points are added until (2k-1) points (where k is the number of points originally input) are obtained in the grid; at which time the ψ grid increment is doubled and the number of points are reduced to k, i.e., only ψ point numbers 1,3,5,7,.....,k are retained by the program. All ψ grid points not in use take on primary stream values.

Physical Coordinates

Once a step in the streamwise direction is taken, the physical coordinate corresponding to all ψ points is calculated through the relations

$$y_o = 0$$

$$y_{m+1} = y_m + \frac{\Delta\psi}{2}\left[\frac{1}{(\rho u)_m} + \frac{1}{(\rho u)_{m-1}}\right] \qquad (A.2)$$

Step Size

As can be seen from Equation (3.53) there is no restriction on the grid size $\Delta\psi$. However, $\Delta\psi$ has to be as small as feasible to ensure finite difference consistency and accuracy, i.e., ε in Equation (3.40) has to be small. An approximate relation between $\Delta\psi$ and the number of grid points may be explained by the following analysis:

The von Mises transformation is

$$\frac{\partial\psi}{\partial y} = \rho u$$

$$\int_0^{y_e} \rho u dy = \int_0^{\psi_e} d\psi$$

Hence,

$$\psi_e = \int_0^{y_e} \rho u dy$$

where the subscript e refers to the lateral coordinate at which flow consists of only the primary stream.

Now as an approximation a step function velocity profile as the initial profile at x = 0 is assumed. Then, pure secondary gas (argon or helium) exists between y = 0 and y = a (where a is the exit height of the secondary stream, i.e., slot height). Hence, ρu is constant from y = 0 to y = a. Therefore

$$\psi_e = (\rho u)_s a$$

The external streamline ψ_e may be related to the number of input grid points by

$$(k - 1)\Delta\psi = \psi_e \tag{A.3}$$

Then

$$\Delta\psi = \frac{a(\rho u)_s}{k - 1} \tag{A.4}$$

The number of input grid points can thus be estimated for a given value of $\Delta\psi$. Obviously, for a given configuration, the smaller the step size $\Delta\psi$, the larger will be the number of grid points. This would result in an inefficient, slow and also expensive program.

For all cases under study, a lateral step size of 5×10^{-3} was used. This resulted in the use of approximately 20 grid points for the helium tests and 50 grid points for the argon tests with about 5 initial points in the mixing zone.

It should be noted that Equation (A.4) is just an approximate analysis to determine an appropriate value $\Delta\psi$. After a value for $\Delta\psi$ is chosen, the actual number of grid points is determined by the experimental curves of ρ, U, T and α_i. Inside the mixing region equal increments of ψ do not yield equal increments of the physical coordinate y. Thus, some iteration with Equation (A.2) is required when putting in the actual initial profiles at some $x = x^*$.

The streamwise step size used was $\Delta x = 4.5 \times 10^{-4}$ feet. However, the stability requirement of Equation (3.53) imposes a restriction on Δx. Thus, given a value of $\Delta\psi$ (i.e., 0.005), the upper limit on Δx was calculated for each grid point. The minimum of the calculate Δx was compared with the value of 4.5×10^{-4} feet.

The smaller of the two values was chosen for the streamwise step size.

One set of helium and argon data were run with streamwise step sizes of 5×10^{-3} and 5×10^{-5} feet to observe the effect of ε, i.e., Equation (3.40), on the results. No differences were detected in either case in comparison to a step size of 4.5×10^{-4} feet. It is deemed that with the use of the stated step size, is insignificant in the streamwise region of interest, i.e., $x/a \leq 20$.

Enthalpy Fits

To initially implement the finite difference scheme, total enthalpies had to be calculated from the input data of temperature, velocity and mass fractions. Then, once the computations had started, temperatures had to be determined from the newly calculated values of total enthalpies.

The species enthalpies (Btu/lbm) were curve fitted by means of the following equation:

$$h_i = A_i + B_i T \qquad T_{low} \leq T \leq T_{high} \tag{A.5}$$

T being the absolute temperature in °R, T_{low} and T_{high} being the range of validity of the curve fit. The value of the constants for each species are given in the following table.

These fits are of data from reference [86] and are based on a reference temperature of 400°R.

It is also noted that the constants B_i correspond to the specific heat at constant pressure of species i.

Table IV. Enthalpy Fit Coefficients.

Species		A_i	B_i	T_{low}(°R)	T_{high}(°R)	Max. Error Due to Curve Fit
1	O_2	-0.47	0.2175	250	550	0.05%
2	N_2	-0.11	0.2481	250	550	0.05%
3	A	-0.05	0.1244	325	550	0.1%
4	He	-0.50	1.2413	325	550	0.1%

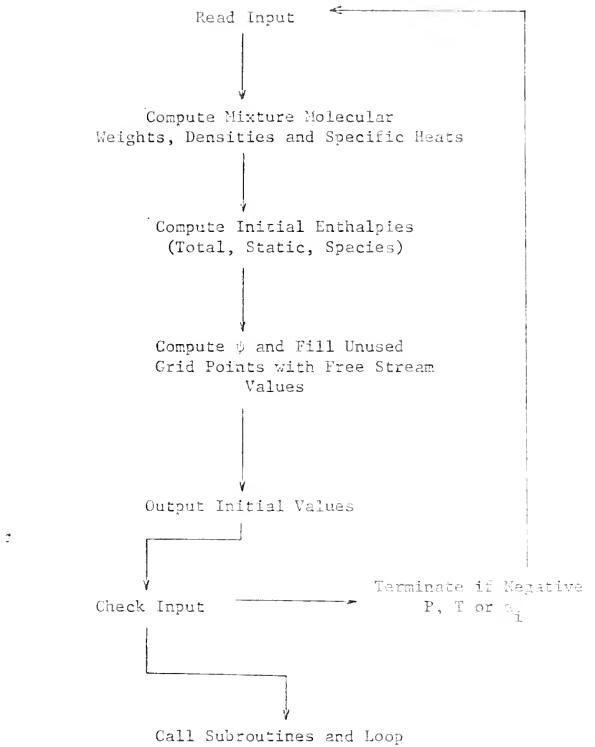

Figure 72 . Flow Diagram for MAIN Routine.

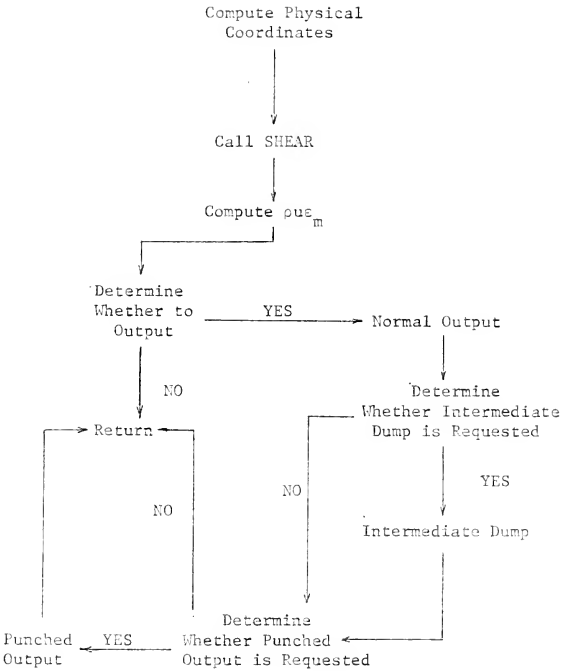

Figure 73 . Flow Diagram for Routine PRELIM.

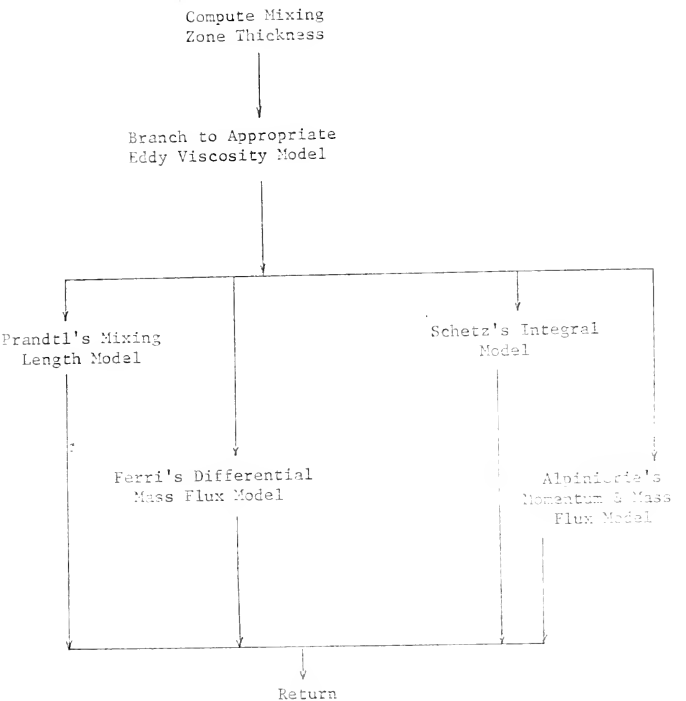

Figure 74 . Flow Diagram for Routine SHEAR.

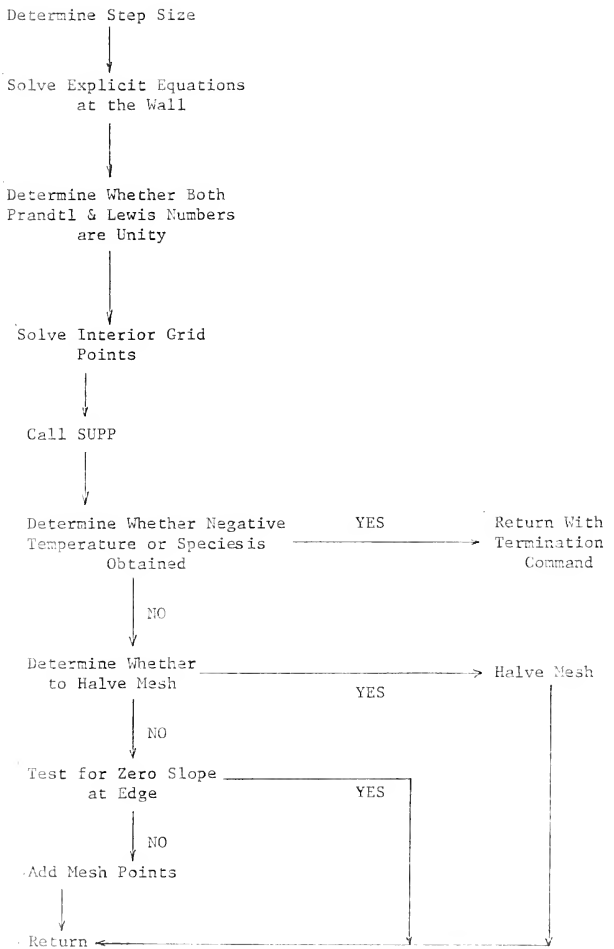

Figure 75 . Flow Diagram for Routine SOLVE.

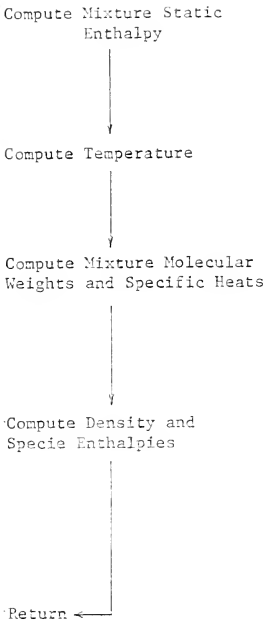

Figure 76 . Flow Diagram for Routine SUPP.

```
C
C       DEFINITION OF VARIABLES IN COMPUTER PROGRAM
C
C       TITLE(18)     :DATA SET ID CARD-ANY 72 CHARACTERS
C       MODEL         :DETERMINES TURBULENT TRANSPORT MECHANISM MODEL
C                      (=1 PRANDTL I)
C                      (=2 MODIFIED FERRI)
C                      (=4 SCHETZ)
C                      (=5 MODIFIED ALPINIERI)
C       MPSI          :NUMBER OF GRID POINTS IN PSI DIRECTION
C       INDUMP        :CONTROLS PRINTED OUTPUT
C                      (=0 NORMAL OUTPUT)
C                      (≠0 NORMAL OUTPUT + INTERMEDIATE DUMP)
C       NOSPEC        :NUMBER OF SPECIES
C       NPUNCH        :CONTROLS PUNCHED OUTPUT
C                      (=0 NO PUNCHED OUTPUT)
C                      (≠0 PUNCHED OUTPUT)
C       IOUT          :CONTROLS WHETHER TO OUTPUT IN INTERVALS
C                      (=0 OUTPUT IN INTERVALS)
C                      (≠0 OUTPUT @ PRESCRIBED X-LOCATIONS)
C       XBAR(9)       :PRESCRIBED X-STATIONS FOR OUTPUT (FT)
C       A(4)          :ENTHALPY FIT COEFFICIENT (BTU/LBM)
C       B(4)          :ENTHALPY FIT COEFFICIENT (BTU/LBM-R)
C       C(4)          :ENTHALPY FIT COEFFICIENT (BTU/LBM-R**2)
C       XPRINT        :INCREMENT IN FEET PROGRAM IS TO OUTPUT
C       XINIT         :INITIAL VALUE OF X IN FEET
C       XFINAL        :FINAL VALUE OF X IN FEET
C       PRNDTL        :PRANDTL NUMBER
C       XLEWIS        :LEWIS NUMBER
C       DELPSI        :MESH INCREMENT IN PSI DIRECTION
C       XMPS          :STABILITY STEP SIZE REGULATOR
C       P             :STATIC PRESSURE IN LBF/FT**2
C       HEIGHT        :SLOT HEIGHT (FT)
C       C1.....C6     :EMPIRICAL TURBULENT VISCOSITY COEFFICIENTS
C       T(200)        :STATIC TEMPERATURE (R)
C       U(200)        :VELOCITY (FT/SEC)
C       PHI(200)      :NON-DIMENSIONAL VELOCITY RATIO (U-UJ)/(UE-UJ)
C       ALFA(4,200)   :SPECIE MASS FRACTIONS
C       WTMOL(4)      :MOLECULAR WEIGHTS OF SPECIES
C       WTMIX(200)    :MOLECULAR WEIGHT OF MIXTURE
C       RHO(200)      :MIXTURE DENSITY (SLUGS/FT**3)
C       HTOT(200)     :MIXTURE TOTAL ENTHALPY (BTU/LBM)
C       HSTAT(200)    :MIXTURE STATIC ENTHALPY (BTU/LBM)
C       HSPEC(4,200):SPECIES STATIC ENTHALPY (BTU/LBM)
C       USQ(200)      :(U*U)/2
C       PSI(200)      :STREAM FUNCTION (SLUGS/FT-SEC)
C       ISTEP         :NUMBER OF STEPS IN X-DIRECTION
C       DX            :DELTA X INCREMENT (FT)
```

```
C       JEXIT        :CONTROLS TERMINATION OF PROGRAM
C       Y(200)       :Y DISTANCE FROM LOWER WALL (FT)
C       EPSI(200)    :TURBULENT VISCOSITY (LBF-SEC/FT**2)
C       SG(200)      :RHO*U*EPSI
C       CPBAR(200)   :MIXTURE SPECIFIC HEATS (BTU/LBM)
C       SIGMA(200)   :CHECK SUM FOR MASS FRACTIONS
C       WU(200)      :VELOCITY (WORKING ARRAY)
C       WALFA(4,200):MASS FRACTIONS (WORKING ARRAY)
C       WH(200)      :TOTAL ENTHALPY (WORKING ARRAY)
C
C
        DIMENSION TITLE(18),A(4),B(4),C(4),T(200),U(200),
       1WTMOL(4),WTMIX(200),RHO(200),HTOT(200),HSTAT(200),
       2USQ(200),PSI(200),Y(200),EPSI(200),SG(200),CPBAR(200),
       3WU(200),WALFA(4,200),WH(200),ALFA(4,200),
       4HSPEC(4,200),SIGMA(200)
C
        COMMON TITLE,MPSI,INDUMP,NOSPEC,NPUNCH,A,B,C,XPRINT,XINIT
        COMMON XFINAL,PRNDTL,XLEWIS,DELPSI,XMPS,P,C1,C2,C3,C4,T,U
        COMMON ALFA,WTMOL,WTMIX,RHO,HTOT,HSTAT,HSPEC,USQ,PSI,ISTEP
        COMMON PCNT,DX,JEXIT,Y,EPSI,SG,CPBAR,SIGMA,WU,WALFA,WH,NPSI
        COMMON X,MINIT,MHALF,IPAGE
        COMMON XBAR(9),IXBAR,PHI(200),BZ,C5,C6,MODEL,HEIGHT
C
C
C       INPUT DATA
C
  100   READ (5,1,END=99)  (TITLE(I),I=1,15)
        READ(5,1969) MODEL
        READ(5,2) MPSI,INDUMP,NOSPEC,NPUNCH,IOUT
        IF (MPSI.EQ.0) GO TO 99
        IF (IOUT.NE.0) READ (5,1970)  XBAR
        DO 4 I=1,NOSPEC
        READ (5,3) A(I),B(I),C(I)
    4   CONTINUE
        READ (5,5)  (WTMOL(I),I=1,NOSPEC)
        READ (5,6) XPRINT,XINIT,XFINAL
        READ (5,7) PRNDTL,XLEWIS,DELPSI,XMPS
        READ (5,8) P,HEIGHT
        READ (5,81) C1,C2,C3,C4,C5,C6
        READ (5,9) (T(I),I=1,MPSI)
        READ (5,9) (U(I),I=1,MPSI)
        DO 12 I=1,MPSI
        READ (5,11) (ALFA(J,I),J=1,NOSPEC)
   12   CONTINUE
C
C       COMPUTE MIXTURE MOLECULAR WEIGHTS AND DENSITIES
C
        DO 14 I=1,MPSI
        SUM=0.0
```

```
      DO 13 J=1,NOSPEC
      SUM=SUM+ALFA(J,I)/WTMOL(J)
 13   CONTINUE
      WTMIX(I)=1./SUM
      RHO(I)=(P*WTMIX(I)/49719.1*T(I))
 14   CONTINUE
C
C     COMPUTE ENTHALPIES
C
      DO 16 I=1,MPSI
      SUM=0.0
      DO 15 J=1,NOSPEC
      HSPEC(J,I)=A(J)+(B(J)+C(J)*T(I))*T(I)
      SUM=SUM+HSPEC(J,I)*ALFA(J,I)
 15   CONTINUE
      HSTAT(I)=SUM
      USQ(I)=U(I)*U(I)/50073.
      HTOT(I)=HSTAT(I)+USQ(I)
 16   CONTINUE
C
C     COMPUTE MIXTURE SPECIFIC HEATS
C
      DO 30 I=1,MPSI
      PHI(I)=(U(I)-U(1))/(U(MPSI)-U(1))
      SUM=0.0
      DO 31 J=1,NOSPEC
      IF (C(J)) 40,41,40
 41   SUM=SUM+B(J)*ALFA(J,I)
      GO TO 31
 40   SUM=SUM+(B(J)+2.*C(J)*T(I))*ALFA(J,I)
 31   CONTINUE
      CPBAR=SUM
 30   CONTINUE
C
C     COMPUTE PSI AND FILL UNUSED GRID POINTS
C     WITH FREE STREAM VALUES
C
      DO 17 I=1,200
      XI=I-1
      PSI=XI*DELPSI
 17   CONTINUE
      DO 18 I=MPSI,200
      RHO(I)=RHO(MPSI)
      T(I)=T(MPSI)
      HTOT(I)=HTOT(MPSI)
      U(I)=U(MPSI)
      PHI(I)=PHI(MPSI)
      CPBAR(I)=CPBAR(MPSI)
      WTMIX(I)=WTMIX(MPSI)
      USQ(I)=USQ(MPSI)
      DO 18 J=1,NOSPEC
```

```
      ALFA(J,I)=ALFA(J,MPSI)
   18 CONTINUE
      ISTEP=0
      NPSI=MPSI-1
      JEXIT=0
      X=XINIT
      DX=0.0
      IPACE=0
      IKBAR=1
C
C     OUTPUT OF INPUT
C
      WRITE (6,19)
      WRITE (6,1) (TITLE(I),I=1,15)
      WRITE (6,1969) MODEL
      WRITE (6,2) MPSI,INDUMP,NOSPEC,NPUNCH,IOUT
      IF (IOUT.NE.0) WRITE (6,1970) XBAR
      DO 20 I=1,NOSPEC
      WRITE (6,3) A(I),B(I),C(I)
   20 CONTINUE
      WRITE (6,5) (WTMOL(I),I=1,NOSPEC)
      WRITE (6,6) XPRINT,XINIT,XFINAL
      WRITE (6,7) PRNDTL,XLEWIS,DELPSI,XMPS
      WRITE (6,8) P,HEIGHT
      WRITE (6,81) C1,C2,C3,C4,C5,C6
      WRITE (6,9) (T(I),I=1,MPSI)
      WRITE (6,9) (U(I),I=1,MPSI)
      DO 22 I=1,MPSI
      WRITE (6,11) (ALFA(J,I),J=1,NOSPEC)
   22 CONTINUE
C
C     CHECK INPUT
C
   29 IF (P.LE.0.0)  GO TO 24
      DO 23 I=1,MPSI
      IF (T(I).LE.0.0)  GO TO 24
      DO 23 J=1,NOSPEC
      IF (ALFA(J,I).LT.0.0.OR.ALFA(J,I).GT.1.0)  GO TO 24
   23 CONTINUE
      GO TO 26
   24 WRITE (6,25)
      GO TO 100
   26 CALL PRELIM
      IF (JEXIT.GT.1)  GO TO 100
      CALL SOLVE
      GO TO 26
C
C
C
    1 FORMAT (18A4)
    2 FORMAT (T8,I3,4I10)
```

```
  3     FORMAT (3F10.5)
  5     FORMAT (4F10.3)
  6     FORMAT (3F10.5)
  7     FORMAT (2F10.2,F10.5,F10.1)
  8     FORMAT (F10.1,6F10.5)
 81     FORMAT (6F10.4)
  9     FORMAT (T10,7F9.1)
1969    FORMAT (T10,I1)
1970    FORMAT (9F8.5)
 11     FORMAT (T10,4F10.4)
 19     FORMAT ('1')
 25     FORMAT ('0',//T21,'***** PROGRAM TERMINATED DUE TO ERROR'
     1,' IN P,T,ALFA *****')
 99     STOP
        END
C
C
C       ------------------------------------------------------
C
C
C
        SUBROUTINE PRELIM
C
C       THIS SUBROUTINE COMPUTES THE PARAMETERS NECESSARY TO
C       IMPLANT THE FINITE DIFFERENCE SCHEME.  THE OUTPUT IS ALSO
C       CONTROLLED BY PRELIM
C
        DIMENSION TITLE(18),A(4),B(4),C(4),T(200),U(200),
       1WTMOL(4),WTMIX(200),RHO(200),HTOT(200),HSTAT(200),
       2USQ(200),PSI(200),Y(200),EPSI(200),SG(200),CPBAR(200),
       3WU(200),WALFA(4,200),WH(200),ALFA(4,200),
       4HSPEC(4,200),SIGMA(200)
C
        COMMON  TITLE,MPSI,INDUMP,NOSPEC,NPUNCH,A,B,C,XPRIMT,XINIT
        COMMON  XFINAL,PRNDTL,XLEWIS,DELPSI,XMPS,P,C1,C2,C3,C4,T,U
        COMMON  ALFA,WTMOL,WTMIX,RHO,HTOT,HSTAT,HSPEC,USQ,PSI,ISTEP
        COMMON  PCNT,DX,JEXIT,Y,EPSI,SG,CPBAR,SIGMA,WU,WALFA,WH,NPSI
        COMMON  X,MINIT,MHALF,IPAGE
        COMMON  PHI(200),BZ,C5,C6,MODEL,HEIGHT
        COMMON  XBAR(9),IXBAR
C
C       COMPUTE PHYSICAL COORDINATES
C
        Y(1)=0.0
        DO 1000 I=2,MPSI
        Y(I)=Y(I-1)+DELPSI*(1./RHO(I)/U(I)+1./RHO(I-1)/U(I-1))/2.
 1000   CONTINUE
C
C       COMPUTE TURBULENT VISCOSITY
C
        CALL SHEAR
        IF (MODEL.EQ.1)  CALL SHEAR1 (&1984)
```

```
      IF (MODEL.EQ.3) CALL SHEAR3 (&1984)
      IF(MODEL.EQ.4)  CALL SHEAR4 (&1984)
      IF (MODEL.EQ.5) CALL SHEAR5 (&1984)
C
 1984 ISTEP=ISTEP+1
      DO 2000 I=1,MPSI
      SG(I)=RHO(I)*U(I)*EPSI(I)
 2000 CONTINUE
C
C     DETERMINE WHETHER TO OUTPUT
C
      IF (JEXIT)  300,100,300
  300 CONTINUE
      IF (X.GE.XFINAL) GO TO 101
      IF (IOUT.NE.0) GO TO 102
      IF (XPRINT.LE.PONT) GO TO 100
      PONT=PONT+DX
      GO TO 350
  102 IF (X.LT.XBAR(IXBAR)) GO TO 350
      IXBAR=IXBAR+1
      GO TO 100
  101 JEXIT=2
      NN=1
   60 WRITE (6,55)
      KK=1
      WRITE (6,62)
      IF (NOSPEC.EQ.3) GO TO 65
      WRITE (6,63)
   65 CONTINUE
      DO 70 I=NN,MPSI
      WRITE (6,67) I,HSTAT(I),(HSPEC(J,I),J=1,NOSPEC)
      KK=KK+1
      IF (KK.LT.25) GO TO 70
      NN=I+1
      GO TO 60
   70 CONTINUE
C
C     COMPUTE SIGMA ALFA AS A CHECK SUM
C
  100 DO 80 I=1,MPSI
      SIGMA(I)=0.0
      DO 80 J=1,NOSPEC
      SIGMA(I)=SIGMA(I)+ALFA(J,I)
   80 CONTINUE
      PONT=0.0
      IPAGE=IPAGE+1
C
C     OUTPUT
C
      NN=1
      WRITE (6,210) (TITLE(I),I=1,15)
```

```
      IF (MODEL.EQ.1) WRITE (6,1971)
      IF (MODEL.EQ.3) WRITE (6,1973)
      IF (MODEL.EQ.4) WRITE (6,1974)
      IF (MODEL.EQ.5) WRITE (6,1975)
      WRITE (6,211)
      XDUM=X/HEIGHT
      DXDUM=DX/HEIGHT
      BZDUM=BZ/HEIGHT
      WRITE (6,212) XDUM,P,PRNDTL,XLEWIS,BZDUM,DXDUM,ISTEP,IPAGE
      WRITE (6,5212)
216   WRITE (6,213)
      KK=1
      DO 214 I=NN,MPSI
      YDUM=Y(I)/HEIGHT
      WRITE (6,215) I,PSI(I),U(I),T(I),RHO(I),EPSI(I),PHI(I),
     1YDUM,I
      KK=KK+1
      IF (KK.LT.25) GO TO 214
      NN=I+1
      WRITE (6,5211)
      GO TO 216
214   CONTINUE
      NN=1
      WRITE (6,210) (TITLE(I),I=1,15)
      IF (MODEL.EQ.1) WRITE (6,1971)
      IF (MODEL.EQ.3) WRITE (6,1973)
      IF (MODEL.EQ.4) WRITE (6,1974)
      IF (MODEL.EQ.5) WRITE (6,1975)
      WRITE (6,310) XDUM,IPAGE
      WRITE (6,5212)
325   WRITE (6,311)
      IF (NOSPEC.LE.3) GO TO 315
      WRITE (6,312)
315   CONTINUE
      KK=1
      DO 324 I=NN,MPSI
      WRITE (6,320) I,SIGMA(I),HTOT(I),CPBAR(I),WTMIX(I),
     1(ALFA(J,I),J=1,NOSPEC)
      KK=KK+1
      IF (KK.LT.25) GO TO 324
      NN=I+1
      WRITE (6,5211)
      GO TO 325
324   CONTINUE
C
C     DETERMINE WHETHER INTERMEDIATE DUMP IS REQUIRED
C
      IF (INDUMP.EQ.0) GO TO 330
      NN=1
341   WRITE (6,210) (TITLE(I),I=1,15)
      IF (MODEL.EQ.1) WRITE (6,1971)
```

```
      IF (MODEL.EQ.3) WRITE (6,1973)
      IF (MODEL.EQ.4) WRITE (6,1974)
      IF (MODEL.EQ.5) WRITE (6,1975)
      WRITE (6,62)
      IF (NOSPEC.LE.3) GO TO 335
      WRITE (6,63)
  335 CONTINUE
      KK=1
      DO 340 I=NN,MPSI
      WRITE (6,67) I,HSTAT(I),(HSPEC(J,I),J=1,NOSPEC)
      KK=KK+1
      IF (KK.LT.25) GO TO 340
      NN=I+1
      GO TO 341
  340 CONTINUE
C
C     DETERMINE WHETHER PUNCHED OUTPUT IS REQUIRED
C
  341 IF (NPUNCH.EQ.0) GO TO 350
      IZ=1
      KK=1
      L=1
      JJ=7
  353 IF (JJ.LT.MPSI) GO TO 351
      JJ=MPSI
  351 WRITE (7,352) IZ,ISTEP,KK,(T(LL),LL=L,JJ)
      IF (JJ.EQ.MPSI) GO TO 450
      L=JJ+1
      JJ=JJ+7
      KK=KK+1
      GO TO 353
  450 CONTINUE
      IZ=2
      KK=1
      L=1
      JJ=7
  452 IF (JJ.LT.MPSI) GO TO 451
      JJ=MPSI
  451 WRITE (7,352) IZ,ISTEP,KK,(U(LL),LL=L,JJ)
      IF (JJ.EQ.MPSI) GO TO 550
      L=JJ+1
      JJ=JJ+7
      KK=KK+1
      GO TO 452
  550 CONTINUE
      IZ=3
      DO 552 I=1,MPSI
      KK=I
      WRITE (7,551) IZ,ISTEP,KK,(ALFA(J,I),J=1,NOSPEC)
  552 CONTINUE
C
```

```
C
C
 55    FORMAT ('1',T9,'***** DUMP OF MIXTURE AND SPECIES STATIC',
      1' ENTHALPIES AT LAST STEP DUE TO NORMAL PROGRAM',
      2' TERMINATION *****')
 62    FORMAT (//T2,'PT.',T10,'STATIC ENTHALPY',T36,'HALPHA(1)',
      1T56,'HALPHA(2)',T76,'HALPHA(3)')
 63    FORMAT ('+',T96,'HALPHA(4)')
 67    FORMAT ('0',T2,I3,1P5E20.6)
210    FORMAT ('1',T25,18A4)
211    FORMAT ('0',T14,'X/A',T32,'PRESSURE',T48,'PRANDTL',T60,
      1'LEWIS',T75,'BZ/A',T92,'STEP SIZE',T107,'STEPS',T115,
      2'PAGE')
212    FORMAT ('0',1P2E20.6,T50,0PF4.2,T61,F4.2,T71,1PE10.4,T82,
      1E20.6,I9,I6)
5212   FORMAT (//)
213    FORMAT ('+',T4,'POINT',T17,'PSI',T30,"VELOCITY',T43,
      1'TEMPERATURE',T61,'DENSITY',T75,'VISCOSITY',T92,'PHI',
      2T108,'Y/A',T116,'POINT')
215    FORMAT ('0',T4,I5,1P7E15.4,2X,I5)
5211   FORMAT ('1')
310    FORMAT ('0',T4,'X/A',1PE12.6,T112,I5)
311    FORMAT ('+',T4,'POINT',T17,'SIGMA',T28,'ENTHALPY',T44,
      1'CPBAR',T59,'WTMIX',T73,'ALPHA(1)',T88,'ALPHA(2)',
      2T103,'ALPHA(3)')
312    FORMAT ('+',T103,'ALPHA(4)')
320    FORMAT ('0',T4,I5,F13.4,1P6E15.4)
352    FORMAT (I1,2I3,T10,7F9.1)
351    FORMAT (I1,2I3,T10,4F10.4)
1971   FORMAT ('+',T85,'PRANDTL I')
1973   FORMAT ('+',T85,'MODIFIED FERRI')
1974   FORMAT ('+',T85,'MODIFIED SCHETZ')
1975   FORMAT ('+',T85,'MODIFIED ALPINIERI')
350    RETURN
       END
C
C      ------------------------------------------------------------
C
C
       SUBROUTINE SOLVE
C
C      THIS SUBROUTINE SOLVES THE FINITE DIFFRENCE EQUATIONS.
C
       DIMENSION TITLE(18),A(4),B(4),C(4),T(200),U(200),
      1WTMOL(200),WTMIX(200),RHO(200),HTOT(200),HSTAT(200),
      2USQ(200),PSI(200),Y(200),EPSI(200),SG(200),CPBAR(200),
      3WU(200),WALFA(4,200),WH(200),ALFA(4,200),HSPEC
      4(4,200),SIGMA(200)
C
       COMMON TITLE,MPSI,INDUMP,NOSPEC,NPUNCH,A,B,C,XPRINT,XINIT
```

```
      COMMON XFINAL,PRNDTL,XLEWIS,DELPSI,XMPS,P,C1,C2,C3,C4,T,U
      COMMON ALFA,WTMOL,WTMIX,RHO,HTOT,HSTAT,HSPEC,USQ,PSI,ISTEP
      COMMON PONT,DX,JEXIT,Y,EPSI,SG,CPBAR,SIGMA,WU,WALFA,WH,NPSI
      COMMON X,MINIT,MHALF,IPAGE
      COMMON PHI(200),BZ,C5,C6,MODEL,HEIGHT
      COMMON XBAR(9),IXBAR
C
C     DETERMINE STEP SIZE
C
      G1=1.
      G2=1./PRNDTL
      G3=XLEWIS/PRNDTL
      G4=(PRNDTL-1.)/PRNDTL
      G5=(XLEWIS-1.)/PRNDTL
      FACTOR=AMAX1(G1,G2,G3,G4,G5)
      XD=FACTOR*6.*RHO(1)*U(1)*EPSI(1)
      DO 1 I=2,NPSI
      DIV=SG(I+1)+SG(I)+SG(I)+SG(I-1)
      DDX=FACTOR*DIV*1.5
      XD=AMAX1(XD,DDX)
    1 CONTINUE
      DX=(DELPSI*DELPSI)/(XD*XMPS)
      DX=AMIN1(DX,4.5E-4)
      XMU=DX/DELPSI/DELPSI/XMPS
C
C     SOLVE EQUATIONS AT THE WALL
C
      WU(1)=U(1)+2.*XMU*SG(1)*(U(2)-U(1))
      SUM=0.0
      DO 2 J=1,NOSPEC
      WALFA(J,1)=ALFA(J,1)+XMU*SG(1)*G3*(ALFA(J,2)-ALFA(J,1))*2.
      SUM=SUM+HSPEC(J,1)*(ALFA(J,2)-ALFA(J,1))
    2 CONTINUE
      T1=SUM*G5
      T2=G4*(USQ(2)-USQ(1))
      T3=G2*(HTOT(2)-HTOT(1))
      WH(1)=HTOT(1)+2.*XMU*SG(1)*(T1+T2+T3)
C
C     SOLVE EXPLICIT EQUATIONS
C
      DO 50 I=2,NPSI
      T4=0.5*(SG(I)+SG(I+1))
      T5=0.5*(SG(I)+SG(I-1))
      WU(I)=U(I)+XMU*(T4*U(I+1)-(T4+T5)*U(I)+T5*U(I-1))
      IF (PRNDTL.GT.0.95.AND.PRNDTL.LT.1.05) GO TO 20
      T6=T4*USQ(I+1)-(T4+T5)*USQ(I)+T5*USQ(I-1)
      T66=G4*XMU*T6
      GO TO 21
   20 T66=0.0
   21 IF (XLEWIS.GT.0.95.ANDXLEWIS.LT.1.05) GOTO 30
      T20=0.0
```

```
      T21=0.0
      T22=0.0
      T23=0.0
      DO 22 J=1,NOSPEC
      T20=T20+.5*(HSPEC(J,I)+HSPEC(J,I+1))*ALFA(J,I+1)
      T21=T21+.5*(HSPEC(J,I)+HSPEC(J,I-1))*ALFA(J,I-1)
      T22=T22+.5*(HSPEC(J,I)+HSPEC(J,I+1))*ALFA(J,I)
      T23=T23+.5*(HSPEC(J,I)+HSPEC(J,I-1))*ALFA(J,I)
 22   CONTINUE
      T202=G5*XMU*T4*T20
      T212=G5*XMU*T5*T21
      T222=G5*XMU*T4*T22
      T232=G5*XMU*T5*T23
      T77=T202+T212+T222-2.*T222-T232
      GO TO 32
 30   T77=0.0
 32   WH(I)=HTOT(I)+XMU*G2*(T4*HTOT(I+1)-(T4+T5)*HTOT(I)+T5*
     1HTOT(I-1))+T66+T77
      DO 33 J=1,NOSPEC
      WALFA(J,I)=ALFA(J,I)+G3*XMU*(T4*ALFA(J,I+1)-(T4+T5)*
     1ALFA(J,I)+T5*ALFA(J,I-1))
 33   CONTINUE
 50   CONTINUE
      DO 51 I=1,MPSI
      U(I)=WU(I)
      PHI(I)=(U(I)-U(1))/(U(MPSI)-U(1))
      HTOT(I)=WH(I)
      USQ(I)=U(I)*U(I)/50073.
      DO 51 J=1,NOSPEC
      ALFA(J,I)=WALFA(J,I)
 51   CONTINUE
C
C     COMPUTE TEMPERATURE, DENSITY, MOLECULAR WEIGHT, ENTHALPIES
C
      CALL SUPP
C
      DO 60 I=1,MPSI
      IF (T(I).LE.0.0) GO TO 66
      DO 60 J=1,NOSPEC
      IF (ALFA(J,I).LT.0.0.OR.ALFA(J,I).GT.1.0) GO TO 66
 60   CONTINUE
      GO TO 61
 66   X=X+DX
      WRITE (6,67) X,DX,ISTEP
      JEXIT=2
      PCNT=XPRINT
      GO TO 2000
 61   IF (JEXIT)3,4,3
C
C     SET HALVING CODE FIRST TIME THRU
C
```

```
      JEXIT=1
      MINIT=MPSI
      MHALF=MPSI+MPSI-1
    3 X=X+DX
      IF (MPSI-MHALF) 999,1500,1500
C
C     TEST FOR ZERO SLOPE AT EDGE
C
  999 IF (ABS(U(NPSI)-U(MPSI))/U(MPSI)-0.001) 1011,1011,1004
 1011 IF (ABS(HTOT(NPSI)-HTOT(MPSI))/HTOT(MPSI)-0.001)
     1  1002,1002,1004
 1002 DO 1003 J=1,NOSPEC
      IF (ABS(ALFA(J,NPSI)-ALFA(J,MPSI))-0.0005) 1003,1003,1004
 1003 CONTINUE
      GO TO 2000
C
C     EXPAND MESH
C
 1004 MPSI=MPSI+1
      NPSI=NPSI-1
      GO TO 2000
C
C     HALVE MESH
C
 1500 JEXIT=0
      DELPSI=DELPSI+DELPSI
      DO 1600 I=1,MINIT
      K=I+I-1
      U(I)=U(K)
      HTOT(I)=HTOT(K)
      USQ(I)=USQ(K)
      PHI(I)=PHI(K)
      WTMIX(I)=WTMIX(K)
      RHO(I)=RHO(K)
      T(I)=T(K)
      HSTAT(I)=HSTAT(K)
      CPBAR(I)=CPBAR(K)
      DO 1650 J=1,NOSPEC
      HSPEC(J,I)=HSPEC(J,K)
      ALFA(J,I)=ALFA(J,K)
 1650 CONTINUE
      XI=I-1
      PSI(I)=XI*DELPSI
 1600 CONTINUE
      MPSI=MINIT
      NPSI=MPSI-1
      DO 1700 I=MINIT,200
      U(I)=U(MPSI)
      PHI(I)=PHI(MPSI)
      HTOT(I)=HTOT(MPSI)
      WTMIX(I)=WTMIX(MPSI)
```

```
      USQ(I)=USQ(MPSI)
      RHO(I)=RHO(MPSI)
      T(I)=T(MPSI)
      HSTAT(I)=HSTAT(MPSI)
      CPBAR(I)=CPBAR(MPSI)
      XI=I-1
      PSI(I)=XI*DELPSI
      DO 1700 J=1,NOSPEC
      ALFA(J,I)=ALFA(J,MPSI)
      HSPEC(J,I)=HSPEC(J,MPSI)
 1700 CONTINUE
   67 FORMAT ('1',T6,'NEGATIVE SPECIES OR TEMPERATURE OBTAINED.'
     1,' PROGRAM TERMINATED.',1P2E20.6,I10)
 2000 RETURN
      END
C
C
C     ------------------------------------------------------------
C
C
      SUBROUTINE SUPP
C
C     THIS IS A COMPLEMENTARY SUBROUTINE TO SUBROUTINE SOLVE.
C     SUPP TAKES VALUES OF TOTAL ENTHALPY, VELOCITY AND MASS
C     FRACTIONS FROM SOLVE AND COMPUTES STATIC ENTHALPY, SPECIES
C     ENTHALPY, AVERAGE CP, MIXTURE MOLECULAR WEIGHT, DENSITY AND
C     TEMPERATURE @ EACH PSI GRID POINT.
C
      DIMENSION TITLE(18),A(4),B(4),C(4),T(200),U(200),
     1WTMOL(4),WTMIX(200),RHO(200),HTOT(200),HSTAT(200),
     2USQ(200),PSI(200),Y(200),EPSI(200),SG(200),CPBAR(200),
     3WU(200),WALFA(4,200),WH(200),ALFA(4,200),
     4HSPEC(4,200),SIGMA(200)
C
      COMMON TITLE,MPSI,LNDUMP,NOSPEC,NPUNCH,A,B,C,XPRINT,XINIT
      COMMON XFINAL,PRNDTL,XLEWIS,DELPSI,XMPS,P,C1,C2,C3,C4,T,U
      COMMON ALFA,WTMOL,WTMIX,RHO,HTOT,HSTAT,HSPEC,USQ,PSI,ISTEP
      COMMON PCNT,DX,JEXIT,Y,EPSI,SG,CPBAR,SIGMA,WU,WALFA,WH,NPSI
      COMMON X,MINIT,MHALF,IPAGE
      COMMON PHI(200),PZ,C5,C6,MODEL,HEIGHT
      COMMON XBAR(9),IXBAR
C
C     CALCULATE MIXTURE STATIC ENTHALPY AND TEMPERATURE
C
      DO 1 I=1,MPSI
      HSTAT(I)=HTOT(I)-USQ(I)
      E1=0.0
      E2=0.0
      E3=0.0
      DO 2 J=1,NOSPEC
      E1=E1+A(J)*ALFA(J,I)
```

```
      E2=E2+B(J)*ALFA(J,I)
      E3=E3+C(J)*ALFA(J,I)
 2    CONTINUE
      IF (E3.EQ.0.0) GO TO 3
      T(I)=(-E2+SQRT(E2*E2-4.*E3*(E1-HSTAT(I))))/(2.*E3)
      GO TO 1
 3    T(I)=(HSTAT(I)-E1)/E2
 1    CONTINUE
C
C     COMPUTE MIXTURE MOLECULAR WEIGHT, CPBAR,DENSITY
C     AND SPECIES ENTHALPIES
C
      DO 5 I=1,MPSI
      SUM=0.0
      DSUM=0.0
      DO 6 J=1,NOSPEC
      HSPEC(J,I)=A(J)+(B(J)*T(I))*T(I)
      SUM=SUM+ALFA(J,I)/WTMOL(J)
      IF (C(J)) 40,41,40
 41   DSUM=DSUM+B(J)*ALFA(J,I)
      GO TO 6
 40   DSUM=DSUM+(B(J)+2.*C(J)*T(I))*ALFA(J,I)
 6    CONTINUE
      CPBAR(I)=DSUM
      WTMIX(I)=SUM
      RHO(I)=(P*WTMIX(I))/(49719.1*T(I))
 5    CONTINUE
      RETURN
      END
C
C
C     ------------------------------------------------------------
C
C
      SUBROUTINE SHEAR
C
C     THIS SUBROUTINE MODELS THE TURBULENT TRANSPORT MECHANISM
C     AND COMPUTES EDDY VISCOSITY THROUGHOUT MPSI GRID POINTS.
C
      DIMENSION TITLE(18),A(4),B(4),C(4),T(200),U(200),
     1WTMOL(4),WTMIX(200),RHO(200),HTOT(200),HSTAT(200),
     2USQ(200),PSI(200),Y(200),EPSI(200),SG(200),CPBAR(200),
     3WU(200),WALFA(4,200),WH(200),ALFA(4,200),
     4HSPEC(4,200),SIGMA(200)
C
      COMMON TITLE,MPSI,INDUMP,NOSPEC,NPUNCH,A,B,C,XPRINT,XINIT
      COMMON XFINAL,PRNDTL,XLEWIS,DELPSI,XMPS,P,C1,C2,C3,C4,T,U
      COMMON ALFA,WTMOL,WTMIX,RHO,HTOT,HSTAT,HSPEC,USQ,PSI,ISTEP
```

```
      COMMON PONT,DX,JEXIT,Y,EPSI,SG,CPBAR,SIGMA,WU,WALFA,WH,NPSI
      COMMON X,MINIT,MHALF,IPAGE
      COMMON PHI(200),BZ,C5,C6,MODEL,HEIGHT
      COMMON XBAR(9),IXBAR
C
C     COMPUTE MIXING ZONE THICKNESS
C
      IF (U(MPSI).LT.U(1)) GO TO 5
      WUMAX=.95*U(MPSI)
      WUMIN=1.05U(1)
      DO 1 I=1,MPSI
      IMAX=I
      IF (U(I).GE.WUMAX) GO TO 2
 1    CONTINUE
 2    CONTINUE
      DO 3 I=1,MPSI
      IMIN=I
      IF (U(I).GE.WUMIN) GO TO 4
 3    CONTINUE
 5    WUMAX=1.05*U(MPSI)
      WUMIN=.95*U(1)
      DO 6 I=1,MPSI
      IMAX=I
      IF (U(I).LE.WUMAX) GO TO 7
 6    CONTINUE
 7    CONTINUE
      DO 8 I=1,MPSI
      IMIN=I
      IF (U(I).LE.WUMIN) GO TO 4
 8    CONTINUE
 4    CONTINUE
      DUM2=WUMIN-U(IMIN)
      DUM3=U(IMIN-1)-U(IMIN)
      DUM4=Y(IMIN-1)-Y(IMIN)
      YMIN=DUM2*DUM4/DUM3+Y(IMIN)
      DUM5=WUMAX-U(IMAX)
      DUM6=U(IMAX-1)-U(IMAX)
      DUM7=Y(IMAX-1)-Y(IMAX)
      YMAX=DUM5*DUM7/DUM6+Y(IMAX)
      BZ=YMAX-YMIN
      RETURN
C
      ENTRY SHEAR1 (*)
C
C     MODEL USED : ************ PRANDTL I ************
C
      EPSI(1)=0.0
      DO 11 I=2,MPSI
      DFDY=ABS((U(I+1)-U(I-1))/(2.*DELPSI))
      EPSI(I)=C1*C1*BZ*BZ*RHO(I)*RHO(I)*U(I)*DYDY
 11   CONTINUE
```

```
 99     RETURN 1
 100    RETURN
C
       ENTRY SHEAR3 (*)
C
C      MODEL USED : ************ MODIFIED FERRI ************
C
       RUMAX=RHO(1)*U(1)
       RUMIN=RHO(1)*U(1)
       DO 13 I=2,MPSI
       RUX=RHO(I)*U(I)
       RUMAX=AMAX1(RUMAX,RUX)
       RUMIN=AMIN1(RUMIN,RUX)
 13    CONTINUE
       DELRU=RUMAX-RUMIN
       VISC=C3*BZ*DELRU
       DO 14 I=1,MPSI
       EPSI(I)=VISC
 14    CONTINUE
 119   RETURN 1
 120   RETURN
C
       ENTRY SHEAR4 (*)
C
C      MODEL USED : ************ SCHETZ ************
C
       DUM=0.0
       DO 15 I=1,MPSI
       DUM=DUM+ABS((RHO(MPSI)*U(MPSI)/RHO(I)/U(I))-1.)
 15    CONTINUE
       VISC=DUM*DELPSI*C4
       DO 21 I=1,MPSI
       EPSI(I)=VISC
 21    CONTINUE
 129   RETURN 1
 130   RETURN
C
       ENTRY SHEAR5 (*)
C
C      MODEL USED : ************ MODIFIED ALPINIERI ************
C
       RATRO=RHO(MPSI)/RHO(1)
       RATMOM=(RHO(MPSI)*U(MPSI)*U(MPSI))/(RHO(1)*U(1)*U(1))
       VISC=C5*BZ*RHO(1)*U(1)*(RATRO+RATMOM)
       DO 16 I=1,MPSI
       EPSI(I)=VISC
 16    CONTINUE
 139   RETURN 1
 140   RETURN
       END
```

BIBLIOGRAPHY

1. Abramovich, G. N., The Theory of Turbulent Jets. MIT Press, Cambridge, Mass. (1963)

2. Pai, S. I., Fluid Dynamics of Jets. D. van Nostrand Company, Inc. (1954)

3. Schlichting, H., Boundary Layer Theory. Sixth Edition, Chapter XXIV, McGraw-Hill Book Co., New York. (1968)

4. Kleinstein, G., "Mixing in Turbulent Axially Symmetric Free Jets." Journal of Spacecraft. 1, 4, 403-408. (1964)

5. Forstall, W., Jr., Shapiro, A. H., "Momentum and Mass Transfer in Coaxial Jets." Journal of Applied Mechanics, Vol. 17, pp. 399-408. (1950)

6. Tollmien, W., "Berechnung turbulenter Ausbreitungs-vor-gange." ZAMM, Vol. 6, pp. 2458-2478. (1926); also available in NACA TM 1085 (1945)

7. Prandtl, L., "Uber die Ausgebildete Turbulenz." ZAMM, Vol. 5, pp. 136. (1925)

8. Kuethe, A. M., "Investigation of the Turbulent Mixing Regions Formed by Jets." Journal of Applied Mechanics, Vol. 2, No. 3. (1935)

9. Gortler, H., "Berechnung von Aufgaben der frein Turbulenz auf Grund eines neuen Naherungsansatzes". ZAMM, Vol 22. (1942)

10. Prandtl, L., "Bemerkungen zur Theorie der freien Turbulenz." ZAMM, Vol. 22, 241. (1942)

11. Howarth, L., "Concerning the Effect of Compressibility on Laminar Boundary Layers and Their Separation." Proceedings of the Royal Society. (London). 194, 16. (1948)

12. Mager, A., "Transformation of the Turbulent Boundary Layer." Journal of Aeronautical Sciences. Vol. 25, pp. 305-311. (1958)

13. Bauer, R. C., "An Analysis of Two-Dimensional Laminar and Compressible Mixing." AIAA Journal, 4, 3, 392-395. (March 1966)

14. Channapragada, R. S., Voolley, J. P., "Turbulent Mixing of Parallel Compressible Non-Isoenergetic Streams." Astronautica Acta, 13, 4, 341-352. (1967)

15. Korst, H. H., Tripp, W., "The Pressure on a Blunt Trailing Edge Separating Two Supersonic Two-Dimensional Air Streams of Different Mach Number and Stagnation Pressure but Identical Stagnation Temperature." Proceedings of the Fifth Midwestern Conference on Fluid Mechanics. (1957)

16. Channapragada, R. S., "Compressible Jet Spread Parameter for Mixing Zone Analysis." AIAA Journal, 1, 9, 2188-2189. (September 1963)

17. Woolley, J. P., "Theoretical and Experimental Study of Supersonic Mixing of Turbulent Dissimilar Streams." NASA CR-66893. (1969)

18. Laufer, J., "Turbulent Shear Flow of Variable Density." AIAA Journal, 7, 4, 706-713. (April 1969)

19. Warren, W. R., "An Analytical and Experimental Study of Compressible Free Jets." Princeton University Department of Aeronautical Engineering. Report 381. (1957)

20. Donaldson, C. duP., Gray, K. F., "Theoretical and Experimental Investigation of the Compressible Free Mixing of Two Dissimilar Gases." AIAA Journal, 4, 11, 2017-2025. (1966)

21. Smoot, L. D., Purcell, W. E., "Model for Mixing of a Compressible Free Jet with a Moving Environment." AIAA Journal, 5, 11, 2049-2052. (1967)

22. Peters, C. E., "A Model for the Free Turbulent Eddy Viscosity." AEDC-TR-65-209. (November 1965)

23. Lamb, J. P., "The Development of Free Turbulent Shear Layers." AEDC-TR-65-184. (November 1965)

24. Lamb, J. P., Bass, R. L., "Some Correlations of Theory and Experiment for Developing Turbulent-Free Shear Layers." Journal of Basic Engineering, Transactions ASME, pp. 572-579. (December 1968)

25. Korst, H. H., Chow, W. L., "On the Correlation of Analytical and Experimental Free Shear Layer Similarity Profiles by Spread Rate Parameters." Journal of Basic Engineering, Transactions ASME, pp. 377-382. (September 1971)

26. Wygnanski, I., Hawaleshka, O., "Effect of Upstream Profile on the Free Mixing of Jets with Ambient Fluid." AIAA Journal, 5, 6, 1057-1062. (June 1967)

27. Korst, H. H., Chow, W. L., "Non-Isoenergetic Turbulent (Pr_t = 1) Jet Mixing Between Two Compressible Streams at Constant Pressure." ME-TN-393-2. Engineering Experiment Station, University of Illinois. (1965)

28. Lamb, J. P., "An Approximate Theory for Developing Turbulent Free Shear Layers." Journal of Basic Engineering, Transactions ASME, Series D. Vol. 89, pp. 633-642. (1967)

29. Pai, S. I., "On the Turbulent Jet Mixing of Two Gases at Constant Temperature." Journal of Applied Mechanics, Transactions ASME, Vol. 22, pp. 41-47. (1955)

30. Baker, R. L., Tao, L. N., Weinstein, H. "The Mixing of Two Parallel Streams of Dissimilar Fluids. Part I: Analytical Development." ASME Paper 70 WA/APM 37, 38, 2, 301, 309. (1971)

31. Zelazny, S. W., Morgenthaler, J. H., Herendeen, D. L., "Reynolds Momentum and Mass Transport in Axi-symmetric Coflowing Streams." Proceedings of the 1970 Heat Transfer and Fluid Mechanics Institute. Stanford University Press. (1970)

32. Carslaw, H. S., Jaeger, J. C., Conduction of Heat in Solids. Oxford: Clarendon Press. (1959)

33. Libby, P. A., "Theoretical Analysis of Turbulent Mixing of Reactive Cases with Application to Supersonic Combustion of Hydrogen". ARS Journal, Vol. 32, pp. 388-396. (March 1962)

34. Ferri, A., Libby, P. A., Zakkay, J., "Theoretical and Experimental Investigation of Supersonic Combustion." Third Congress, International Council of the Aeronautical Sciences. Spartan Books. Baltimore, Maryland. (1964)

35. Alpinieri, L. J., "Turbulent Mixing of Coaxial Jets." AIAA Journal, 2, 9, 1560-1567. (March 1965)

36. Schetz, J. A., Supersonic Diffusion Flames, Supersonic Flow, Chemical Processes and Radiative Transfer. AGARD. Pergamon Press Book. (1964)

37. Weinstein, H., Todd, C. A., "Analysis of Mixing of Coaxial Streams of Dissimilar Fluids Including Energy Generation Terms." NASA TN D-2123. (March 1964)

38. Edelman, R., Fortune, O., "An Analysis of Mixing and Combustion in Ducted Flows." AIAA pre-print, 68-114. (1968)

39. Peters, C. E., Phares, W. J., Cunningham, T. H. M., "Theoretical and Experimental Studies of Ducted Mixing and Burning of Coaxial Streams." AIAA pre-print, 69-85. (1969)

40. Craya, A., Curtet, R., "On the Spreading of a Confined Jet." Comtes-rendus Academie des Sciences, Vol. 241, pp. 621-622. Paris. (1955)

41. Curtet, R., "Confined Jets and Recirculation Phenomena with Cold Air." Combustion and Flame. (London). Vol. 2, No. 4 (December 1958)

42. Curtet, R., "On the Flow of an Enclosed Jet." (In French). Translation by: U.S. Department of Commerce, Office of Technical Services, Joint Publications Research Service. "On Confined Jet Flow." DO-49-186-003-03535 JPRS; R-2934-D. (January 1963)

43. Curtet, R., Ricou, F. P., "On the Tendency of Self-Preservation in Axi-symmetric Ducted Jets." Journal of Basic Engineering, Transactions ASME. (December 1966)

44. Curtet, R., Barchilon, M., "Some Details of the Structure of an Axi-symmetric Confined Jet with Backflow." Journal of Basic Engineering, Transactions ASME. (December 1966)

45. Hill, P. G., "Turbulent Jets in Ducted Streams." Journal of Fluid Mechanics, Vol. 22. (1965)

46. Hill, P. G., "Incompressible Jet Mixing in Converging-Diverging Axi-Symmetric Ducts." Journal of Basic Engineering, Transactions ASME. (1966)

47. Dealy, J. M., "The Confined Circular Jet with Turbulent Source." Symposium on Fully Separated Flows. ASME. New York. (November 1960)

48. Trapani, R. D., "An Experimental Study of Bounded and Confined Jets." Advances in Fluidics. ASME, pp. 1-13. (1967)

49. Peters, C. E., Cunningham, T. H. M., "Further Experiments on Mixing of Bounded Coaxial Systems." AEDC-TR-68-136. (October 1968)

50. Peters, C. E., "Turbulent Mixing and Burning of Coaxial Streams Inside a Duct of Arbitrary Shape." AEDC-TR-68-220. (January 1969)

51. Emmons, D. L., "Analysis of the Turbulent Mixing Between a Reactive Gas-Particle Rocket Exhaust and a Confined Airstream." AIAA Paper No. 65-609. (June 1965)

52. Cohen, L. S., "An Analytical Study of the Mixing and Nonequilibrium Chemical Reaction of Ducted Compressible Streams." AIAA Paper No. 66-617. Second Propulsion Joint Specialist Conference. Colorado Springs, Colorado. (June 1966)

53. Ghia, K. N., Torda, T. P., Lavan, Z., "Turbulent Mixing in the Initial Region of Heterogeneous Axi-symmetric Coaxial Confined Jets." NASA CR-1615. (March 1970)

54. Ruden, P., "Turbulence Ausbreitungsvorgange im Freistrahl." Die Naturwiss, Vol. 21, Heft 21/23, pp. 375-378. (May 1933)

55. Keagy, W. R., Weller, A. E., "A Study of Freely Expanding Inhomogeneous Jets." Proceedings of the 1949 Heat Transfer and Fluid Mechanics Institute. ASME, pp. 89-98. New York. (1949)

56. Corrsin, S., Uberoi, M. S., "Further Experiments on the Flow and Heat Transfer in a Heated Turbulent Air Jet." NACA Report 998. (1950)

57. Yates, C. L., "Two-Dimensional Supersonic Mixing of H_2 and Air Near a Wall." NASA CR-1793. (March 1971)

58. Zakkay, V., Krause, E., Woo, S. D. L., "Turbulent Transport Properties for Axi-symmetric Heterogeneous Mixing." AIAA Journal, 2, 11, 1939-1947. (1964)

59. Abramovich, G. N., Yakovlevsky, O. V., Smirnova, A. N., Krasheninnikov, S. Yu., "An Investigation of the Turbulent Jets of Different Gases in a General Stream." Astronautica Acta, 14, 3, 229-240. (1969)

60. Van Driest, E. R., "Turbulent Boundary Layer in Compressible Fluids." J. Aeronautical Sciences, 18, 3, 145-153. (1951)

61. Boussinesq, T. V., Mem. pres. Acad. Sci., Third Edition, XXIII, 46, Paris. (1877)

62. Bird, R. B., Stewart, W. E., Lightfoot, E. N., Transport Phenomena. John Wiley & Sons, Inc. (1960)

63. Richtmyer, R. D., Morton, K. W., Difference Methods for Initial Value Problems. Second Edition, John Wiley & Sons, Inc. (1967)

64. Isaacson, E., Keller, H. B., Analysis of Numerical Methods. John Wiley & Sons, Inc. (1966)

65. Strang, W. G., "Accurate Partial Difference Methods II: Non-Linear Problem." Numer. Math., Vol. 6, p. 37. (1964)

66. Bradshaw, P., Ferris, D. H., Atwell, N. P., "Calculation of Boundary Layer Development Using the Turbulent Energy Equation." J. Fluid Mechanics, 28, 3, 593-616. (1967)

67. Lee, S. C., Harsha, P. T., "The Use of Turbulent Kinetic Energy in Free Mixing Studies." AIAA pre-print, 69-683. (1969)

68. Nee, V. W., Kovasznay, L. S. G., "Simple Phenomenological Theory of Turbulent Shear Flows." Physics of Fluids, 12, 3, 473-84. (1969)

69. Schetz, J. A., "Unified Analysis of Turbulent Jet Mixing." NASA CR-1382. (1969)

70. Ting, L., Libby, P. A., "Remarks on the Eddy Viscosity in Compressible Mixing Flows." J. Aerospace Sci, Vol. 27, No. 10, pp. 797-798. (1960)

71. Eggers, J. M., "Velocity Profiles and Eddy Viscosity Distributions Downstream of a Mach 2.2 Nozzle Exhausting to Quiescent Air." NASA TN-3601. (1966)

72. Ragsdale, R. G., Edwards, O. J., "Data Comparisons and Photographic Observations of Coaxial Mixing of Disimilar Gases at Nearly Equal Stream Velocities." NASA TND-3131. (1965)

73. Ragsdale, R. G., Edwards, O. J., "Turbulent Coaxial Mixing of Dissimilar Gases at Nearly Equal Stream Velocities." NASA TMX-52082. (1965)

74. Hokenson, G. J., Schetz, J. A., "Free Turbulent Mixing in Axial Pressure Gradients." Paper No. 72-WA/APM-31. (1972)

75. McNair, H. M., Bonelli, E. J., Basic Gas Chromatography. 5th Edition, Berkeley, California; Varian Aerograph publications. (1969)

76. Horn, R. C., Lard, E. W., "Separation and Determination of Argon, Oxygen and Nitrogen by Gas Chromatography." Analytical Chemistry, Vol. 32, No. 7, pp. 878-879. (June 1960)

77. Heylmun, G. W., "Improved Analysis of Argon-Oxygen-Nitrogen Mixtures by Gas Chromatography." Journal of Gas Chromatography, pp. 82-84. (March 1965)

78. Present, R. D., Kinetic Theory of Gases. McGraw-Hill Book Co. (1958)

79. Shapiro, A. H., The Dynamics and Thermodynamics of Compressible Fluid Flow. The Ronald Press Co. (1953)

80. Morgenthaler, J. H., "Supersonic Mixing of Hydrogen and Air." NASA CR-747. (1967)

81. Eggers, J. M., Torrence, M. G., "An Experimental Investigation of the Mixing of Compressible Air Jets in an Coaxial Configuration." NASA TN D-5315. (July 1965)

82. Torrence, M. G., "Concentration Measurements of an Injected Gas in a Supersonic Stream." NASA TN D-3860. (1967)

83. Masson, B. S., "Diffusive Separation of a Gas Mixture Approaching a Sampling Probe." Tech. Rep. HE-150-206 Inst. Eng. Res., University of California. (October 1962)

84. Chow, R. R., "On the Separation Phenomenon of Binary Gas Mixture in an Axi-symmetric Jet." Rep. No. HE-150-175. Inst. Eng. Res., University of California. (November 1959)

85. Reis, V. H., Fenn, J. B., "Separation of Gas Mixtures in Supersonic Jets." J. Chem. Phys., Vol. 39, No. 12, 3240-3250. (December 1963)

86. Keenan, J. H., Kaye, J., Gas Tables. John Wiley & Sons, Inc. (1966)

BIOGRAPHICAL SKETCH

Seyfeddin Tanrikut was born July 15, 1947 in Istanbul, Turkey. In June 1964, he was graduated from Robert Academy, Istanbul, Turkey, majoring in sciences. In June 1968, he received the degree of BS in Mechanical Engineering from Robert College in Istanbul. In September 1968, he enrolled in the Graduate School of the University of Florida and in Auguat 1970, received the degree of MS in Engineering. He is a graduate assistant in the Mechanical Engineering Department and until the present time, has pursued his work toward the degree of Ph.D. in Engineering.

He is married to former Yasar Balkose, and has a daughter, Cigdem.

I certify that I have read this study and that in my opinion it conforms to acceptable standards of scholarly presentation and is fully adequate, in scope and quality, as a dissertation for the degree of Doctor of Philosophy.

R. B. Gaither, Chairman
Professor of Mechanical Engineering

I certify that I have read this study and that in my opinion it conforms to acceptable standards of scholarly presentation and is fully adequate, in scope and quality, as a dissertation for the degree of Doctor of Philosophy.

V. P. Roan, Co-Chairman
Associate Professor of Mechanical Engineering

I certify that I have read this study and that in my opinion it conforms to acceptable standards of scholarly presentation and is fully adequate, in scope and quality, as a dissertation for the degree of Doctor of Philosophy.

R. A. Gater
Associate Professor of Mechanical Engineering

I certify that I have read this study and that in my opinion it conforms to acceptable standards of scholarly presentation and is fully adequate, in scope and quality, as a dissertation for the degree of Doctor of Philosophy.

C. K. Hsieh
Associate Professor of Mechanical Engineering

I certify that I have read this study and that in my opinion it conforms to acceptable standards of scholarly presentation and is fully adequate, in scope and quality, as a dissertation for the degree of Doctor of Philosophy.

U. H. Kurzweg
Associate Professor of Engineering Science, Mechanics and Aerospace

I certify that I have read this study and that in my opinion it conforms to acceptable standards of scholarly presentation and is fully adequate, in scope and quality, as a dissertation for the degree of Doctor of Philosophy.

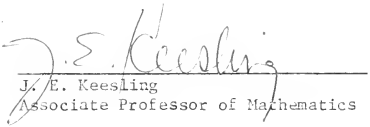

J. E. Keesling
Associate Professor of Mathematics

This dissertation was submitted to the Dean of the College of Engineering and to the Graduate Council, and was accepted as partial fulfillment of the requirements for the degree of Doctor of Philosophy.

December, 1973

Dean, College of Engineering

Dean, Graduate School